UNIVERSITY OF CALIFORNIA

Santa Barbara

Development of Device Technology for Micro-Light-Emitting Diodes

A dissertation submitted in partial satisfaction of the requirements for the degree

Doctor of Philosophy

in

Materials

by

Matthew S. Wong

Committee in charge

Professor Steven P. DenBaars, Chair

Professor Shuji Nakamura

Professor James S. Speck

Dr. Tal Margalith

December 2020

The dissertation of Matthew S. Wong is approved.

Tal Margalith

James S. Speck

Shuji Nakamura

Steven P. DenBaars, Committee chair

September 2020

Development of Device Technology for Micro-Light-Emitting Diodes

Copyright © 2020

by

Matthew S. Wong

To my grandparents and parents,

for all their care and love

Acknowledgments

There are many people throughout my graduate school life that I would need to acknowledge for their supports, since my PhD path has been rugged. I started the graduate school journey at UCSB in August 2015, working on organic semiconductor materials, and did not join Professor Steve DenBaars' group until September 2016. I would first like to thank my advisor, Professor Steve DenBaars, for taking me into his group, when I had no idea on LEDs or inorganic semiconductor materials, for giving me many opportunities during graduate school, and for believing in me to do well in his group. I would also want to thank my committee members for all their supports: Professor Shuji Nakamura has been offering his encouragements on my research projects and various opportunities. Professor Jim Speck has been teaching me numerous useful knowledge and giving me beneficial insights, where his mentoring style keeps me continue to gain new knowledge. Dr. Tal Margalith has been a wonderful mentor and friend, where he has been helping me on a variety of aspects and offering great advice.

I would want to thank Professor Umesh Mishra, Dr. Dan Cohen, and Dr. Aidan Taylor for all the discussions on the device and material perspectives. Moreover, other SSLEEC staff, including Stacia Keller, Fukiko, Tara, David Whitlatch, Mike Iza, Yukina, and Emi, have been offering many supports.

Many of my research would not be possible without my mentors: David Hwang, Changmin Lee, and Sang Ho Oh. David has been educating me patiently

on cleanroom fabrication, device measurements, and semiconductor knowledge, where giving me a solid foundation in GaN based LEDs. Changmin has been a good friend who gives many advices on my PhD path and on paper writing. Sang Ho has been offering encouragements and supports whenever I need to.

I would like to acknowledge my office mates: Jianfeng Wang and Cheyenne Lynsky for all conversations in the office. I want to thank all MOCVD growers and LED and microLED team members for showing me new knowledge every time. Other than that, the cleanroom staff: Brian T., Tom, Aidan, Mike S., Mike D., Don, Luis, Demis, Bill, Brian L., Lee, and Biljana, and friends, including Sean D., Paula, Noel, Kevin, Jason A., Felipe, Joan, Greg, Erissa, Marty, Cesar, and John, have been giving me enjoyable times in the cleanroom.

There are many friends who have supported me throughout the entire PhD journey: Kenny W., Michael F., Paolo, Anthony L., Srinivas, Haojun, Bei, Yujie, and Maggie C. I also want to thank Yahya, Srinivas, Anthony, Bei, Haojun, Changmin, and Kenny for getting delicious food with me.

Finally, my families: Simon, Nancy, aunts, grandparents, and parents, have been giving me continuous support and care throughout graduate school and in life in general.

Curriculum Vitae
September 2020

Matthew S. Wong

Santa Barbara, CA, 93111
(224) 795-3322 | m_wong@ucsb.edu

Summary

I have 5-year thorough experience and understanding in InGaN- and AlGaInP-based semiconductor materials for visible optoelectronic applications, with extensive materials growth, hands-on cleanroom device fabrication, device testing and failure analysis, and computational simulations. Other than inorganic semiconductors, I also have 3-year detailed practices in organic polymeric and perovskite materials for biomedical and photonic uses, including material synthesis and physiochemical characterizations, thin-film coating, and device construction. I have authored/co-authored 26 academic publications and 7 international conference presentations. I have invented 8 patents related to devices for display applications and display integration system. Other than the academic achievements, I have taken technical courses related to visual perception and machine learning.

Education

University of California, Santa Barbara **Sept 2015 – Sept 2020**

- Doctor of Philosophy – Materials
- Advisor: Steven P. DenBaars
- Research focus: Development of Device Technology for MicroLEDs

University of Wisconsin – Madison **Aug 2010 - Jun 2015**

- Bachelor of Science – Chemical Engineering
- Dual Major: Chemistry
- Research advisor: David M. Lynn
- Research project: Azlactone-Functionalized Polymers

Experience

UCSB Materials Department – Graduate Student Researcher **Sept 2016 – Present**

- Demonstrated improved microLED performances with post-etch fabrication techniques by conducting InGaN and AlGaInP device processing, testing, characterizations, and packaging
- Characterized microLED and laser diode devices using infrared (IR) camera and focus ion beam (FIB) for failure analysis
- Performed optical, electrical, and thermal modeling for microLEDs by LightTools and Lumerical
- Deep knowledge with the device architectures, color gamut, and limitations of current display technologies: LCD and OLED displays
- Wrote and grew recipes for GaN LED, microLED, and p-n diode on planar and patterned sapphire substrates using metalorganic chemical vapor deposition (MOCVD)
- Mentored four graduate students on cleanroom fabrication

UCSB Beyond Academia – Finance Co-chair **June 2017 – June 2019**

- Maintained sustainable budgets and managed the reimbursements from other subcommittees
- Communicated with local startups, companies, and departments at UCSB for sponsorships
- Worked with people from various backgrounds as a team to achieve different tasks
- Supervised the finance committee and retained a good teamwork environment

UCSB Chemistry Department – Graduate Student Researcher **Sept 2015 – Sept 2016**

- Synthesized water-soluble conjugated polyelectrolytes (CPEs) and conjugated polymers for organic photovoltaic (OPV) and organic light-emitting diode (OLED) applications
- Characterized the structural and chemical properties of CPEs using GPC, NMR, and DLS
- Characterized the optical properties and film morphology of CPEs using SEM, AFM, and UV-Vis spectroscopy

UW – Madison Chemical Engineering Department – Undergraduate Researcher A**ug 2014 – June 2015**

- Developed methods to fabricate partially hydrolyzed PVDMA polymers from homo-PVDMA polymer
- Determined the hydrolysis percentage of PVDMA using quantitative ^{13}C NMR
- Characterized the growth of films made from partially hydrolyzed PVDMA polymers using ellipsometry and IRRAS

Skills

- Team communication in managing projects and daily stand-ups

Lab Skills

- Material characterizations: AFM, ESR, GPC, IR spectroscopy, mass spectroscopy, NMR, TEM, TGA, UV-Vis, XRD, SIMS, EDX
- Failure analysis: SEM, FIB, IR camera, laser-scanning confocal microscope
- Thin-film and soft material inspection: IRRAS, contact-angle measurement, cyclic voltammetry, ellipsometry

Computer Skills

- Device and computational simulations: COMSOL, Lumerical DEVICE, MATLAB, LightTools, Python
- CAD: L-Edit
- Chemical process design: ASPEN

Fabrication Processes

- 4-year cleanroom experience
- Vacuum deposition: ALD, PECVD, RF sputtering, ICP-PECVD, e-beam evaporation, ion-beam deposition
- Etching: ICP, RIE, ion mill

Awards

Outstanding Graduate Student Research Achievement Award **November 2019**

- Recognition in outstanding research achievement in SSLEEC

UCSB New Venture Competition Honorable Mention and Impact Award **May 2019**

- One of the six finalist teams: MicroPrint

Outstanding Graduate Student Research Achievement Award **November 2018**

- Recognition in outstanding research achievement in SSLEEC

Phi Lambda Upsilon National Honorary Chemical Society Member **Spring 2016**

- Recognition in outstanding academic achievement in Chemistry

Roger J. Altpeter Award **Spring 2014**

- Recognition in excellent technical writing skills in Transport Phenomena Lab

UW – Madison College of Engineering Dean's List **Spring 2013**

- Recognition in strengths, passion, and academic excellence in Chemical Engineering

Otter Chemistry Award **Spring 2012**

- Recognition in outstanding research and academic performances in Chemistry

Selected publications

1. M. S. Wong, D. Hwang, A. I. Alhassan, C.Lee, R. Ley, S. Nakamura, and S. P. DenBaars, *High Efficiency of III-Nitride Micro-Light-Emitting Diodes by Sidewall Passivation Using Atomic Layer Deposition*, Optics Express, 26(16), 21324 (2018)
2. M. S. Wong, C. Lee, D. J. Myers, D. Hwang, J. A. Kearns, T. Li, J. S. Speck, S. Nakamura, and S. P. DenBaars, *Size-independent Peak Efficiency of III-Nitride Micro-Light-Emitting Diodes using Chemical Treatment and Sidewall Passivation*, Applied Physics Express, 12, 097004 (2019)
3. M. S. Wong, S. Nakamura, and S. P. DenBaars, *Review–Progress in High Performance III-Nitride Micro-Light-Emitting Diodes*, ECS J. Solid State Sci., 9, 015012 (2020)
4. M. S. Wong, J. A. Kearns, C. Lee, J. M. Smith, C. Lynsky, G. Lheureux, H. Choi, J. Kim, C. Kim, S. Nakamura, J. S. Speck, S. P. DenBaars, *High Performance of AlGaInP Red Micro-Light-Emitting Diodes with Sidewall Treatments*, Optics Express, 28(4), 5787 (2020)
5. M. S. Wong, S. Nakamura, S. P. DenBaars, *Progress in High Efficiency III-Nitride Micro-Light-Emitting Diodes*, Semiconductors and Semimetals, manuscript in preparation

Patents

1. Reduction in Leakage Current and Increase in Efficiency of III-Nitride MicroLEDs, UC Case 2018-256, *Patent Pending*
2. Continuous Fluidic Printing of MicroLEDs, UC Case 2019-164, *Patent Pending*
3. MicroLEDs with ultralow leakage current, UC Case 2019-393, *Patent Pending*
4. Integration and mass transfer of microLEDs, UC Case 2019-420, *Patent Pending*
5. Formation of Transparent Integrated MicroLED Displays, UC Case 2019-430, *Patent Pending*
6. Integration of Gallium-containing MicroLEDs for Displays, UC Case 2019-979, *Patent Pending*
7. Fluidic Printing System for Optoelectronic Devices, UC Case 2020-078, *Patent Pending*
8. Method to Improve Performance of Gallium-Containing Light-Emitting Devices, UC Case 2020-086, *Patent Pending*

Conferences and presentations

1. Solid State Lighting and Energy Electronics Center (SSLEEC) Review, Santa Barbara, USA, 2017
2. 19th International Conference on Metalorganic Vapor Phase Epitaxy (ICMOVPE), Nara, Japan, 2018
3. 60th Electronic Materials Conference (EMC), Santa Barbara, USA, 2018, presented by Dr. C. Lee
4. SSLEEC Review, Santa Barbara, USA, 2018
5. International Workshop on Nitride Semiconductors (IWN), Kanazawa, Japan, 2018
6. Compound Semiconductor Week (CSW), Nara, Japan, 2019
7. UCSB Photonics Society Student Seminar, Santa Barbara, USA, 2019
8. 13th International Conference on Nitride Semiconductors (ICNS), Bellevue, USA, 2019
9. SSLEEC Review, Santa Barbara, USA, 2019
10. SSLEEC Nitrides Seminar, Santa Barbara, USA, 2020

Technical courses

1. Machine Learning, Stanford University, Coursera
2. Deep Learning Specialization, deeplearning.ai, Coursera

3. Graphic Elements of Design: Color Theory and Image Formats, University of Colorado Boulder, Coursera
4. Visual Perception and the Brain, Duke University, Coursera
5. Perception: Vision, University of California, Santa Barbara (PSY 130)
6. Introduction to Statistical Machine Learning, University of California, Santa Barbara (PSTAT 231)

Abstract

Development of Device Technology for Micro-Light-Emitting Diodes

by

Matthew S. Wong

Due to rapid developments of wearable and portable devices in recent years, displays with better efficiency and higher resolution performances are greatly desired. Inorganic micro-light-emitting diodes (μLEDs) have been considered as one of the promising candidates for next-generation display applications, and demonstrations of μLED displays have shown outstanding performances as compared to liquid crystal displays (LCDs) and organic-light-emitting-diode (OLED) displays. However, it has been shown that the maximum efficiency drops as the device dimensions shrink. This dissertation describes post-etch fabrication techniques that suppress or mitigate the size effect in InGaN and AlGaInP μLEDs.

In this dissertation, the concepts of current display technologies, namely LCDs and OLED displays, and μLEDs will be first introduced. Moreover, the mechanism of the reduction in efficiency will also be addressed. Followed by the first chapter, a series of fabrication methods and their improvements to the device performances will be discussed in the chapters 2-4. In chapter 2, the optoelectrical improvements in the InGaN μLEDs with dielectric sidewall passivation using atomic layer deposition (ALD) will be illustrated. This is the first demonstration that the InGaN μLED efficiency can be partially recovered using post-etch

technique. Due to the greater surface recombination velocity and minority carrier diffusion length, the effects of ALD sidewall passivation on AlGaInP μLEDs are investigated in chapter 3. This chapter also reveals the excellent optical properties of AlGaInP red emitters, and the potential elimination of the size effect in AlGaInP devices is also shown. In chapter 4, a detailed report on the performances of InGaN devices with the combination of chemical treatment and ALD sidewall passivation is presented, where this is the first demonstration of size-independent efficiency from 100×100 to 10×10 μm^2 devices. Since the size effect is mitigated in InGaN and AlGaInP devices, chapter 5 shows a possible mass transfer method that employs fluidic assembly with external forces. Lastly, other critical challenges in μLED displays, brief μLED device process follower, and outlook are discussed concisely in chapter 6.

Table of Contents

Chapter 1: Introduction

1.1 Overview 1
1.2 Current Display Technologies 2
1.3 μLED Displays 10
1.4 An Outline of the Dissertation 24

Chapter 2: μLEDs with ALD sidewall passivation

2.1 Motivation 33
2.2 μLED Design 34
2.3 Device Performances 35
2.4 Summary 47

Chapter 3: Red μLEDs

3.1 Visual Perception on Red Emission 51
3.2 Optical Comparisons Between Red μLEDs 53
3.3 AlGaInP μLEDs with ALD Sidewall Passivation 59
3.4 Summary 67

Chapter 4: μLEDs with chemical and sidewall treatments

4.1 μLEDs with Improved Performances 72
4.2 LEDs with Chemical Treatments 73
4.3 Devices with Chemical and Sidewall Treatments 75
4.4 Summary 88

Chapter 5: Mass transfer of μLEDs

5.1 Liftoff Methods 92
5.2 Fluidic Assembly with External Forces 95
5.3 Devices on Transparent Substrate 99
5.4 Summary 100

Chapter 6: Conclusion

6.1 Challenges in μLED Displays 104
6.2 Outlook 106
6.3 μLED Process Followers 107
6.4 Conclusion 108

1

Introduction

1.1 Overview

Since the development of portable, wearable, and other consumer electronics, the standard of displays has been improving rapidly and the desire of better displays has gained dramatic research attention in both academia and industry. The use of electronic devices becomes significantly important and has been infiltrated in our daily lives, from smart phones/tablets and laptops to automotive displays and large TV monitors[1,2]. Due to the huge demand of displays, market-research companies forecast the display panel market will grow more than 30 billion USD from 2019 to 2024 globally, and the increase is attributed to displays not only with better quality in color gamut and resolution but also for other emerging display applications, including near-eye displays for virtual reality (VR) and augmented reality (AR), head-up displays, and flexible displays[3]. This dissertation will first introduce the two widely used display technologies, namely liquid-crystal displays (LCDs) and organic-light-emitting diode (OLED) displays, and their basic operating principles. After that, the advantages and the main challenges of a new display technology: micro-light-emitting-diode (μLED)

displays will be discussed. In later chapters, some μLED problems will be addressed from the device perspective.

1.2 Current Display Technologies

Display panels have been the most critical component in any electronic devices since the first demonstration, because they deliver information from the devices to our eyes. Full-color displays usually contain elements that can produce red, green, and blue emissions individually. Moreover, a pixel is formed with red, green, and blue lighting elements, but sometimes more colors, for example white color, can be found as the fourth color in a pixel. In the history of displays, LCDs are probably the most mature display technology, because the first patent on liquid crystal light valve was filed in 1936[4]. Since then, LCD digital displays were employed in various of applications, including calculators and digital watches. Before the development of OLED displays in the early 2000s, LCDs were the dominant display technology in the market because of their low-cost and well-established manufacturing processes although other technologies, such as cathode-ray tube and plasma displays, had participated in the market temporarily. LCDs remain the mainstream display technology in a variety of applications; however, OLED displays have been penetrating the LCD market aggressively, especially in the portable and entertainment markets[3,5]. In the following sections, the general working principles of LCDs and OLED displays are presented. Moreover, the benefits and drawbacks of each technology are also highlighted.

1.2.1 Liquid-crystal Displays (LCDs)

As mentioned above, LCDs are the most established display technology and the first study of liquid crystal with electromagnetic fields can be traced back to 1929[4]. There are two types of LCDs, full-color displays and digital displays, both having similar functioning concepts. In this dissertation, LCDs are referred to the full-color displays and not the digital displays. Even though LCD digital displays are still being utilized in calculators, watches, and other applications, full-color LCDs provide a practical and comprehensive comparison with OLED and μLED displays.

An LCD panel can be separated into four parts: backlight unit (BLU), polarizer, liquid crystal and thin-film-transistor arrays (TFT), and color filters, where a schematic of an LCDs is shown in Fig 1.1. The BLU consists of a backlight source, light-guide plate, and brightness enhancement films. For the backlight sources, InGaN based light-emitting diodes (LEDs) with phosphor conversion are commonly used to generate white light, and these LEDs are usually mounted at one edge of the display panel. The light emitted from the LEDs is then transmitted to a light-guide plate, where it distributes light from one edge to the entire panel area and the back side of the light-guide plate usually contains reflective mirror to direct light and minimize light absorption. The light is passed through a series of brightness enhancement films[2]. The objectives of the brightness enhancement films are to define viewing angle of the displays, to recycle refracted light, and to enhance light extraction efficiency of the BLU. After that, the light is polarized

using polarizer and reaches the liquid crystal and TFT structure. Before entering the liquid crystal layer, only 55% of the light emitted from the LEDs escapes from the polarizer, and the light that is trapped within the BLU and polarizer will be recycled to increase the overall efficiency. Liquid crystal is a class of organic compounds, usually small molecules with aromatic structure, in which the crystal orientation can be altered when applying electric field. Additionally, the optical property, either optically clear or opaque, of the liquid crystal can be modulated by changing the crystal orientation[4]. As a result, the TFT controls whether light is transmitted or scattered in the liquid crystal layer. However, liquid crystal is not very efficient for light transmission, thus more than 30% of the light is absorbed in the liquid crystal. Finally, the light gets to the color filters that typically consisted of red, green, and blue colors. These color filters can be a variety of materials from organic to inorganic, and more recently quantum dots for superior color gamut quality. Ultimately, only 5% of the light emitted from the backlight LEDs is delivered[6].

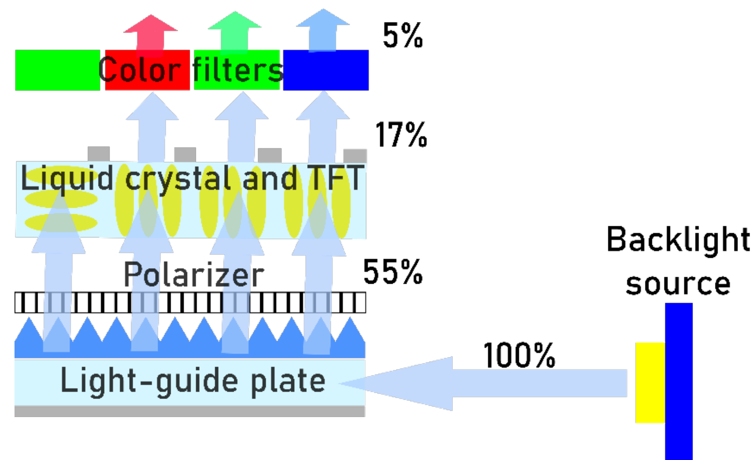

Figure 1.1. Schematic of an LCD pixel and the net percentage of light escaping in each layer

After discussing the basics of LCDs, it should be evident that the energy efficiency of LED backlight plays a crucial role to the success of LCDs, because majority of the light is lost within the LCD architecture. To date, InGaN based LEDs are the most energy efficient light source and the efficiency of InGaN blue LEDs has exceeded more than 80% in the literature[7]. In fact, one of the advantages of LCDs is their high brightness, which is a consequence of the highly efficient LED backlight[6,8]. For indoor and sunlight readable displays, the minimum luminance or brightness requirement is about 300 and 800 nits (1 nit = 1 cd/m^2), respectively[6]. LCDs can easily achieve luminance greater than 1,000 nits by inputting more current to the LEDs without any degradation or damage in the display architecture[2,8]. In addition, LCDs offer long operating lifetime and low manufacturing cost. On the other hand, there are disadvantages due to the intrinsic design of LCDs. First, the framework of LCDs is bulky and the light lost within liquid crystal is significant. Although each layer is less than 100 μm, the layers add up and the overall LCD module thickness ranges from 300 to 700 μm. Furthermore, many of the layers, such as the TFT, are mechanically brittle and inflexible, and this makes the realization of flexible displays challenging with LCDs[9]. Additionally, the contrast ratio is another important aspect for improvement. The contrast ratio of LCDs depends strongly on the LCD modes, which the contrast ratio is between 1,000:1 and 5,000:1[2]. The need for higher contrast ratio is a part of achieving high dynamic range (HDR), and HDR is a fundamental technology for next-generation display applications and requires the

contrast ratio more than 100,000:1[8,10]. There are two ways to enlarge the contrast ratio, by either increasing the peak brightness or improving the dark state. The issue for LCDs is the dark state, also known as the off-state brightness. As discussed previously, the light-guide plate spreads light across the entire panel area, and off-state brightness is controlled by the liquid crystal and TFT. Since light scattering is the primary mechanism to turn off a pixel in conventional LCDs, light leakage through the liquid crystal is the reason for the low contrast ratio[8]. Similarly, response time is also an issue from the liquid crystal and TFT structure, because response time is mainly responsible for the motion blurriness. In LCDs, the response time is limited by the responsivity of liquid crystal to electric field. In short, most of the benefits of LCDs come from the LED backlight while the downsides of LCDs are caused by the fundamental design burdens of liquid crystal.

1.2.2 Organic-light-emitting Diode (OLED) Displays

The potential of organic materials as OLEDs and organic photovoltaics (OPVs), respectively, for light-emitting and light-harvesting applications was first discovered in the 1980s[11]. Since then, a lot of attention has been spent on the development of organic semiconductors, including small molecules and polymeric materials. For typical organic materials, mostly composed of carbon and hydrogen atoms with covalent bonding, they are electrically insulative materials owing to the lack of pi conjugation. A conjugated system offers delocalized electrons within the organic structure and this can affect the electrical, thermal, or optical properties of the overall organic compound. By varying the conjugation network

and the molecular structure of organic semiconductors, OLEDs with different emission wavelengths and physiochemical characteristics can be synthesized[12,13]. For a simple OLED configuration, four components: anode, cathode, light-emitting layer, and encapsulation layer are necessary. Figure 1.2 shows a diagram of an OLED pixel with red, green, and blue subpixels. Anode is usually optically transparent and electrically conductive materials for hole injection, such as indium-tin oxides (ITO) or a conductive polymer PEDOT: PSS, and cathode is reflective metals, such as aluminum or silver, for electron injection[14]. The light-emitting layer is where electrons and holes recombine radiatively. However, in modern OLED design, a variety of electron and hole transport layers are added between the electrodes and the light-emitting layer to boost the injection efficiency, and this is especially crucial for hole injection[15]. Finally, the encapsulation layer is most critical ingredient among the four elements for reliability and operation under ambient condition. The intend of the encapsulation layer is to avoid moisture and oxygen from ambient reacting with the light-emitting layer since moisture and oxygen have detrimental impacts to the performance of light-emitting layer. The barrier requirement is extremely rigorous, where the water vapor transmission rate and oxygen transmission rate must be less than 10^{-6} $g/m^2/day$ and 1×10^{-6} $cm^3/m^2/day$, respectively[16]. This means that no more than a drop of water can diffuse across six football stadium within a day[17], which gives high manufacturing caution to OLED displays even though the architecture is much more straightforward than that of LCDs. As seen in Fig. 1.2, color filters,

polarizer, and liquid crystal are absent in OLED design, hence OLED displays are considered a self-emissive display technology. Nevertheless, organic materials are not very efficient for light-emitting application even with the assistance of electron and hole transport layers, and this attributes to low internal quantum efficiency[18]. Therefore, OLED displays only yield 10% in overall efficiency.

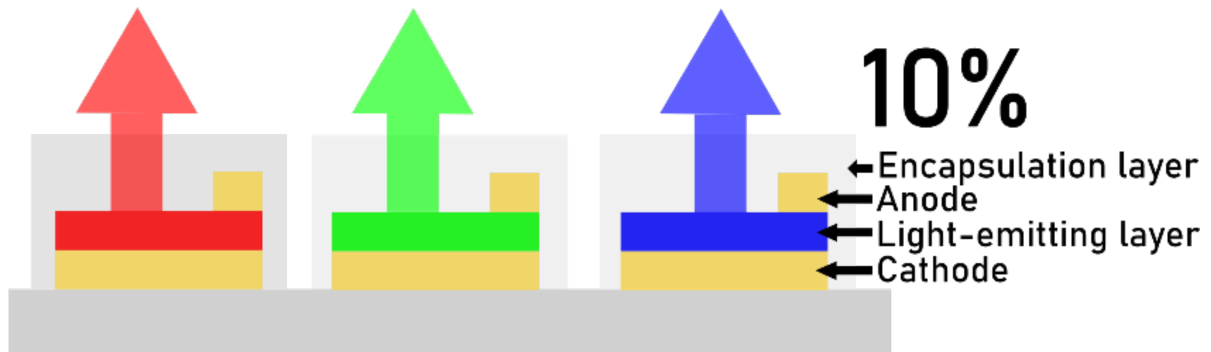

Figure 1.2. Schematic of an OLED pixel with the net percentage of light output efficiency

OLED displays are the first pioneer self-emissive display technology that are employed for commercial products. One of the biggest advantages of self-emissive OLED displays is the outstanding dark state for getting high contrast ratio since the pixel is completely turn off to give true black state[2]. Moreover, the OLEDs render better color gamut than conventional LCDs. Because of the uncomplicated framework, it provides high degree of freedom in device design and can be incorporated easily. Additionally, since organic materials are solution processable and OLEDs have simple design, the total thickness of OLED displays is usually less than 1 μm and are considerably thinner than LCDs[2]. Due to the solution processable feature of OLEDs, the substrate choice can have many variations in terms of mechanical flexibility and optical transparency and with

great capability of scaling for mass production. Although OLEDs have such improvements than LCDs, there are several disadvantages that need more research attention before utilizing them for next-generation display applications. The first issue is the chemical stability of OLEDs. As discussed in the last paragraph, a meticulous encapsulation layer is needed to ensure the operating lifetime and the performance of OLEDs. Otherwise, both the lifetime and light output performance degrade severely[17]. Also, because of the stability of LEDs, the maximum light output of OLEDs drops over time and the decay rate depends on the driving current; this effect is more pronounced in green and blue light emitters[17]. Not to mention OLEDs usually have low carrier mobility and carrier concentration resulting in low injection efficiency[2]. More importantly, the substrate choice could have influences on the water and oxygen transmission rates of the display panel. In traditional OLED design, glass is usually the substrate. If plastic substrate is used, the differences in water and oxygen transmission rates must be evaluated, because normal plastic substrates have orders of higher magnitude transmission rates than glass, and are insufficient to prevent moisture and oxygen reactions with OLEDs[16]. Other than the inherent structural challenges of OLEDs, there are other display related difficulties with OLED displays besides the well-known burn-in problem. Typically, the peak brightness of commercial OLED displays is about 600 nits, which does not satisfy for sunlight readable displays where minimum of 800 nits is required. Likewise, the low brightness of OLEDs affects the contrast ratio feature. OLED displays can

theoretically achieve infinite contrast ratio due to the true black off state, yet this is only correct under true dark condition and invalid under sunlight and indoor environments[2]. Secondly, the cost of OLED displays are more expensive compared to LCDs due to the transfer process to the display panels[17,19–21]. More details of transfer processes will be presented in section 1.3.4. In summary, although OLED displays serve as the first self-emissive display technology in commercial products, which introduces new display architectures and novel display devices to both the industry and market, but the inherent physiochemical properties of OLEDs are the major constraint for futuristic display applications.

1.3 Micro-light-emitting Diode (μLED) Displays

From above sections, it should be obvious that the main benefit of LCDs relies on the energy efficient LED backlighting and the success of OLED displays comes from the simplicity of the display architecture. The basic concept of μLED displays employs highly efficient inorganic LEDs while maintaining uncomplicated display panel design, as shown in Fig. 1.3.

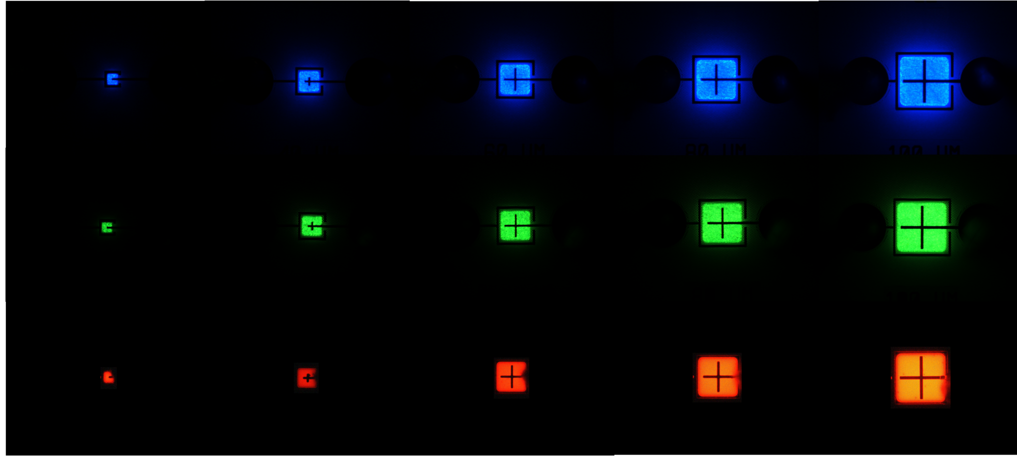

Figure 1.3. Red, green, and blue μLEDs from 100×100 to 20×20 μm²

Before exploring the technical details of μLEDs, let us review briefly on the significance of μLEDs from the industry standpoint. The μLED market is expected to grow from 254 million USD in 2017 to 20,501 million USD by 2025, which the growth percentage is much greater than the overall display panel market. μLEDs are an innovative technology that offers extensive business opportunities for startups and developed corporations and μLEDs can be employed for a variety of influential applications, including displays, short-range visible light communication (VLC), bioelectronics, sensing, and illumination[22–26] giving them an important market value. Although μLEDs have versatile potential usages, there are new challenges that needed to be resolved before the realization of μLED commercial products. In the remaining sections, a general background of μLEDs and the difficulties of μLED displays will be introduced.

1.3.1 What are μLEDs?

μLEDs are inorganic LEDs in micron dimensions, yet the size range of μLEDs is not well defined in the literature[27,28]. In this dissertation, μLEDs refer to LEDs with device dimensions no more than 100×100 μm^2. For conventional LEDs for solid-state lighting applications, the typical top light-emitting area ranges from 0.1 to 1 mm^2, which indicates at least one edge of the device is larger than 300 μm[29–32]. Recently, there are some research interests in employing mini-LEDs, LEDs in the sizes from 100 to 200 μm, for the backlight source in LCDs to boost the contrast ratio, to reduce the complexity of LCD architecture, and to improve other display parameters, such as viewing angle and aperture ratio[33]. Since μLEDs are on the microscopic scale, each μLED represents a pixel in monochromic displays or three red, green, and blue μLEDs form a pixel in full-color displays, and the pixels are unnoticeable by human eyes. In fact, μLED displays with ultrahigh resolution more than 5,000 pixels per inch (PPI) have been demonstrated[1,34]. Moreover, similar to OLEDs, μLEDs are self-emissive technology that means μLEDs can attain the same, if not better, dark state in contrast ratio and simple display panel design[33]. Other than that, μLEDs are comprised of mature inorganic semiconductor materials, such as InGaN or AlGaInP, that provides advantages superior than LCDs, including high peak brightness, remarkable energy efficiency, chemical robustness, and long operating lifespan[1]. As a result, μLEDs combine the benefits of LCDs and OLED displays and abolish the drawbacks in these two display technologies mostly because of the

material and device advantages. To complete the μLED story, it is inevitable to know the basics of the materials for μLEDs – III-nitride.

III-nitride material system consists of the chemical formula $Ga_xAl_yIn_zN$ where $0 \leq x \leq 1$, $0 \leq y \leq 1$, $0 \leq z \leq 1$, and $x + y + z = 1$. Because majority of the research attention focuses on InGaN based μLEDs, although there are little research on UV-A AlGaN μLEDs for display applications, this dissertation will concentrate on InGaN μLEDs and most of the techniques described in this dissertation should be applicable to AlGaN μLEDs[35,36]. One of the most vital advantages of the InGaN material system is the emission wavelength tunability by varying the composition percentage of indium and gallium in the active region, also known as the quantum wells, since the bandgaps of GaN and InN are 3.4 eV and 0.7 eV, respectively, and the alloy of InGaN system can theoretically cover the entire visible spectrum [37,38]. More details about emission wavelength and color gamut will be discussed in section 1.3.3. Additionally, InGaN materials are grown on sapphire (Al_2O_3) or silicon substrates using metalorganic chemical vapor deposition (MOCVD). Depending on the reactor dimensions, the wafer diameter can be scaled from 2-inch to 6-inch for sapphire substrates or up to 18-inch for silicon substrates, and this scalability is ideal for mass production with low material cost. Besides the scalable flexibility, the use of heterogeneous substrates, such as sapphire or silicon, offers straightforward and damage-free methods to remove fabricated devices from the heterogeneous substrates to other substrates or display panels[23,39–41]. These damage-free substrate removal methods can be

very beneficial to transfer μLEDs from their heterogeneous substrates to other substrates, for example mechanically flexible or optically transparent substrates. Moreover, the thickness of traditional LEDs grown on heterogenous substrates is usually less than 5 μm, which provides freedom for thin-film displays and the InGaN device thickness is comparable with OLEDs after encapsulation[42]. Unlike OLEDs, InGaN μLEDs are stable under ambient condition without any degradation in device performances, and the devices do not require any encapsulation for reliability purposes. As mentioned in section 1.2.1, one of the key successes of LCDs is due to the high luminous efficiency of the InGaN LED backlights. Because μLEDs are InGaN LEDs smaller than 100×100 μm^2, the advantageous performances of conventional InGaN LEDs are inherited by InGaN μLEDs. The fact that μLEDs provides simple display architecture on any substrates like OLED displays while giving brighter luminous efficiency and better reliability characteristics than LCDs is very appealing for next-generation display applications.

Although μLEDs have great potentials in display and other emerging applications, there are some challenges needed to be addressed before the realization of commercial products for mass production. In the following sections, three essential issues of InGaN μLEDs: size-dependent efficiency, color gamut (long-wavelength emission), and mass-transfer techniques are discussed with some potential solutions of each problem provided in later chapters.

1.3.2 Size-dependent Efficiency

As indicated in previous sections, one of the main benefits of μLEDs is the chemical robustness of III-nitride materials. However, chemical robustness also serves as a drawback in terms of device fabrication. Because the III-nitride material system is inert to almost all chemicals for wet etching to give significant etch rate, chloride-based plasma dry etching is always employed to define the light-emitting area of devices[43]. The use of plasma etching creates plasma-induced damage, such as surface states and dangling bonds, at the sidewalls and has negative impacts to the optoelectrical characteristics, including increased ideality factor, greater reverse breakdown voltage, and higher reverse leakage current[44–46]. For conventional LEDs that are used for solid-state lighting, it has been shown that plasma damage induces increase in leakage current and lower photoluminescence (PL) and electroluminescence (EL) intensities[47,48]. Therefore, different approaches have been developed on recovering the electrical and optical performances of LEDs[49–52]. Conventional LEDs usually have large top emitting area device design to reduce carrier concentration in the active region to avoid the influences of efficiency droop[30]. Due to this large emitting area and low sidewall perimeter, or low perimeter-to-area ratio, device design, the performance of conventional LEDs is limited by other dominating factors, such as light extraction efficiency and device design, other than sidewall damage, and tremendous efforts have been dedicated to develop LEDs with greater efficiency[7,53,54].

The detailed investigation on the size effect of μLEDs was first published in 2012, where the report demonstrated μLEDs can achieve higher current density at the same applied voltage, compared to larger device dimensions, although the peak EQE value decreases and the corresponding peak current density increases as the μLED size shrinks[55]. The reduction of the peak EQE was attributed to the increase in Shockley-Read-Hall (SRH) non-radiative recombination, also known as the A coefficient in the ABC model, which has a significant impact at low current density and is a contribution from surface states, dangling bonds, surface recombination, and sidewall damage[56,57]. The ABC model that describes the internal quantum efficiency is the following

Equation 1. ABC model for internal quantum efficiency

$$IQE = \frac{B \cdot n^2}{A \cdot n + B \cdot n^2 + C \cdot n^3}$$

where n is the carrier concentration, A is the SRH non-radiative recombination, B represents the bimolecular radiative recombination, and C is associated with Auger non-radiative recombination. It has been shown experimentally and computationally that the B and C coefficients are almost independent with device dimensions and can be assumed as constant[56,58]. Since EQE is the product of internal quantum efficiency and light extraction efficiency, and light extraction efficiency is constant for identical device design, the ABC model provides useful insights to improve the efficiency of μLEDs[56].

Researchers have suggested that device fabrication is responsible for the decrease in maximum EQE, increase in ideality factor, and light emission inhomogeneity[59–61]. Moreover, it has shown that the EQE was recovered by thermal annealing, indicating that the drop in EQE can be recovered partially or, possibly, mitigated completely by employing different post-etch fabrication techniques. Other than the peak efficiency aspect, researchers have found out that smaller μLEDs have less efficiency droop than the larger μLEDs, which is due to better current and thermal spreading and the results have confirmed with simulations[59,60,62,63]. The influences of size-dependent efficiency are fatal for μLED displays, because μLEDs are ideal for emerging display applications, like near-eye displays, with pixel sizes less than 20 μm and these pixel sizes must scale down below 10 μm to be cost-competitive to LCD and OLED display panels[36]. Therefore, it is crucial to maintain the high energy efficiency in conventional LEDs while shrinking down device dimensions less than 20 μm.

1.3.3 Color Gamut

The need of wide color gamut is an essential requirement for any full-color displays, because wide color gamut enables true color representation and gives better display quality. There are multiple standards, such as Rec. 2020, that define the metrics of full-color displays, including color gamut, contrast ratio, refresh rate, and viewing angle[64,65]. In this thesis, only the wavelength shift and the bandwidth, or full-width at half maximum (FWHM), of light emission in long-wavelength devices will be discussed, because these two elements are relevant

from the material and device standpoints whereas other components, such as refresh rate and contrast ratio, are more related to the system level. According to Rec. 2020, the wavelength definitions of three primary colors are 467 nm for blue, 532 nm for green, and 630 nm for red. Although III-nitride based blue and green LEDs have shown excellent bandwidth results that are less than 30 nm, the blueshift in wavelength can be problematic in typical green and red *c*-plane InGaN LEDs, as our eyes are more sensitive in the green and red wavelength ranges. Moreover, due to the high indium percentage in the active region and material challenges, red InGaN LEDs suffer from poor optical properties and low efficiency [66–68]. As a result, this section will focus on the issues of InGaN green μLEDs and other potential red emitters for display applications.

Typical commercial InGaN blue and green LEDs are grown on flat or patterned sapphire substrates (PSS) on *c*-plane polar crystal orientation. Because *c*-plane has the highest total electric field in the active region, the overlap between electron and hole wavefunctions are poor, and thus the blueshift in wavelength is more significant in polar crystal orientation than in crystal orientations with flat-band active region[69–71]. This phenomenon is commonly known as the quantum-confined Stark effect (QCSE). The effects of QCSE on InGaN blue and green LEDs are presented in Fig 1.4, where the emission spectra of the InGaN blue and green and AlGaInP red μLEDs at 1 and 100 A/cm^2 are shown, and the shifts in wavelength are clearly observed for the InGaN devices particularly in the green devices. Based upon Fig. 1.4, the blueshift worsens as the emission wavelength

gets longer, where the shift is 5 nm for blue and 13 nm for green. For the AlGaInP red μLED, where QCSE is absent, the wavelength exhibits a redshift in wavelength of 2 nm from 1 to 100 A/cm^2 due to the increase in junction temperature at high current density. To mitigate or eliminate the influences of QCSE, one option is to fabricate efficient long-wavelength LEDs on semi-polar or non-polar GaN substrates improving optical benefits which have been demonstrated[72–74]. However, these GaN substrates are difficult to scale up in size and costly for display applications. Hence, it is desirable to develop methods that provide the optical advantages as semi-polar devices with high scalability.

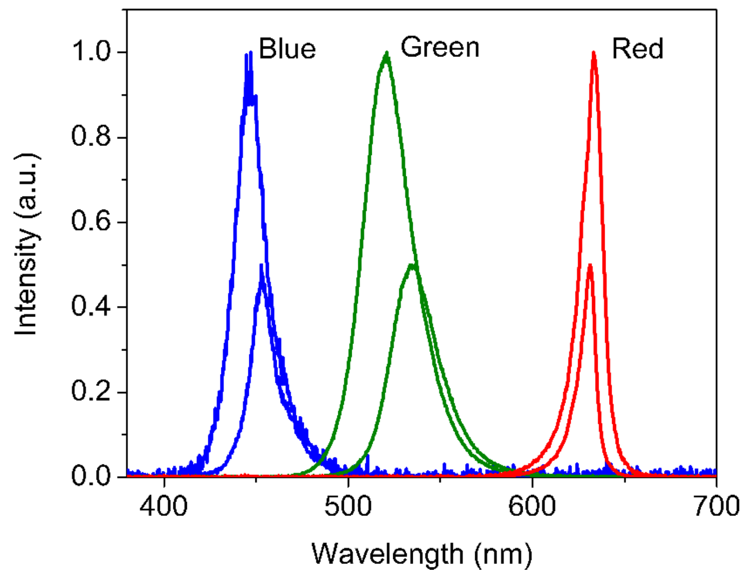

Figure 1.4. Emission spectra of InGaN blue and green and AlGaInP red μLEDs, where the spectra at 1 A/cm^2 have the maximum intensity of 0.5 and the spectra at 100 A/cm^2 have the maximum intensity of 1.

On the other hand, the realization of red, green, and blue LEDs utilizing the III-nitride material system has been a great aspiration since the early development of InGaN LEDs[67]. To date, the red *c*-plane InGaN LED with 3% peak

EQE demonstrated by Hwang *et al.* holds the record of red InGaN LEDs[68]. Because the performance of red InGaN LEDs is constrained by the material barriers, such as the strain between InGaN and GaN, several novel growth approaches are proposed for better material growth of red InGaN LEDs[75].

While the research of red InGaN LEDs are ongoing, there are a variety of mature red emitters and many of them have employed in commercial applications. Color conversion using quantum dots is one of the most popular approaches in the literature[1,76,77]. In fact, this approach has been considered to convert from blue or UV-A to green or red emissions[36,78]. Color conversion using quantum dots offer several advantages for μLED displays. By employing quantum dots, monolithic blue μLED arrays can be used to generate red, green, and blue colors without the need of long-wavelength InGaN μLEDs. Moreover, due to monolithic μLEDs being used, the mass transfer of μLEDs is unnecessary and solution-based inkjet printing is utilized to transfer quantum dots[76,79]. In terms of color gamut, quantum dots have demonstrated outstanding optical properties with FWHM about 30 nm, which is comparable with OLEDs[5,35]. Additionally, unlike conventional phosphor materials, quantum dots are in the dimensions less than 1 μm that can be uniformly coated and result in homogenous light emission[36]. Even though quantum dots give convenient solutions to yield full-color μLED displays, there are problems with this technique. Quantum dots that are employed in μLED demonstrations composed of heavy metals, such as cadmium (Cd), and these heavy metals are toxic and harmful to the environment[35,76]. Heavy-metal free

quantum dots have been reported, but their optical performances are not as good as the quantum dots with heavy metals, and more improvements are required[80–82]. Other than that, since most quantum dots are perovskite materials, thermal stability and long-term degradation might bring in potential reliability issues to commercial products[77]. More importantly, the use of quantum dots will increase the manufacturing cost of μLED displays. The cost consists of two parts: material cost and integration cost. For material cost, quantum dots might allow lower or comparable cost than using long wavelength LED wafers. Nevertheless, the integration cost of quantum dots is questionable. Although inkjet printing can be employed for deposition of quantum dots, the rate and accuracy of inkjet printing are key parameters to yield low integration cost. As of now, all the inkjet printing methods are on an academic lab scale, hence the optimizations on rate, accuracy, and scalability for commercial applications are ongoing[76].

Besides color conversion materials, AlGaInP based materials have been used as the red emitters for many practical applications, including automotive and signaling[83]. Red AlGaInP LEDs are one of the most studied optoelectronic material systems since its discovery in early 1960s. After years of optimizations in epitaxy and device structures, AlGaInP LEDs have the optimal optical characteristics, such as narrow bandwidth and high EQE, for illumination applications. Furthermore, red AlGaInP LEDs have the highest efficiency (>50%) and the smallest bandwidth (15-18 nm) than self-emissive OLEDs, quantum dots, and InGaN LEDs, which makes red AlGaInP LEDs very attractive for μLED

display applications[5,53,68,82]. Yet, AlGaInP materials have greater minority carrier diffusion length and surface recombination velocity than III-nitride system, and these have deleterious effects on the optoelectrical features of AlGaInP μLEDs[61]. Also, if AlGaInP and InGaN μLEDs are used, efficient mass-transfer techniques are required to transfer AlGaInP red and InGaN green and blue μLEDs from source wafers to display panels, which the transfer will introduce new challenges from conventional manufacturing scheme.

1.3.4 Mass-transfer techniques

The mass transfer of μLEDs is a unique problem for display manufacturers, since the specifications and principles for transferring μLEDs are disparate from the well-developed LCD and OLED display assembly approaches. For μLED displays, each red, green, and blue device represent a pixel, and ten or hundred million pixels are needed for display applications. Despite of the numerous devices for mass transfer, the ideal mass-transfer methods should have rapid transfer rate with high yield and selectivity of dead or defective pixels. This is particularly difficult for display builders, because current transfer techniques cannot satisfy all mass-transfer requirements for μLED displays. There are ways that can provide fast transfer rate but resulted in low yield and selectivity, or vice versa. It is beneficial to review the transfer methods for LCD and OLED displays to understand the pros and cons of each approach. Then follow up with the different potential mass-transfer techniques for μLED displays.

Pick-and-place method is the standard approach for transferring LEDs not only in LCD manufacturing but also in solid-state lighting packaging. Since the LED backlights occupy only one edge of the displays, the number of LEDs required to transfer is manageable with robotic arm pick-and-place method, and the transfer rate is about 15,000 chips per hour. In addition, the size range of the transferred LEDs is significantly greater than the μLED dimensions, so individual device handling is possible for large LEDs[84,85]. The typical pick-and-place method is not suitable for the transfer of μLED displays, because it would take months to assembly enough μLEDs onto display panels and it cannot give direct positioning due to the miniature size of μLEDs.

On the other hand, the OLED transfer approaches are fundamentally different from LCDs because of their solution-processable nature. There are two common techniques to deposit OLED materials onto display panels: thermal evaporation and inkjet printing, which the former method has been applied in industry setting since the preliminary stage of OLED displays and the latter being a relatively new method from 2017[17]. Thermal evaporation of OLED materials is very similar to regular thermal evaporation for metal deposition in cleanroom, where the OLED material is deposited to desired area under vacuum and a shadow mask is used to covered other areas. This method offers high deposition precision with the use of shadow mask, yet wastes many OLED materials during deposition, which attributes to the high cost of OLED displays. Roll-to-roll manufacturing is one of the most important advantages to yield cost-effective

OLED displays, because the high throughput rate of roll-to-roll manufacturing can produce high quantity of OLED displays continuously without losing noticeable amount of OLED materials in the process. However, roll-to-roll manufacturing has not been realized until the development of inkjet printing technique. With the first demonstration of inkjet printing for OLED displays, other potential applications with the same transfer technique could be revealed[86].

One of the well-known illustrations of μLED mass transfer was developed using plastic elastic stamps by Rogers *et al.*, and the mechanism of this approach has been studied extensively and different heterogenous integrations have been reported[87–90]. Also, this method is material independent and has been employed to transfer different inorganic semiconductors onto flexible and transparent substrates[23,91–93]. Although the stamping method has shown great μLED transfer ability, the drawback is that the yield and selectivity relies on the number of repeatability with the plastic stamp, which could cause reliability issues for μLED displays[23]. Apart from the stamping approach, other μLED mass-transfer techniques remain in the research and development stage, hence more research attention on this perspective is ideal. Additionally, besides advancing the μLED transfer technology for display applications, there are other emerging usages, including biomedical and optogenetic, for heterogeneous integration of inorganic semiconductors on flexible and transparent substrates[22,25,94,95]. A mass transfer fluidic assembly method using acoustic focusing and magnetic field will be

introduced, where the transfer employs acoustic focusing to control the device alignment and magnetic field to modulate the device orientation of μLEDs.

1.4 An Outline of the Dissertation

Chapter 2 discusses the optoelectrical characteristics of blue InGaN μLEDs using dielectric sidewall passivation by atomic layer deposition (ALD). Chapter 2 emphasizes the significant improvements of ALD sidewall passivation by comparing the device performances with plasma-enhanced chemical vapor deposition (PECVD), a common dielectric deposition method in industry. Chapter 2 also serves as the foundation for later chapters.

Chapter 3 covers the use of ALD sidewall passivation on commercial AlGaInP μLEDs. Because the differences in material properties and minority carrier diffusion length, the miniature dimensions of μLEDs have greater negative effects on AlGaInP materials than the III-nitride system. Chapter 3 also touches on the influences of a plasma-based surface pretreatment before ALD on AlGaInP and InGaN μLED performances. Finally, chapter 3 provides insights about size-independent EQE performance in AlGaInP devices.

Chapter 4 reveals the first demonstration of size-independent EQE performance of etched InGaN mesa dimensions range from 10×10 to 100×100 μm^2. The size-independent EQE feature is achieved by employing the combination of potassium hydroxide (KOH) chemical treatment and ALD sidewall passivation. Chapter 4 reports the details about chemical treatments under various conditions.

Chapter 5 explores a novel approach to assemble InGaN μLEDs in solution using non-damaging external forces, namely acoustic focusing and magnetic field. Chapter 5 discusses the liftoff methods for InGaN μLEDs from sapphire substrates and the design of the printing devices. This chapter shows the demonstrations of ordered μLED alignment using acoustic focusing and controllable device orientation by magnetic field, and preliminary EQE results of μLEDs on transparent substrate. Chapter 5 hypothesizes a potential assembly technique to realize full-color μLED displays using mass transfer approach.

Chapter 6, lastly, concludes the work and foresees future expectations on μLEDs for display and other emerging applications. For those who are passionate to understand about the cleanroom fabrication or are interested in trying at their own risk, the brief process follower is included at the end of the chapter.

References

1. Jung, T., Choi, J. H., Jang, S. H. & Han, S. J. Review of Micro-light-emitting-diode Technology for Micro-display Applications. *SID Symp. Dig. Tech. Pap.* **50**, 442–446 (2019).

2. Chen, H.-W., Lee, J.-H., Lin, B.-Y., Chen, S. & Wu, S.-T. Liquid crystal display and organic light-emitting diode display: present status and future perspectives. *Light Sci. Appl.* **7**, 17168 (2018).

3. Lin, Y. *et al.* Mini-LED and Micro-LED: Promising Candidates for the Next Generation Display Technology. *Appl. Sci.* **8**, 1557 (2018).

4. Castellano, J. A. The History of LCD Development. *Flat Panel Displays Int. Conf.* (2005).

5. Levermore, P. P. *et al.* Ink-Jet-Printed OLEDs for Display Applications. *SID Symp. Dig. Tech. Pap.* **47**, 484–486 (2016).

6. Display Optics 101, 3M United States https://www.3m.com/3M/en_US/display-solutions-us/the-science-behind-the-display/display-optics-101/.

7. Hurni, C. A. *et al.* Bulk GaN flip-chip violet light-emitting diodes with optimized efficiency for high-power operation. *Appl. Phys. Lett.* **106**, (2015).

8. Tan, G., Huang, Y., Li, M.-C., Lee, S.-L. & Wu, S.-T. High dynamic range liquid crystal displays with a mini-LED backlight. *Opt. Express* **26**, 16572 (2018).

9. Harding, M. J., Horne, I. P. & Yaglioglu, B. Flexible LCDs Enabled by OTFT. *SID Symp. Dig. Tech. Pap.* **48**, 793–796 (2017).

10. Chen, H., Zhu, R., Li, M.-C., Lee, S.-L. & Wu, S.-T. Pixel-by-pixel local dimming for high-dynamic-range liquid crystal displays. *Opt. Express* **25**, 1973 (2017).

11. Schwambera, M. *et al.* 52.3: Invited Paper: OLED Manufacturing by Organic Vapor Phase Deposition. *SID Symp. Dig. Tech. Pap.* **34**, 1419 (2003).

12. Moon, S. *et al.* Hole transport layer based on conjugated polyelectrolytes for polymer solar cells. *J. Colloid Interface Sci.* **518**, 21–26 (2018).

13. Lee, B. R. *et al.* Conjugated Polyelectrolytes as Efficient Hole Transport Layers in Perovskite Light-Emitting Diodes. *ACS Nano* **12**, 5826–5833 (2018).

14. Brown, T. *et al.* Built-in field electroabsorption spectroscopy of polymer light- emitting diodes incorporating a doped poly(3,4-ethylene dioxythiophene) hole injection layer. *Appl. Phys. Lett.* **75**, 1679–1681 (1999).

15. de Jong, M. P., van IJzendoorn, L. J. & de Voigt, M. J. a. Stability of the interface between indium-tin-oxide and poly(3,4-ethylenedioxythiophene)/poly(styrenesulfonate) in polymer light-emitting diodes. *Appl. Phys. Lett.* **77**, 2255–2257 (2000).

16. Park, J. S., Chae, H., Chung, H. K. & Lee, S. I. Thin film encapsulation for flexible AM-OLED: A review. *Semicond. Sci. Technol.* **26**, (2011).

17. Kateeva. Inkjet Printing for Manufacturing of Flexible and Large-size OLEDs. 1–30 (2017).

18. Chen, L. M., Xu, Z., Hong, Z. R. & Yang, Y. Interface investigation and engineering - achieving high performance polymer photovoltaic devices. *J. Mater. Chem.* **20**, 2575–2598 (2010).

19. Apple iPhone 8+ Preliminary Cost Summary, IHS Markit.

20. Apple iPhone X Preliminary Cost Summary, IHS Markit.

21. Madigan, C. Inkjet Technology For OLED SSL Mass Production. (2015).

22. Park, J. *et al.* Soft, smart contact lenses with integrations of wireless circuits, glucose sensors, and displays. *Sci. Adv.* **4**, 1–12 (2018).

23. He, J., Nuzzo, R. G. & Rogers, J. A. Inorganic materials and assembly techniques for flexible and stretchable electronics. *Proc. IEEE* **103**, 619–632

(2015).

24. McKendry, J. *et al.* Structured illumination for communications and bioscience using GaN micro-LED arrays interfaced to CMOS. (2017).

25. Poher, V. *et al.* Micro-LED arrays: a tool for two-dimensional neuron stimulation. *J. Phys. D. Appl. Phys.* **41**, 94014 (2008).

26. Lingley, A. R. *et al.* A single-pixel wireless contact lens display. *J. Micromechanics Microengineering* **21**, 125014 (2011).

27. Lee, V. W., Twu, N. & Kymissis, I. Micro-LED Technologies and Applications frontline technology. *Inf. Disp. (1975).* **32**, 16–23 (2016).

28. Wong, M. S., Nakamura, S. & DenBaars, S. P. Review—Progress in High Performance III-Nitride Micro-Light-Emitting Diodes. *ECS J. Solid State Sci. Technol.* **9**, 015012 (2020).

29. Li, P. P. *et al.* Very high external quantum efficiency and wall-plug efficiency 527 nm InGaN green LEDs by MOCVD. *Opt. Express* **26**, 33108 (2018).

30. Oh, S. H. *et al.* Semipolar III-nitride light-emitting diodes with negligible efficiency droop up to ~1 W. *Appl. Phys. Express* **9**, 7–10 (2016).

31. Li, H. *et al.* Efficient Semipolar (11-22) 550 nm Yellow/Green InGaN Light-Emitting Diodes on Low Defect Density (11-22) GaN/Sapphire Templates. *ACS Appl. Mater. Interfaces* **9**, 36417–36422 (2017).

32. Becerra, D. L. *et al.* High-power low-droop violet semipolar (30 3 ¯ 1 ¯) InGaN/GaN light-emitting diodes with thick active layer design. *Appl. Phys. Lett.* **105**, 171106 (2014).

33. Huang, Y. *et al.* Prospects and challenges of mini-LED and micro-LED displays. *J. Soc. Inf. Disp.* 1–15 (2019). doi:10.1002/jsid.760

34. Day, J. *et al.* III-Nitride full-scale high-resolution microdisplays. *Appl. Phys. Lett.* **99**, 2–4 (2011).

35. Gong, Z. *et al.* Efficient flip-chip InGaN micro-pixellated light-emitting diode arrays: Promising candidates for micro-displays and colour conversion. *J. Phys. D. Appl. Phys.* **41**, 094002 (2008).

36. Ding, K., Avrutin, V., Izyumskaya, N., Özgür, Ü. & Morkoç, H. Micro-LEDs, a manufacturability perspective. *Appl. Sci.* **9**, 1206 (2019).

37. Alhassan, A. I. *et al.* Development of high performance green c- plane III-nitride light-emitting diodes. *Opt. Express* **26**, 5591–5601 (2018).

38. Nakamura, S., Senoh, M. & Mukai, T. High-power InGaN/GaN double-heterostructure violet light emitting diodes. *Appl. Phys. Lett.* **62**, 2390–2392 (1993).

39. Zou, X., Zhang, X., Chong, W. C., Tang, C. W. & Lau, K. M. Vertical LEDs on Rigid and Flexible Substrates Using GaN-on-Si Epilayers and Au-Free Bonding. *IEEE Trans. Electron Devices* **63**, 1587–1593 (2016).

40. Carreira, J. F. C. *et al.* Integration of Micro-LED Array on CMOS by Transfer Printing. *31st Annu. Conf. IEEE Photonics Soc. IPC 2018* 6–7 (2018). doi:10.1109/IPCon.2018.8527266

41. Wong, W. S. & Sands, T. Damage-free separation of GaN thin films from sapphire substrates. *Appl. Phys. Lett.* **72**, 599–601 (1998).

42. Chwang, A. B. *et al.* Thin film encapsulated flexible organic electroluminescent displays. *Appl. Phys. Lett.* **83**, 413–415 (2003).

43. Zhuang, D. & Edgar, J. H. Wet etching of GaN, AlN, and SiC: A review. *Mater. Sci. Eng. R Reports* **48**, 1–46 (2005).

44. Ping, A. T. *et al.* Characterization of reactive ion etching-induced damage to n-GaN surfaces using schottky diodes. *J. Electron. Mater.* **26**, 266–271 (1997).

45. Martinez, G. L., Curiel, M. R., Skromme, B. J. & Molnar, R. J. Surface recombination and sulfide passivation of GaN. *J. Electron. Mater.* **29**, 325–331 (2000).

46. Cao, X. A. *et al.* Electrical effects of plasma damage in p-GaN. *Appl. Phys. Lett.* **75**, 2569–2571 (1999).

47. Lee, J.-M., Huh, C., Kim, D.-J. & Park, S.-J. Dry-etch damage and its recovery in InGaN/GaN multi-quantum-well light-emitting diodes. *Semicond. Sci. Technol.* **18**, 530–534 (2003).

48. Yang, Y. & Cao, X. A. Removing plasma-induced sidewall damage in GaN-based light-emitting diodes by annealing and wet chemical treatments. *J. Vac. Sci. Technol. B Microelectron. Nanom. Struct.* **27**, 2337 (2009).

49. Kometani, R. *et al.* A high-temperature nitrogen plasma etching for preserving smooth and stoichiometric GaN surface. *Appl. Phys. Express* **6**, (2013).

50. Liu, Y. J. *et al.* A low damage GaN-based light-emitting diode with textured/inclined sidewalls and an air-buffer layer. *Displays* **31**, 111–114 (2010).

51. Liu, H. *et al.* Al2O3 Passivation Layer for InGaN / GaN LED Deposited by Ultrasonic Spray Pyrolysis. *IEEE Photonics Technol. Lett.* **26**, 1243–1246 (2014).

52. Kim, H. M., Huh, C., Kim, S. W., Park, N. M. & Park, S. J. Suppression of leakage current in InGaN/GaN multiple-quantum well LEDs by N 2 O plasma treatment. *Electrochem. Solid-State Lett.* **7**, 241–243 (2004).

53. Krames, M. R. *et al.* High-power truncated-inverted-pyramid (AlxGa1-x)0.5In0.5P/GaP light-emitting diodes exhibiting >50% external quantum

efficiency. *Appl. Phys. Lett.* **75**, 2365–2367 (1999).

54. Oh, S. H. High-efficiency Light-emitting Devices based on Semipolar III-Nitrides. (University of California, Santa Barbara, 2017).

55. Tian, P. *et al.* Size-dependent efficiency droop of blue InGaN micro-light emitting diodes. *Appl. Phys. Lett.* **101**, 231110 (2012).

56. Olivier, F., Daami, A., Licitra, C. & Templier, F. Shockley-Read-Hall and Auger non-radiative recombination in GaN based LEDs: A size effect study. *Appl. Phys. Lett.* **111**, 022104 (2017).

57. Verzellesi, G. *et al.* Efficiency droop in InGaN/GaN blue light-emitting diodes: Physical mechanisms and remedies. *J. Appl. Phys.* **114**, 071101 (2013).

58. Karpov, S. ABC-model for interpretation of internal quantum efficiency and its droop in III-nitride LEDs: a review. *Opt. Quantum Electron.* **47**, 1293–1303 (2015).

59. Hwang, D., Mughal, A., Pynn, C. D., Nakamura, S. & DenBaars, S. P. Sustained high external quantum efficiency in ultrasmall blue III-nitride micro-LEDs. *Appl. Phys. Express* **10**, 032101 (2017).

60. Olivier, F. *et al.* Influence of size-reduction on the performances of GaN-based micro-LEDs for display application. *J. Lumin.* **191**, 112–116 (2017).

61. Oh, J.-T. *et al.* Light output performance of red AlGaInP-based light emitting diodes with different chip geometries and structures. *Opt. Express* **26**, 11194 (2018).

62. Bulashevich, K., Konoplev, S. & Karpov, S. Effect of Die Shape and Size on Performance of III-Nitride Micro-LEDs: A Modeling Study. *Photonics* **5**, 41 (2018).

63. Konoplev, S. S., Bulashevich, K. A. & Karpov, S. Y. From Large-Size to Micro-LEDs: Scaling Trends Revealed by Modeling. *Phys. Status Solidi Appl. Mater. Sci.* **215**, 1700508 (2018).

64. Zhu, R., Luo, Z., Chen, H., Dong, Y. & Wu, S.-T. Realizing Rec 2020 color gamut with quantum dot displays. *Opt. Express* **23**, 23680 (2015).

65. Chen, H. W. *et al.* Going beyond the limit of an LCD's color gamut. *Light Sci. Appl.* **6**, e17043-10 (2017).

66. Nakamura, S. *et al.* Super-bright green InGaN single-quantum-well-structure light-emitting diodes. *Jpn. J. Appl. Phys.* **34**, L1332 (1997).

67. Mukai, T., Yamada, M. & Nakamura, S. Characteristics of InGaN-Based UV/Blue/Green/Amber/Red Light-Emitting Diodes. *Jpn. J. Appl. Phys.* **38**, 3976–3981 (1999).

68. Hwang, J.-I., Hashimoto, R., Saito, S. & Nunoue, S. Development of InGaN-based red LED grown on (0001) polar surface. *Appl. Phys. Express* **7**, 071003 (2014).

69. Feezell, D. F., Speck, J. S., Denbaars, S. P. & Nakamura, S. Semipolar (2021) InGaN/GaN light-emitting diodes for high-efficiency solid-state lighting. *IEEE/OSA J. Disp. Technol.* **9**, 190–198 (2013).

70. Feezell, D. F., Schmidt, M. C., DenBaars, S. P. & Nakamura, S. Development of Nonpolar and Semipolar InGaN/GaN Visible Light-Emitting Diodes. *MRS Bull.* **34**, 318–323 (2009).

71. Farrell, R. M., Young, E. C., Wu, F., DenBaars, S. P. & Speck, J. S. Materials and growth issues for high-performance nonpolar and semipolar light-emitting devices. *Semicond. Sci. Technol.* **27**, 024001 (2012).

72. Zhao, Y. *et al.* Green Semipolar (20-2-1) InGaN Light-Emitting Diodes with Small Wavelength Shift and Narrow Spectral Linewidth. *Appl. Phys. Express* **6**, 062102 (2013).

73. Yamamoto, S. *et al.* High-efficiency single-quantum-well green and yellow-green light-emitting diodes on semipolar $(20\bar{2}1)$ GaN substrates. *Appl. Phys. Express* **3**, 18–21 (2010).

74. Masui, H., Nakamura, S., DenBaars, S. P. & Mishra, U. K. Nonpolar and semipolar III-nitride light-emitting diodes: Achievements and challenges. *IEEE Trans. Electron Devices* **57**, 88–100 (2010).

75. Pasayat, S. S. *et al.* Growth of strain-relaxed InGaN on micrometer- sized patterned compliant GaN pseudo-substrates. *Appl. Phys. Lett* **116**, 111101 (2020).

76. Huang Chen, S.-W. *et al.* Full-color monolithic hybrid quantum dot nanoring micro light-emitting diodes with improved efficiency using atomic layer deposition and nonradiative resonant energy transfer. *Photonics Res.* **7**, 416 (2019).

77. Leitão, M. F. *et al.* Pump-power-dependence of a CsPbBr 3 -in-Cs 4 PbBr 6 quantum dot color converter. *Opt. Mater. Express* **9**, 3504 (2019).

78. Wierer, J. J. & Tansu, N. III-Nitride Micro-LEDs for Efficient Emissive Displays. *Laser Photon. Rev.* **1900141**, 1900141 (2019).

79. Han, H.-V. *et al.* Resonant-enhanced full-color emission of quantum-dot-based micro LED display technology. *Opt. Express* **23**, 32504 (2015).

80. Pickett, N. L., Harris, J. A. & Gresty, N. C. Heavy Metal-Free Quantum Dots for Display Applications. *SID Symp. Dig. Tech. Pap.* **46**, 168–169 (2015).

81. Pickett, M. L., Gresty, N. C. & Hines, M. A. Heavy Metal-Free Quantum

Dots Making Inroads for Consumer Applications. *SID Symp. Dig. Tech. Pap.* **47**, 425–427 (2016).

82. Won, Y.-H. *et al.* Highly efficient and stable InP/ZnSe/ZnS quantum dot light-emitting diodes. *Nature* **575**, 634–638 (2019).

83. Stringfellow, G. B. *High brightness light emitting diodes. Academic Press* **34683**, (1997).

84. Nabat, V., De La O Rodriguez, M., Company, O., Krut, S. & Pierrot, F. Par4: Very high speed parallel robot for pick-and-place. *2005 IEEE/RSJ Int. Conf. Intell. Robot. Syst. IROS* 1202–1207 (2005). doi:10.1109/IROS.2005.1545143

85. Saeedi, E., Kim, S. S., Etzkorn, J. R., Meldrum, D. R. & Parviz, B. A. Automation and yield of micron-scale self-assembly processes. *Proc. 3rd IEEE Int. Conf. Autom. Sci. Eng. IEEE CASE 2007* 375–380 (2007). doi:10.1109/COASE.2007.4341776

86. Singh, M., Haverinen, H. M., Dhagat, P. & Jabbour, G. E. Inkjet printing-process and its applications. *Adv. Mater.* **22**, 673–685 (2010).

87. Cok, R. S. *et al.* Inorganic light-emitting diode displays using micro-transfer printing. *J. Soc. Inf. Disp.* **25**, 589–609 (2017).

88. Meitl, M. a. *et al.* Transfer printing by kinetic control of adhesion to an elastomeric stamp. *Nat. Mater.* **5**, 33–38 (2006).

89. Sun, Y. & Rogers, J. A. Inorganic semiconductors for flexible electronics. *Adv. Mater.* **19**, 1897–1916 (2007).

90. Park, S. *et al.* Printed Assemblies of Inorganic Light-Emitting Diodes for Deformable and Semitransparent Displays. *Science (80-.).* **325**, 977–982 (2009).

91. Kim, H. -s. *et al.* Unusual strategies for using indium gallium nitride grown on silicon (111) for solid-state lighting. *Proc. Natl. Acad. Sci.* **108**, 10072–10077 (2011).

92. Kim, R.-H. *et al.* Waterproof AlInGaP optoelectronics on stretchable substrates with applications in biomedicine and robotics. *Nat. Mater.* **9**, 929–37 (2010).

93. Yoon, J. *et al.* GaAs photovoltaics and optoelectronics using releasable multilayer epitaxial assemblies. *Nature* **465**, 329–33 (2010).

94. Kim, T. *et al.* Injectable, Cellular-Scale Optoelectronics with Applications for Wireless Optogenetics. *Science (80-.).* **340**, 211–216 (2013).

95. Rein, M. *et al.* Diode fibres for fabric-based optical communications. *Nature* **560**, 214–218 (2018).

2

μLEDs with ALD sidewall passivation

2.1 Motivation

In the beginning stage of μLED development, many reports focused on the capabilities and the advantages of μLEDs for display, communication, and other interesting applications[1–5]. However, the performance details of device in different sizes was poorly understood until recently[6]. It has been shown that the peak efficiency drops significantly as the device dimensions shrink by several research groups, and this phenomenon is observed in both InGaN and AlGaInP material systems[7–10]. Despite μLEDs offer greater light extraction efficiency and better thermal and electrical current spreading due to their small sizes, size-dependent efficiency is problematic for μLEDs[11]. Even though μLEDs with outstanding EQE have been demonstrated, it is critical to understand the reasons of efficiency drop and find ways to recover it. The decrease in efficiency is caused by the enhancement in non-radiative recombination coefficient in the ABC model. According to the ABC model (equation 1), A and C are attributed to non-radiative

recombination while B corresponds to the radiative recombination coefficient. B and C are dominated mainly by bulk material properties, such as defects or impurities at the active region, and do not vary much with device size[12,13]. On the other hand, A represents the SRH non-radiative recombination coefficient and it is determined by dangling bonds, surface states, and fabrication damage. Moreover, it has been shown that the A coefficient increases linearly with perimeter-to-area ratio, suggesting that the reduction in peak EQE is a consequence of increased sidewall damage or defects, leakage current, and surface recombination[8,12,14]. In this chapter, the optoelectrical effects from employing ALD sidewall passivation on InGaN μLEDs are examined.

2.2 μLED Design

Before going into the specific of device performances, the details of μLED device architecture should be addressed. The devices were designed by Hwang *et al*. and the device sizes range from 100×100 to 10×10 μm^2 with squared mesa structures[15]. This μLED design is used throughout this dissertation to investigate the size effect and the improvements from different post-etch sidewall treatments, and the device fabrication scheme is modified from Hwang's process development. Figures 2.1(a) and (b) show the scanning-electron microscope (SEM) images of the six μLEDs and a micrograph of a 40×40 μm^2 device with metal contact pads dimensions, respectively. This mask design employs Al/Ni/Au as the common metal contacts, and 110 nm of indium-tin oxide (ITO) is deposited using electron-

beam evaporation as a transparent and ohmic *p*-contact. More details of the device design can be found elsewhere[9,15].

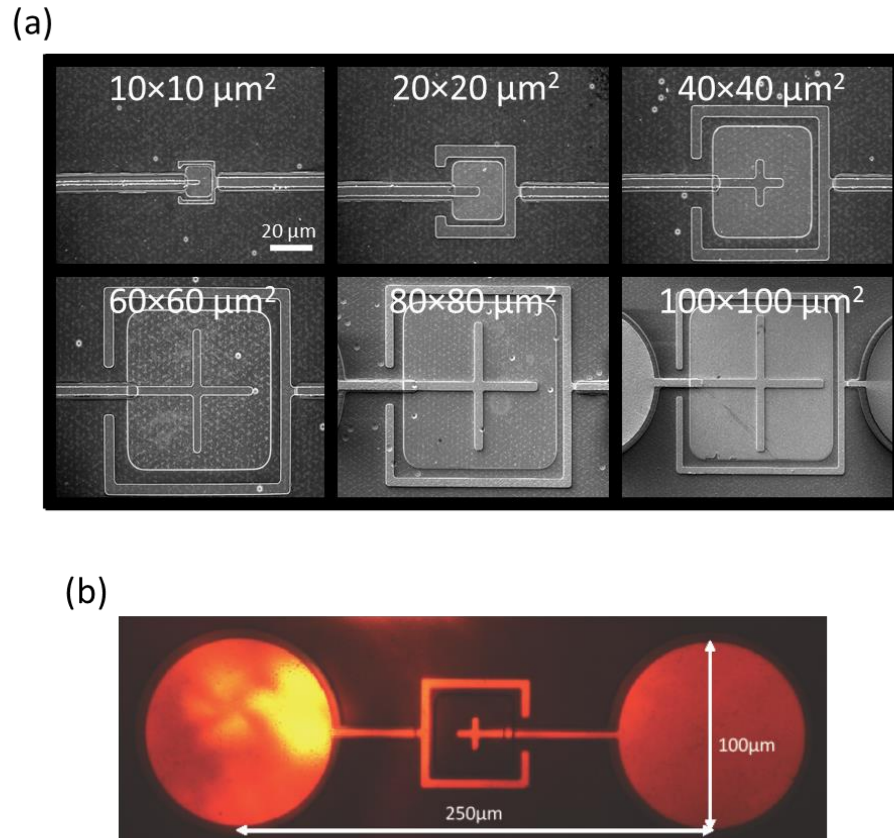

Figure 2.1. (a) SEM images of six μLEDs described in this dissertation and (b) a micrograph of a 40×40 μm² μLED with metal contact dimensions

2.3 Device Performances

Dielectric sidewall passivation of silicon dioxide (SiO_2), silicon nitride (Si_3N_4), or aluminum oxide (Al_2O_3) is a common approach to suppress the influences of surface recombination and leakage current, and this is typically performed using PECVD[16,17]. PECVD possesses several advantages, including cheap precursors, fast deposition rate, and high scalability, that are advantageous

to mass production of devices. However, as the device dimensions shrink, the device performances become increasingly sensitive to dielectric material quality, pre-deposition surface treatments, and the deposition method, compared to devices with low perimeter-to-area ratio[18]. ALD offers superior dielectric material quality with less impurity incorporations and matching stoichiometric ratio than PECVD dielectric materials, which could be beneficial to µLED performances[19].

Four InGaN samples with different sidewall passivation methods: without sidewall passivation (reference), with PECVD SiO_2 sidewall passivation, and two samples with ALD SiO_2 sidewall passivation, were used to determine the µLED optoelectrical characteristics using ALD and PECVD. In the three samples with passivation, 50 nm of SiO_2 was deposited, yet this thickness was not optimized and passivation with thinner film was possible. Figure 2.2 illustrates schematics of a device with the epitaxy information. From Fig. 2.2, it should be clear that the whole device was covered by the SiO_2 layer, including the sidewalls. The optical properties of different sidewall passivation methods are now discussed.

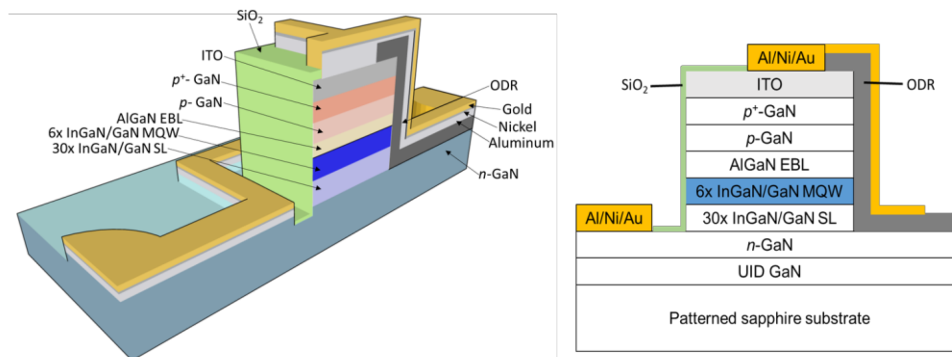

Figure 2.2. Schematics of a µLED with dielectric sidewall passivation

2.3.1 Optical Performances

The µLEDs with ALD sidewall passivation gained better optical characteristics, including uniform light emission and greater light output power for smaller µLEDs, compared to devices without sidewall passivation and with PECVD sidewall passivation[20]. Figures 2.3 (a) and (b) show electroluminescence (EL) pictures of devices with different sidewall passivation methods at 1 A/cm^2 and the current-light output power characteristics of 20×20 µm^2 devices.

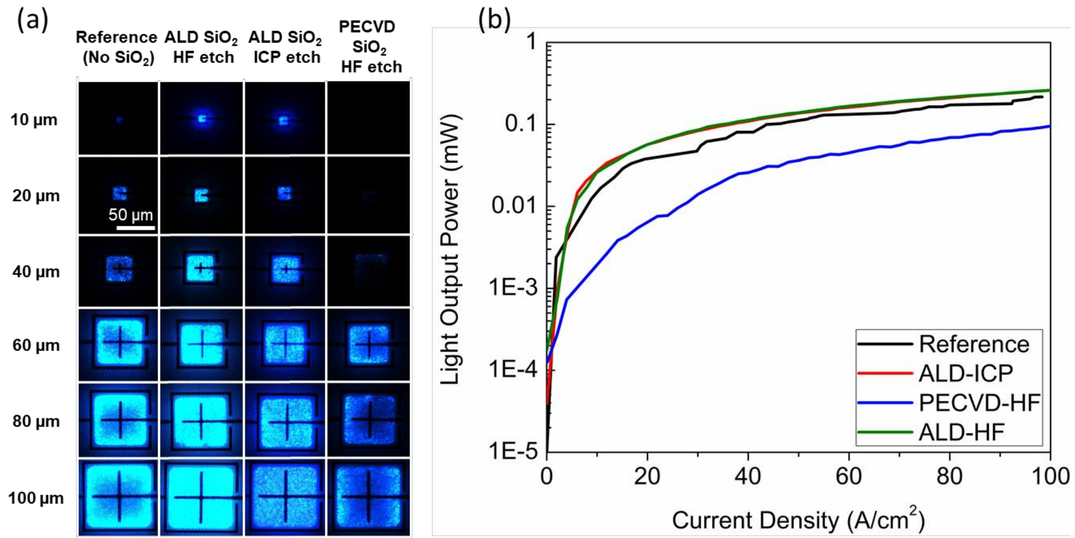

Figure 2.3. (a) EL images of µLEDs with different sidewall passivation methods at 1 A/cm^2 and (b) current-light output power performances of 20×20µm^2 µLEDs

The reference samples exhibited two distinct behaviors from the EL images, where light emission was crowded at the edges for devices larger than 40×40 µm^2 while homogeneous light emission was observed in smaller µLEDs. The light inhomogeneity could be accounted for current crowding due to plasma-induced etch damage, where the *p*-GaN at edges might be compensated or converted to *n*-GaN because of the generation of nitrogen vacancies during mesa etch[21–23].

Typically, current crowding issues are attributed to the highly resistive *p*-GaN, with current crowding around the *p*-contact. The surrounding area of *p*-contact (or around the center in this case) would be brighter than normal with current crowding. Since light emission was crowded at the edges, it indicated that there are more leakage current or less high-resistance paths at the sidewalls, thus resulting in the difference in current spreading between the center and the sidewalls. Moreover, this light emission nonuniformity has been observed by other researchers and the inhomogeneity behavior disappears at higher applied current density[8,9]. On the other hand, µLEDs that are 40×40 μm^2 or smaller yielded uniform light emission, but the light emission intensity was dimmer than the bigger devices. The uniform light emission in small µLEDs was attributed to uniform current spreading due to the miniature dimensions, yet the light intensity was reduced because of the increase in SRH non-radiative recombination[9,12,24].

In the case of PECVD sidewall passivation, the light intensity was less than the reference and the ALD samples. The decrease in light intensity was attributed to the drop in optical transparency of the ITO film. In the PECVD system, silane (SiH_4) was the silicon precursor, where hydrogen radicals were created during the deposition. It has been reported the generated hydrogen radicals react with the ITO surface to form metallic indium and tin oxides that are less transparent than ITO itself[25]. Figure 2.4 shows the transmittance data of ITO film on double-side polished sapphire substrates between as-deposited and after dielectric depositions. From Fig. 2.4, the ITO film after PECVD resulted in 48% decrease in

transmittance, with only a 5% decrease with ALD, compared to the as-deposited ITO film at 450 nm. Moreover, the ITO sheet resistivity was measured with a four-point resistivity mapper, and the resistivities were 33.6 Ω/sq, 45.2 Ω/sq, and 19.0 Ω/sq for the as-deposited, after ALD, and after PECVD samples, respectively. Based upon the transmittance and sheet resistivity results, ITO after PECVD became less transparent and more electrically conductive, confirming the results that the reduction of ITO to metallic indium by hydrogen radicals in the literature[25]. Therefore, in Fig. 2.3(b), the light output power of the 20×20 μm^2 device with PECVD sidewall passivation was about 80% lower than that of the reference device at 20 A/cm^2.

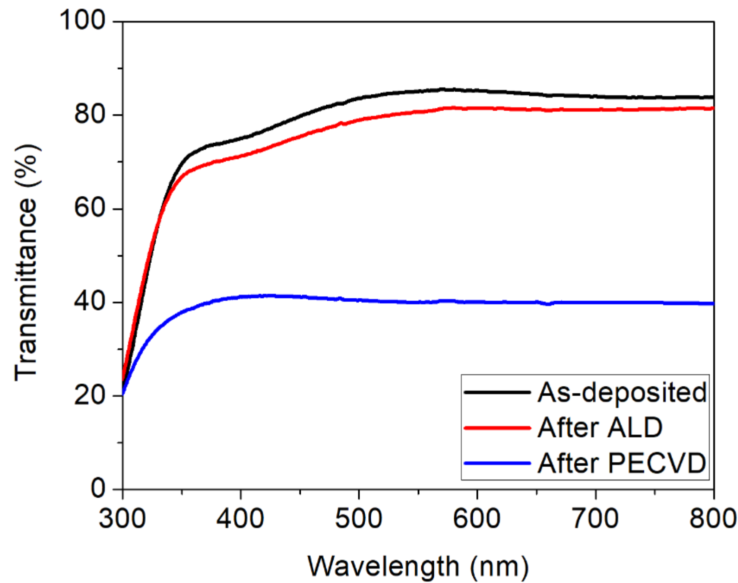

Figure 2.4. Transmittance data of ITO films on double-side polished sapphire substrates

For devices with ALD sidewall passivation, the two samples revealed similar behaviors including homogeneous light emission and comparable light output power. The main difference between "ALD-ICP" and "ALD-HF" was the

etch technique to remove ALD SiO_2 before metal deposition. Because ALD operates at 300°C, photoresist was not an option and blanket deposition was employed. To access electrical contacts, some area of SiO_2 must be removed for metal deposition, so two etch methods were used: inductively coupled plasma (ICP) dry etch and buffered hydrofluoric acid (HF) wet etch. In fact, the two SiO_2 removal methods not only had negligible impacts from a light emission perspective but also shared similar optical characteristics, as shown in Fig. 2.3(a). The ALD samples yielded uniform light emission among all device sizes and the light intensity was maintained in smaller devices. Furthermore, the light output power with ALD sidewall passivation was enhanced by 50% compared to the reference sample at 20 A/cm^2. The boost in light output power indicated ALD sidewall passivation is effective to suppress SRH non-radiative recombination and to recover some of the lost due to surface recombination and sidewall damage.

To determine the efficacy of ALD sidewall passivation, the EQE performances must be considered. Figures 2.5 (a) and (b) present the EQE of 100×100 and 20×20 μm^2 devices with different sidewall passivation methods, respectively. For the 100×100 μm^2 devices, the maximum EQE values for all samples were close to each other, where the values ranged between 36% and 41%, with deviation arising from small variations in growth and fabrication. This suggested dielectric sidewall passivation does not have critical effects on EQE for bigger μLEDs, because the influences of sidewall damage and passivation technique were trivial for devices with low perimeter-to-area dimensions.

Although the peak EQE values were equivalent, the EQE curves with different sidewall passivation methods were distinguishable. The device with PECVD passivation yielded greater EQE at high current density, whereas the EQE decayed dramatically after reaching the maximum for the ALD-HF device. Since the dissimilar behaviors occurred after the peak efficiency, Auger non-radiative recombination should be the dominant contributor for the change in EQE curves, and the cause could be either thermal or charge carrier aspects[26,27]. As mentioned before, the ITO resistivity decreased significantly after PECVD, hence the device possibly resulted in less heat or better current spreading at high current density, but the reasons for different EQE features remain unknown. As a result, further investigations are necessary on the droop behavior and carrier dynamics with different device dimensions and sidewall treatments.

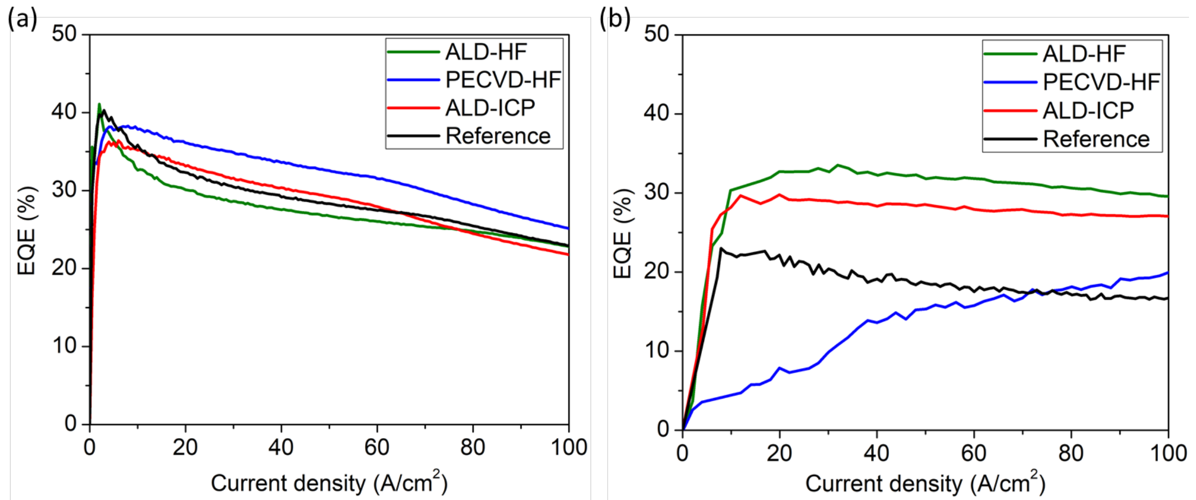

Figure 2.5. EQE characteristics of (a) 100×100 and (b) 20×20 μm² devices with different sidewall passivation methods

For the 20×20 μm² devices, disparate EQE performances were observed. The peak EQE decreased from 40% to 24% for the reference sample when shrinking the

dimensions from 100×100 to 20×20 μm^2, which corresponded to 40% reduction in EQE. Because of the lower ITO transparency in the PECVD sample, the light emission was too dim to detect by the photodetector of the integrating sphere at low current density regime. Therefore, the EQE curve of the PECVD sample provided an abnormal trend compared to the other μLEDs. In contrast, the ALD samples showed improvements that the peak EQE values are partially recovered, where the peak EQE dropped from 41% to 34% with a change of 20%, regardless of the SiO_2 removal methods. The EQE enhancement was a consequence of improved light output power due to the suppression in surface recombination and sidewall damage, yet ALD sidewall passivation alone did not mitigate the size effect, since the EQE performances retained some of its size dependence.

2.3.2 Electrical Characteristics

Besides the optical performances, the electrical features of μLEDs are addressed to reveal the benefits of ALD sidewall passivation. Figure 2.6 plots the current density-voltage characteristics of 20×20 μm^2 μLEDs with different sidewall passivation methods. From the current density-voltage measurements, the distinctive behavior between SiO_2 removal methods was identified, whereas the optical performances were weakly correlated with the SiO_2 removal methods. Additionally, it realized the effectiveness of different sidewall passivation approaches based upon forward- and reverse leakage current information.

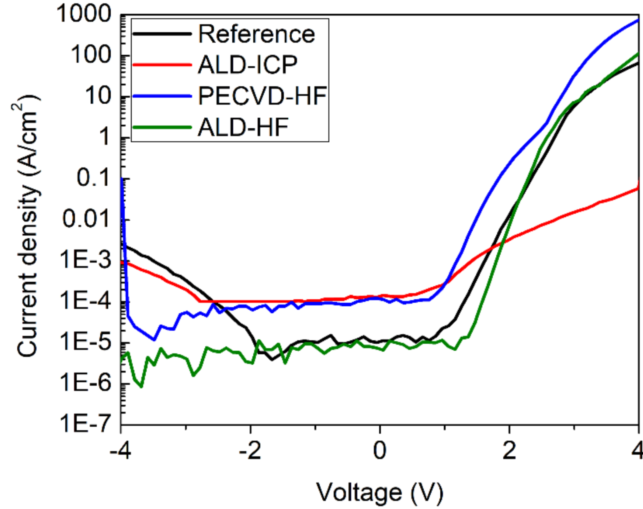

Figure 2.6. Current density-voltage characteristics from -4 to +4 V of 20×20 μm² devices with different sidewall passivation techniques

For the reference device, it resulted in significant forward- and reverse leakage, where the device started to breakdown gradually as the reverse bias increases beyond -2 V. The ALD-HF sample sustained lower forward- and reverse leakage compared to the reference device, and did not possess a breakdown feature up to -4 V. On the other hand, both the PECVD and ALD-ICP samples yielded an order of magnitude higher leakage current between 0 and -2 V, indicating more leakage paths were introduced in the devices than the reference device. In the case of ALD-ICP, SiO_2 removal using dry etching resulted in further damage in the ITO layer, and the ITO damage can be observed. Figure 2.7 shows a cross-sectional SEM image of the ITO/SiO_2 interface prepared using focus-ion beam (FIB), where the ITO layer under Al/Ni/Au metal contact was thinner than the region covered by SiO_2. The thinner ITO layer was caused by the over etch of the ICP etch during SiO_2 removal and additional damage was created, hence the ALD-ICP device performed not only with more leakage but also the most resistive device. This

highly resistive performance was noticed even with PECVD-ICP device, which provided consistency on the drawback of ICP dry etch SiO_2 removal approach. However, the PECVD-ICP devices showed dimmer and resistive optoelectrical characteristics as mentioned previously in the PECVD-HF and ALD-ICP cases, thus the PECVD-ICP data was not included in the dissertation.

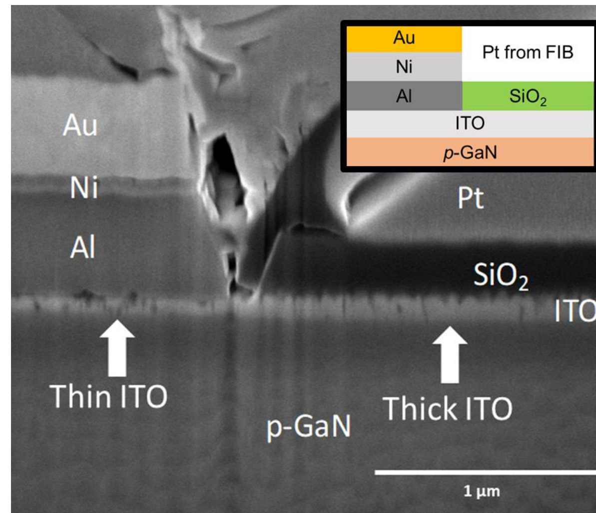

Figure 2.7. Cross-sectional SEM image of ITO layer after metal deposition. The left side of ITO layer was exposed by ICP etch to remove SiO_2 before metal deposition. The inset shows a diagram of the SEM image

ALD sidewall passivation was the most effective technique to lessen leakage current by comparing the leakage current density at -4 V among all six sizes, shown in Fig. 2.8. It should be straightforward that µLEDs without sidewall passivation yielded the highest leakage current among all device dimensions since they suffered from the influences of surface recombination and sidewall damage. For devices with PECVD sidewall passivation, this technique was sufficient to suppress leakage current for device dimensions greater than 60×60 μm^2 and leakage current increased significantly for smaller devices. The increase in

leakage current with smaller sizes indicated the impact of PECVD sidewall passivation on leakage is reduced. The leakage current density was close to that of device without sidewall passivation at 10×10 and 20×20 μm^2. Additionally, the ALD-ICP devices resulted in a similar trend as with the PECVD devices, as the damage in ITO created more leakage paths in the ALD-ICP devices. Nevertheless, the ALD-HF sample possessed the least amount of leakage current density among all device dimensions. The ability of suppressing leakage current could be related to the dielectric material quality or chemical reaction at the semiconductor interface, where ALD provided superior materials and created different surface chemistry for nucleation of dielectric materials[18,19,28]. Although ALD sidewall passivation has illustrated excellent reduction in leakage current, leakage current continues to increase with smaller devices, suggesting ALD sidewall passivation alone do not resolve the size effect and more rigorous approaches are required for future development.

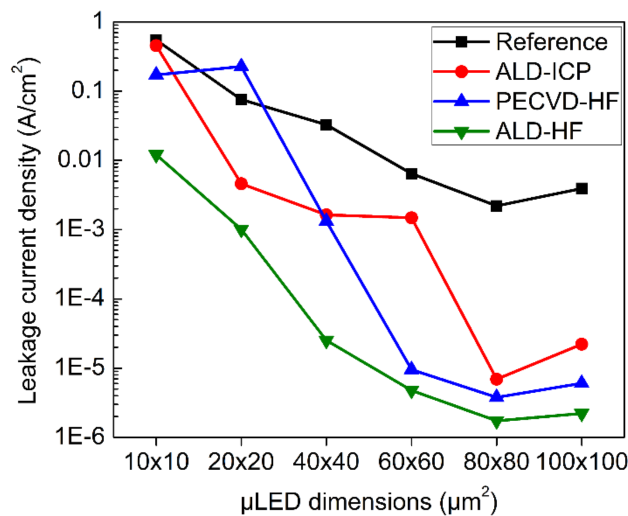

Figure 2.8. Leakage current density at -4 V for μLEDs with different sidewall passivation methods

Finally, the wall-plug efficiency (WPE) of μLEDs with different sidewall passivation methods was analyzed. WPE is defined as the ratio of optical power to electrical power, where it takes both current and voltage into the calculation. For commercial portable products, WPE is more important than EQE, because WPE gives a clearer idea about power consumption that is strongly related to battery lifetime, whereas EQE merely considers how efficient the device converts electrons to photons. In this study, the optical power was measured in the integrated sphere to collect as much light emitted from the devices as possible and the electrical power was determined from the current-voltage characteristics. Figures 2.9 (a) and (b) present the WPE of 100×100 and 20×20 μm^2 devices, respectively. Similar to Fig. 2.5, the enhancements of ALD sidewall passivation were more effective in smaller μLEDs. In the 100×100 μm^2 devices, the maximum WPE improved from 35% to 39% by employing ALD sidewall passivation and was attributed to the better current-voltage characteristics. However, the resistive feature in the ALD-ICP device caused significantly lower WPE than other devices. For the 20×20 μm^2 devices, the WPE and the EQE performances were alike, where the ALD-HF device was the most efficient among all devices.

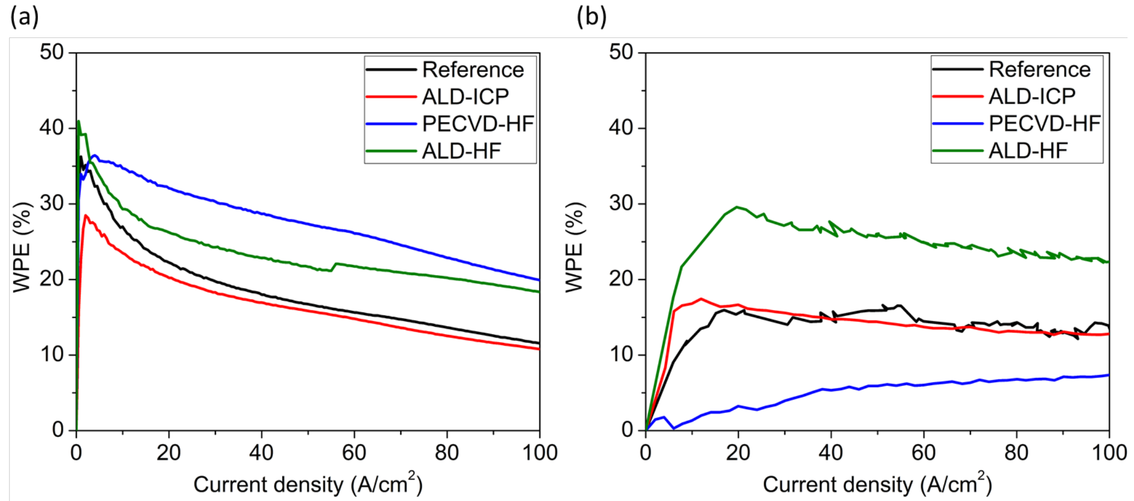

Figure 2.9. WPE performances of (a) 100×100 and (b) 20×20 μm² μLEDs with different sidewall passivation methods

2.4 Summary

In summary, the advantages of ALD sidewall passivation in μLEDs were demonstrated in terms of optical and electrical aspects. In terms of the optical properties, the light emission homogeneity and the light output power of 20×20 μm² device were improved. Additionally, devices with ALD sidewall passivation showed enhancements in current-voltage characteristics and suppression in leakage current. Compared to PECVD, a conventional sidewall passivation technique, the hydrogen radicals from PECVD reduced the optical transparency of ITO and failed to lessen leakage current in small μLEDs. Therefore, ALD sidewall passivation with proper SiO_2 removal method gained greater EQE and WPE performances than devices without sidewall passivation and with PECVD sidewall passivation.

This was the first detailed study on recovering the μLED efficiency using post-etch technique. Based upon this finding, it was confirmed that the efficiency

lost in μLEDs is attributed from surface recombination and sidewall damage, where some of the preliminary evidences were determined from the EQE curves, but more precise studies are needed. Secondly, this work addressed the success of ALD sidewall passivation and emphasized the enhancements in device performances, especially for devices smaller than 60×60 μm^2. Although ALD sidewall passivation alone did not resolve the size effect, it provided insightful direction and potential methods to mitigate the negative impacts of the size effect. Further understanding and improvements on the ALD sidewall treatments will be discussed in later chapters.

References

1. Jiang, H. X., Jin, S. X., Li, J., Shakya, J. & Lin, J. Y. III-nitride blue microdisplays. *Appl. Phys. Lett.* **78**, 1303–1305 (2001).
2. Gong, Z. *et al.* Matrix-addressable micropixellated InGaN light-emitting diodes with uniform emission and increased light output. *IEEE Trans. Electron Devices* **54**, 2650–2658 (2007).
3. McKendry, J. J. D. *et al.* High-speed visible light communications using individual pixels in a micro light-emitting diode array. *IEEE Photonics Technol. Lett.* **22**, 1346–1348 (2010).
4. Wun, J. M. *et al.* GaN-based miniaturized cyan light-emitting diodes on a patterned sapphire substrate with improved fiber coupling for very high-speed plastic optical fiber communication. *IEEE Photonics J.* **4**, 1520–1529 (2012).
5. Lingley, A. R. *et al.* A single-pixel wireless contact lens display. *J. Micromechanics Microengineering* **21**, 125014 (2011).
6. Wong, M. S., Nakamura, S. & DenBaars, S. P. Review—Progress in High Performance III-Nitride Micro-Light-Emitting Diodes. *ECS J. Solid State Sci. Technol.* **9**, 015012 (2020).
7. Tian, P. *et al.* Temperature-dependent efficiency droop of blue InGaN micro-light emitting diodes. *Appl. Phys. Lett.* **105**, 4–7 (2014).
8. Olivier, F. *et al.* Influence of size-reduction on the performances of GaN-

based micro-LEDs for display application. *J. Lumin.* **191**, 112–116 (2017).

9. Hwang, D., Mughal, A., Pynn, C. D., Nakamura, S. & DenBaars, S. P. Sustained high external quantum efficiency in ultrasmall blue III-nitride micro-LEDs. *Appl. Phys. Express* **10**, 032101 (2017).

10. Oh, J.-T. *et al.* Light output performance of red AlGaInP-based light emitting diodes with different chip geometries and structures. *Opt. Express* **26**, 11194 (2018).

11. Ding, K., Avrutin, V., Izyumskaya, N., Özgür, Ü. & Morkoç, H. Micro-LEDs, a Manufacturability Perspective. *Appl. Sci.* **9**, 1206 (2019).

12. Olivier, F., Daami, A., Licitra, C. & Templier, F. Shockley-Read-Hall and Auger non-radiative recombination in GaN based LEDs: A size effect study. *Appl. Phys. Lett.* **111**, 022104 (2017).

13. Myers, D. J. *et al.* Evidence for trap-assisted Auger recombination in MBE grown InGaN quantum wells by electron emission spectroscopy. *Appl. Phys. Lett.* **116**, (2020).

14. Kou, J. *et al.* Impact of the surface recombination on InGaN / GaN-based blue micro-light emitting diodes. *Opt. Express* **27**, 643–653 (2019).

15. Hwang, D. Epitaxial Growth, Nanofabrication, and Mass Transfer of InGaN Micro-LEDs for Displays. (2018).

16. Chen, W. *et al.* High-performance, single-pyramid micro light-emitting diode with leakage current confinement layer. *Appl. Phys. Express* **8**, 032102 (2015).

17. Yang, C.-M. *et al.* Enhancement in Light Extraction Efficiency of GaN-Based Light-Emitting Diodes Using Double Dielectric Surface Passivation. *Opt. Photonics J.* **02**, 185–192 (2012).

18. Le Maoult, C. *et al.* Analysis of InGaN surfaces after chemical treatments and atomic layer deposition of Al2O3 for µLED application. *Proc. SPIE* (2020). doi:10.1117/12.2544787

19. Dingemans, G., Van De Sanden, M. C. M. & Kessels, W. M. M. Influence of the deposition temperature on the c-Si Surface passivation by Al2 O3 films synthesized by ALD and PECVD. *Electrochem. Solid-State Lett.* **13**, (2010).

20. Wong, M. S. *et al.* High Efficiency of III-Nitride Micro-Light-Emitting Diodes by Sidewall Passivation Using Atomic Layer Deposition. *Opt. Express* **26**, 21324–21331 (2018).

21. Lee, J.-M., Huh, C., Kim, D.-J. & Park, S.-J. Dry-etch damage and its recovery in InGaN/GaN multi-quantum-well light-emitting diodes. *Semicond. Sci. Technol.* **18**, 530–534 (2003).

22. Nedy, J. *et al.* Low damage dry etch for III-nitride light emitters. *Semicond. Sci. Technol.* **30**, 85019 (2015).

23. Cao, X. A. *et al.* Electrical effects of plasma damage in p-GaN. *Appl. Phys. Lett.* **75**, 2569–2571 (1999).

24. Konoplev, S. S., Bulashevich, K. A. & Karpov, S. Y. From Large-Size to Micro-LEDs: Scaling Trends Revealed by Modeling. *Phys. Status Solidi Appl. Mater. Sci.* **215**, 1700508 (2018).

25. Son, K. S., Lim Choi, D., Nyeon Lee, H. & Geon Lee, W. The interfacial reaction between ITO and silicon nitride deposited by PECVD in fringe field switching device. *Curr. Appl. Phys.* **2**, 229–232 (2002).

26. Iveland, J., Martinelli, L., Peretti, J., Speck, J. S. & Weisbuch, C. Direct measurement of auger electrons emitted from a semiconductor light-emitting diode under electrical injection: Identification of the dominant mechanism for efficiency droop. *Phys. Rev. Lett.* **110**, 2–6 (2013).

27. Piprek, J. How to decide between competing efficiency droop models for GaN-based light-emitting diodes. *Appl. Phys. Lett.* **107**, (2015).

28. Kim, K. *et al.* Efficiency enhancement of InGaN/GaN blue light-emitting diodes with top surface deposition of AlN/Al2O3. *Nano Energy* **43**, 259–269 (2018).

3

Red µLEDs

3.1 Visual Perception on Red Emission

For full-color display applications, it is critical to consider human-orientated factors, such as color science and visual perception, because the main purpose of displays is to deliver numerous information while preserving all the color and visual details as much as possible from different devices to our visual system[1,2]. Therefore, it is important to understand the basics of the visual perception before addressing the need of long-wavelength devices.

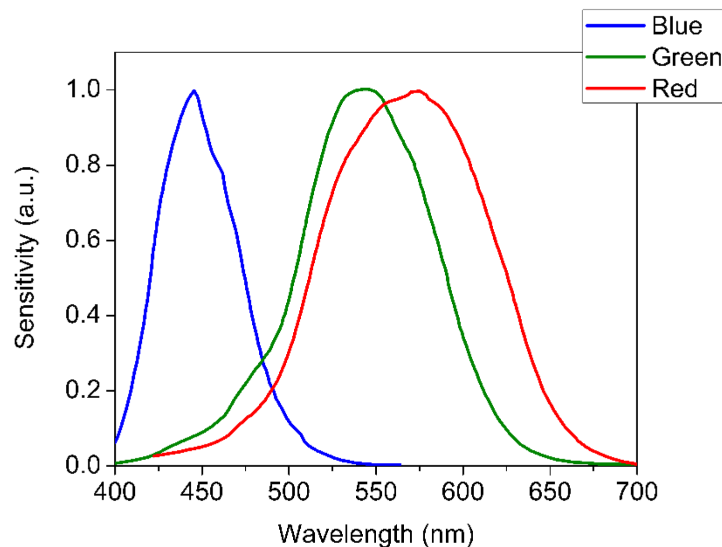

Figure 3.1. Sensitivities of the three types of cone cells

Cone cells in the retina of the eyes are responsible for the color vision under photopic condition, where the stimulus luminance level is beyond several cd/m^2, and the normalized response curves of the three types of cone cells are shown in Fig. 3.1. As shown in Fig. 3.1, the maximum sensitivities of the cone cells are about 445, 545, and 575 nm, roughly corresponding to blue, green, and yellow emissions, respectively. Among all three colors, green has the greatest sensitivity and blue yields the least response under photopic condition, and the overall sensitivity is optimal at the green-red region[2]. Although green is the most sensitive color, it has been shown that the influences due to QCSE to the optical performances of InGaN green μLEDs can be lessened from the material and system levels[3–5]. Thus, red could result in a bigger problem than the other two colors. Since the cone cells that are responsible for red emission have the highest sensitivity in the yellow color, it is crucial to have a red emitter that can provide proper color accuracy. In the next section, the differences in optical properties between AlGaInP and InGaN red μLEDs will be discussed. Because the material and device developments in AlGaInP red LEDs are much more mature than InGaN red LEDs, the electrical characteristics and absolute efficiency feature will not be included due to the early stage of InGaN red μLEDs[6,7]. There are other demonstrated methods to generate red emission, such as the use of quantum dots or nanorod structure, yet they have a variety of drawbacks and challenges that are beyond the scope of this dissertation[8–17].

3.2 Optical Comparisons Between Red μLEDs

As mentioned above, AlGaInP red LEDs with excellent optical and electrical performances have been employed extensively for various commercial applications, including traffic lights and automotive taillight[18]. On the other hand, InGaN amber/red LEDs have been demonstrated for more than twenty years, but the progress in InGaN LEDs towards red emission has been slow and more novel developments in the active region have been performed in recent years[19–21]. The optical properties of the recent InGaN red LEDs have shown similar results with the historical reports, and thus the optical properties between the two red μLEDs are valid to compare[22,23]. The peak wavelength and bandwidth are two of the most important parameters to consider for full-color display applications, because they have dramatic influences on the display quality and the color gamut.

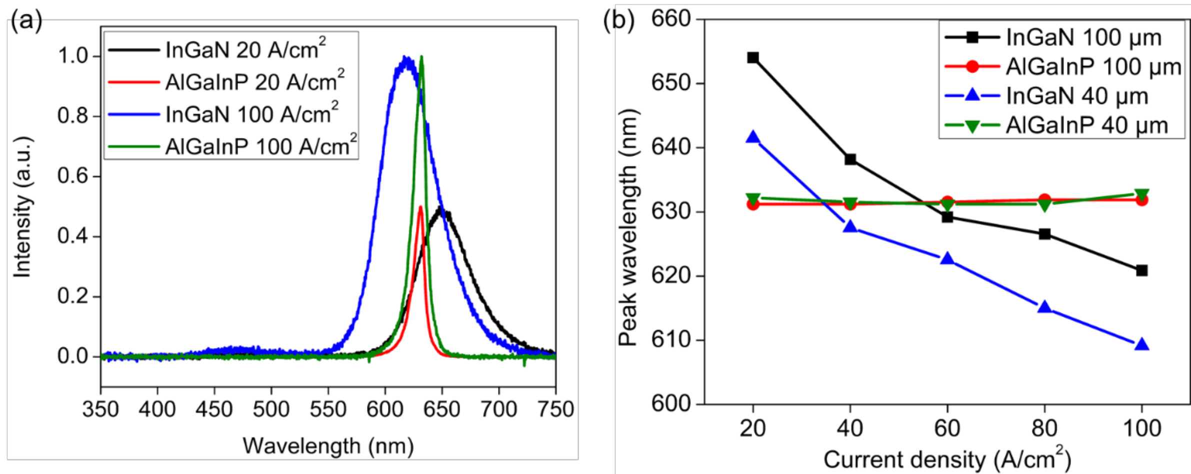

Figure 3.2. (a) The emission spectra of 100×100 μm² devices at 20 and 100 A/cm² under room temperature and (b) the dependence of peak wavelength on current density of 100×100 and 40×40 μm² devices at room temperature

The emission spectra of AlGaInP and InGaN 100×100 μm² red μLEDs at 20 and 100 A/cm² under room temperature are shown in Fig. 3.2(a), to illustrate the

differences in emission spectra between the two red emitters. For the InGaN devices, the peak wavelength exhibited a blueshift in wavelength of about 31 nm from 647 nm at 20 A/cm^2 to 616 nm at 100 A/cm^2. The large blueshift in peak wavelength was a consequence of the QCSE caused by the piezoelectric field in the active region, which is a typical issue for InGaN long-wavelength devices[24–26]. Figure 3.2(b) reveals the significance of the blueshift in wavelength of InGaN devices due to QCSE. Other than the main peak, there was an additional weak emission at about 460 nm, attributed to the possible decomposition of the InGaN at the active region[7,21,23]. Whereas in the case of AlGaInP devices, since the piezoelectric field and thus the QCSE are absent from the AlGaInP material system, the emission spectra at 20 and 100 A/cm^2 were almost identical, with a difference of 2 nm in the peak wavelength and bandwidth. The peak wavelength of the AlGaInP devices was 631 nm at 20 A/cm^2 and increased to 633 nm at 100 A/cm^2, where the slight shift in peak wavelength could be attributed to the increase in junction temperature at high current density[27]. Moreover, the peak wavelength experienced a gradual increase in peak wavelength, as shown in Fig. 3.2(b), confirming that the redshift in peak wavelength is attributed to the increase in the junction temperature due to high current injection.

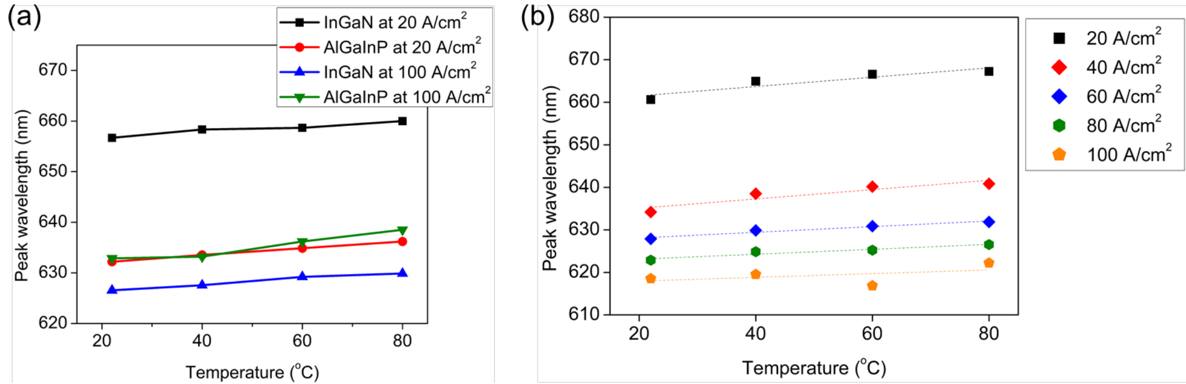

Figure 3.3. (a) The dependence of peak wavelength of 40×40 μm² AlGaInP and InGaN devices at 20 and 100 A/cm² with stage temperature and (b) the dependence of peak wavelength of 100×100 μm² InGaN devices on stage temperature at different current densities.

Because temperature can have distinguishable optical impacts to the devices, as shown in Fig. 3.2(b), the redshift in wavelength with temperature should be considered for displays, where small changes in wavelength can be easily observed. Figure 3.3(a) shows the temperature-dependent wavelength characteristics of 40×40 μm² devices, where the temperature was defined and controlled by a heated stage. Both InGaN and AlGaInP devices yielded redshift in wavelength, yet the degree of redshift was distinctive in the two devices. The redshift in wavelength is caused by bandgap shrinkage at elevated temperature[7,23,26]. The AlGaInP device resulted in higher redshift rates of 0.069 and 0.097 nm/°C at 20 and 100 A/cm², respectively, while the InGaN μLED exhibited the redshift coefficients of 0.052 and 0.060 nm/°C, and the lower redshift coefficients in InGaN devices were due to the compensation of blueshift from the QCSE. To determine the effectiveness of the blueshift compensation of the redshift behavior, the relationship between the peak wavelength and stage temperature at different current densities is shown in Fig. 3.3(b). The redshift rates were 0.110,

0.110, 0.067, 0.058, and 0.044 nm/°C at 20, 40, 60, 80, and 100 A/cm^2, respectively. The data shows that the redshift in wavelength was the greatest at low current densities and the redshift reduced gradually as the current density increases. The blueshift compensation due to the QCSE enhanced with smaller InGaN device dimensions. The results suggested that AlGaInP devices should operate at low current density, as the junction temperature would not increase significantly with lower redshift rate. In contrast, InGaN devices offers the advantage of compensation in wavelength shift because of QCSE, where the redshift rate diminished as the device operating at higher current density range. Besides the peak wavelength emission, the light output power of devices is also influenced by temperature.

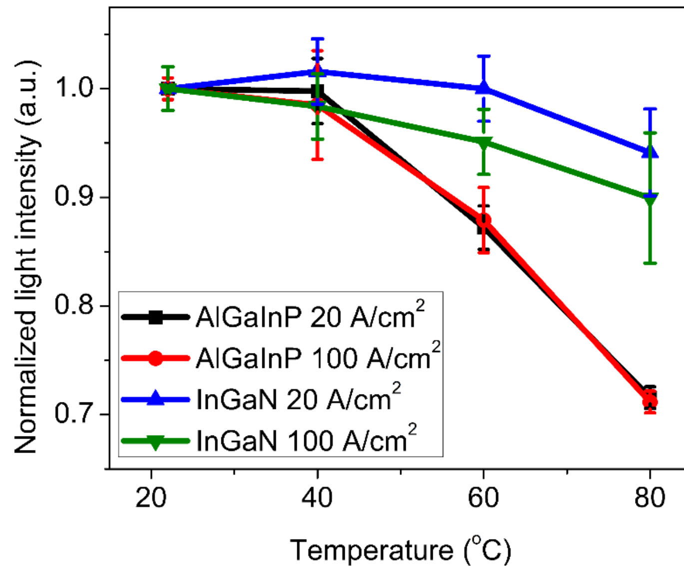

Figure 3.4. The dependence of normalized light output power of 40×40 μm^2 AlGaInP and InGaN devices at 20 and 100 A/cm^2 on stage temperature

Similar to other inorganic semiconductor devices, thermal degradation could be a major problem, especially from the reliability aspect for commercial

products. The performances of AlGaInP and InGaN devices behaved disparately under elevated temperature conditions[27]. The light output power of AlGaInP and InGaN devices with various temperatures is shown in Fig. 3.4. For the InGaN devices, they yielded great thermal stability with about 10% reduction in light output power between room temperature and 80°C, and the decrease was attributed to the thermal droop in efficiency[27,28]. In the case of AlGaInP μLEDs, they suffered more from the thermal degradation for two main factors, namely the direct-indirect (Γ-X) bandgap transition and smaller band offset, where both are related to the intrinsic AlGaInP material properties. The direct-indirect bandgap transition is caused by the change in carrier population from direct bandgap to indirect bandgap as temperature increases[18,29]. The transition leads to a reduction in radiative recombination and enhancement in non-radiative recombination. The smaller band offset in AlGaInP LEDs, compared to typical InGaN devices, yields greater carrier leakage and overflow. The combination of these two factors resulted in 30% lost in light output power at 80°C. Although the AlGaInP devices show significant drop in light output power, compared to the InGaN devices, AlGaInP red LEDs have demonstrated the highest efficiency more than 50%, yet the best efficiency of InGaN red LEDs is 3%[21,30]. Therefore, AlGaInP LEDs remain the ideal candidate for the red emitter of μLED displays. Moreover, AlGaInP LEDs have lower emission bandwidth than that of the InGaN red devices, which is another critical benefit for AlGaInP LEDs, as shown in Fig. 3.5.

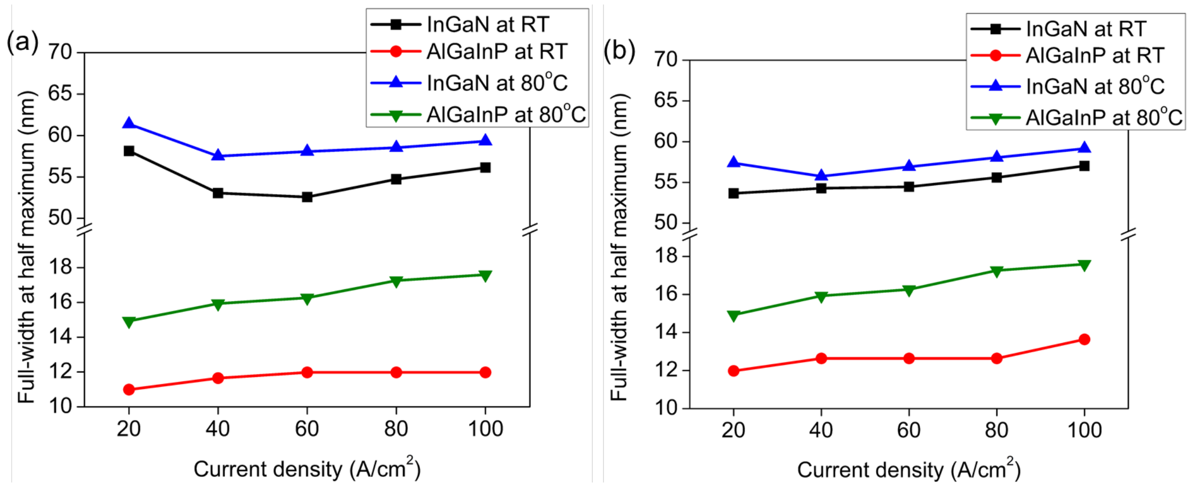

Figure 3.5. The dependence of bandwidth, or FWHM, on current density of (a) 100×100 and (b) 40×40 μm² devices at room temperature and at 80°C

The AlGaInP devices yielded narrower bandwidth than that of the InGaN devices. Additionally, the bandwidth in both devices increases with temperature. The broadening in the bandwidth was attributed to the bandgap normalization or generation of non-radiative recombination sites due to an increase in junction temperature[19,21,26]. For conventional red emitters, including OLED, LCDs, and self-emissive quantum dot LEDs, the emission bandwidth is about 30 nm[9,31]. Nevertheless, the bandwidth of AlGaInP μLEDs is lower than all commercially available red emitters, indicating the exceptional optical characteristics of AlGaInP μLEDs. The need for narrow bandwidth can be explained by using Fig. 3.6, where it shows the cone cells that are responsible for red emission and the emission spectra of InGaN and AlGaInP red μLEDs. Based upon the response curve of red cone cells, the maximum sensitivity is about 560 nm, corresponding to yellow emission. Because InGaN μLEDs have wide bandwidth, as shown in Fig. 3.5, the excitation not only covers the red emission but also includes the orange and yellow regions, and hence the perceived hue appears more towards yellow or

orange color. By the same token, AlGaInP μLEDs yield narrow bandwidth and merely excite small part of the cone cells, and thus the narrow bandwidth provides better color accuracy.

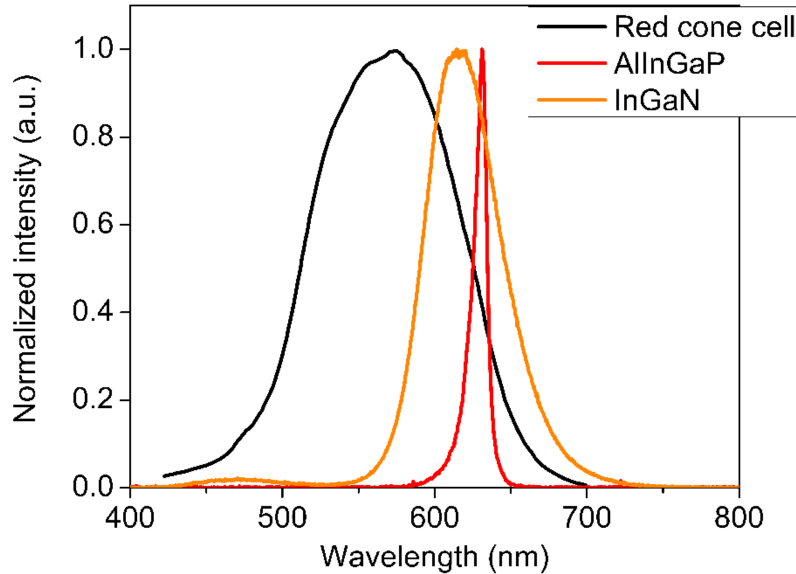

Figure 3.6. The response curve of red cone cells and emission spectra of InGaN and AlGaInP red μLEDs

3.3 AlGaInP μLEDs with ALD Sidewall Passivation

From the previous section, AlGaInP μLEDs could be applicable as the red emitter for μLED displays due to their excellent optical characteristics and the immature technology in InGaN red devices. However, the AlGaInP material system has a higher surface recombination velocity and minority diffusion length, resulting in severe drop in efficiency, which is detrimental for μLED displays[32–34]. As demonstrated before, ALD sidewall passivation is effective to suppress leakage current due to surface recombination and to enhance the light output power and efficiency. In this section, the improved performances of AlGaInP μLEDs using ALD sidewall passivation will be discussed. The enhancements in AlGaInP μLEDs

using sidewall treatments indicate that the size-dependent efficiency characteristic can be recovered, or even mitigated, by employing proper sidewall treatments.

The device design of the AlGaInP μLEDs are identical as the InGaN devices, where ITO is used as the ohmic and transparent *p*-contact. Although current spreading in the p-type layer is not a problem for the AlGaInP material system, the use of ITO is a common approach and the fabrication procedure is limited by the current lithography design. Nevertheless, the device design described here is sufficient to address the size effect of μLEDs, and further device optimizations can be performed later. Ge/Au/Ni/Au metal stacks, typically used as the *n*-contact, are used for both *n*- and *p*- metal pads. The circular transmission line measurement (CTLM) characteristics of ITO and Ge/Au/Ni/Au metal contact indicate ohmic contact behavior, as shown in Fig. 3.7(a), and a cross-sectional schematic of the AlGaInP μLEDs presents in Fig. 3.7(b).

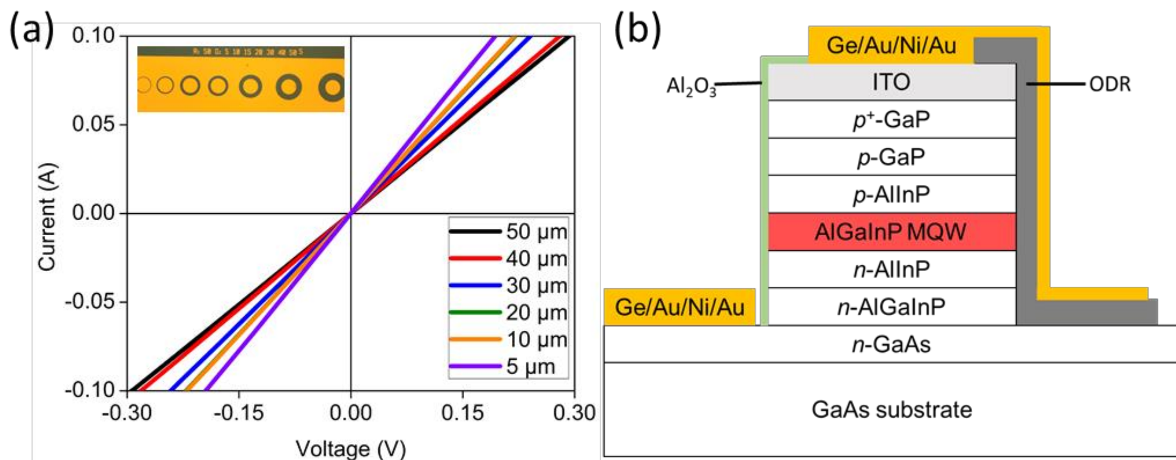

Figure 3.7. (a) The CTLM characteristics of ITO and Ge/Au/Ni/Au metal contact and (b) a cross-sectional schematic of the AlGaInP μLEDs with ALD Al_2O_3 sidewall passivation

To determine the effectiveness of ALD sidewall passivation, three sets of devices were fabricated using different fabrication processes, namely reference for devices without sidewall passivation, ALD refers to devices with ALD Al_2O_3 sidewall passivation, and ALD+N indicates devices with trimethyl aluminum (TMA)/nitrogen plasma followed by ALD Al_2O_3 sidewall passivation.

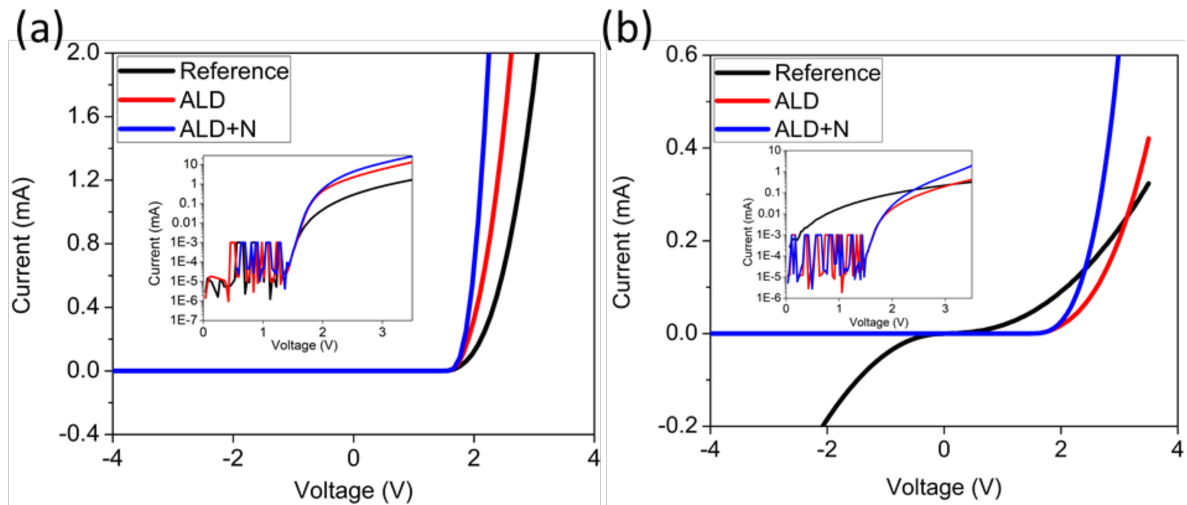

Figure 3.8. Current-voltage characteristics of 100×100 and 20×20 μm² AlGaInP μLEDs. The insets are the identical graphs in semi-log plots for better visualization

Since surface recombination is the main drawback of the AlGaInP μLEDs, the electrical performances of AlGaInP devices with different sidewall passivation are first compared. By employing ALD sidewall passivation, the devices yielded better forward current-voltage characteristics, as shown in Fig. 3.8[35]. In the case of the larger devices, the devices resulted in better turn-on performances than the device without sidewall passivation, and this could be attributed to the greater parasitic resistance at the device surface, in the form of surface defects, for devices without sidewall passivation. The devices with TMA/nitrogen plasma pretreatment offered sharper turn-on feature, or less resistive behavior, from the

forward current-voltage characteristics for both 100×100 and 20×20 μm^2 devices. There is a possible reason to account for the improved forward current-voltage characteristic with the pretreatment. The pretreatment could be a more effective method to eliminate dangling bonds and surface defects, by forming very thin layer of aluminum nitride at the surface, thus the surface parasitic resistance and traps are further reduced[36–38]. For the small devices, the device without sidewall passivation suffered greatly in leakage current for both forward- and reverse- bias, confirming the poor AlGaInP device performances as the device dimensions shrink due to surface recombination[39]. Nevertheless, leakage current was suppressed effectively by using ALD sidewall passivation, regardless of the use of TMA/nitrogen plasma pretreatment, and the forward current-voltage characteristic was enhanced further with the pretreatment.

To investigate the influences of size effect on the electrical performances, the dependences of leakage current and the ideality factor on device sizes are presented in Fig. 3.9(a) and (b), respectively. Similar to InGaN devices, leakage current increased as device dimensions shrink, yet the increase in leakage current was more rigorous than that of InGaN devices. The difference in surface recombination velocity and minority diffusion length can be accounted for the disparate leakage current characteristics in AlGaInP and InGaN devices, since AlGaInP materials have greater surface recombination velocity and minority diffusion length, the AlGaInP devices suffered more severe impacts from sidewall damage and surface recombination. The abrupt increase in leakage current

between the 60×60 and the 40×40 μm^2 devices could be due to the difference in perimeter-to-area ratio, where the 60×60 μm^2 devices have the ratio of 0.067 and the 40×40 μm^2 devices have the ratio of 0.1, and the increase in perimeter-to-area ratio could introduce more impacts due to the sidewall damage and surface recombination. Besides leakage current, the ideality factor also provides insightful information in terms of the effectiveness of ALD sidewall passivation. The ideality factor gives a sense between ideal diode and the actual device, as shown in Fig. 3.9(b), where the ideality factor is calculated from the forward current-voltage characteristics. Greater ideality factor could be attributed to leakage current generated from defects or epitaxy structure design issue, and qualitative comparisons can be made by devices fabricated from the same LED wafer[40,41]. For devices without sidewall passivation, the ideality factor increased moderately from 2 to 3.3 as the device dimensions shrink, indicating the electrical characteristics were influenced by the sidewall damage and surface recombination[39,42,43]. In contrast, the devices with ALD sidewall passivation yielded lower and nearly constant ideality factor among all device sizes, illustrating the improvements with ALD sidewall passivation.

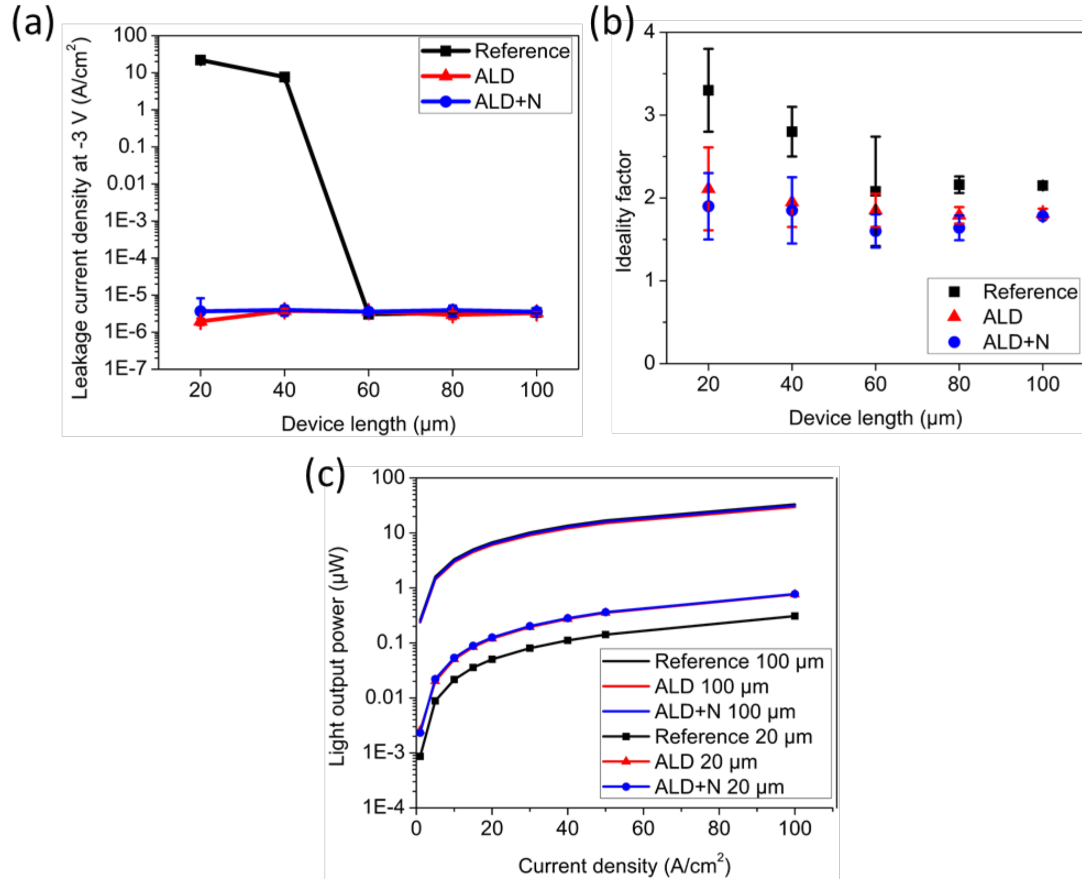

Figure 3.9. (a) The dependence of leakage current density at -3 V and (b) the ideality factor on AlGaInP device sizes with different sidewall treatments. (c) The light output characteristics of 100×100 and 20×20 μm² devices with different sidewall treatments

Moreover, the benefits of using ALD sidewall passivation not only in the electrical aspect but also in the optical perspective. Figure 3.9(c) shows the light output power features of the 100×100 and 20×20 μm² devices with different sidewall passivation techniques. The larger devices provided very similar light output power, regardless of the sidewall passivation methods, which was attributed to the trivial perimeter-to-area ratio. While the smaller devices resulted in an enhancement in light output power across all current density range for devices with ALD sidewall passivation, and the improvement was more than 150% at 100 A/cm². The improvement in light output power was a consequence of the increase

in light extraction efficiency and the reduction in surface defects and dangling bonds[35,44].

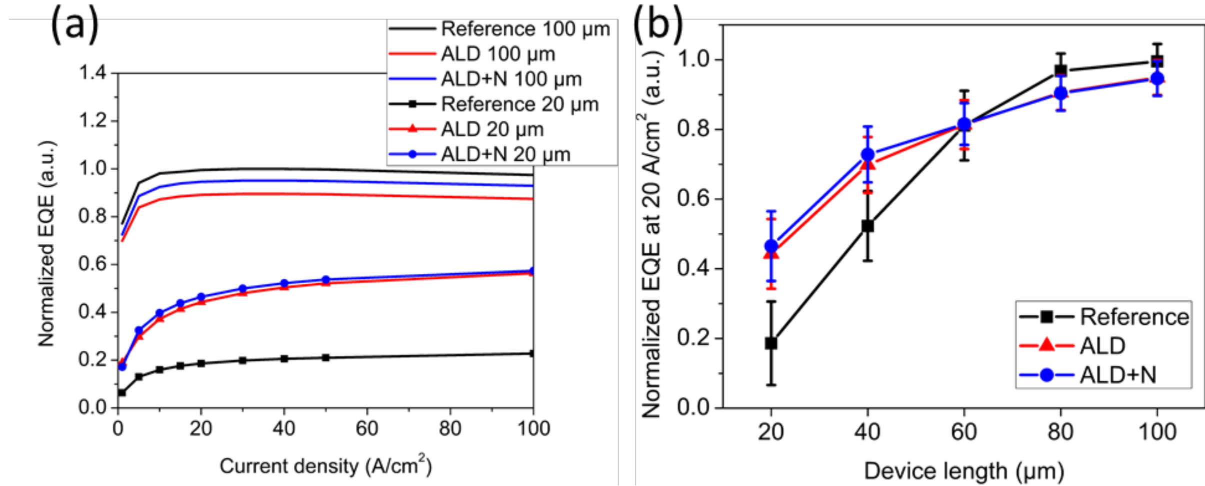

Figure 3.10. (a) The dependence of EQE on current density and (b) the size-dependent normalized EQE at 20 A/cm^2 with different sidewall passivation techniques

Because ALD sidewall passivation has demonstrated to be effective to boost the optoelectrical performances of AlGaInP μLEDs, it is also important to show the effectiveness in EQE, as shown in Fig. 3.10. As in the case of InGaN devices, larger AlGaInP μLEDs did not experience huge effect on the EQE characteristic and they showed similar EQE curves within 10% deviation possibly caused by fabrication and/or growth variations. However, the advantage of ALD sidewall passivation can be distinguished from the EQE of the smaller devices, as shown in Fig. 3.10. The drop in EQE was 80% from decreasing the device size from 100×100 to 20×20 μm^2 for devices without sidewall passivation, while the devices with ALD sidewall passivation exhibited partial recovery in EQE to about 50%. By comparing all sizes from 100×100 to 20×20 μm^2, the reduction in EQE was significant for devices without sidewall passivation, especially for devices below

60×60 μm^2. The severe drop in EQE was expected based upon the high surface recombination velocity and minority carrier diffusion length, leading to the high non-radiative recombination and thus detrimental EQE drop as size decreases. The use of ALD sidewall passivation suppressed the effects of surface defects and lessened the decrease in EQE. Hence, the overall drop in EQE was about 50%, which was not as critical as in the devices without sidewall passivation, as shown in Fig. 3.10(b). With further optimizations on the sidewall treatment techniques, the EQE performance can be greatly enhanced and size-independent EQE characteristic can be achieved in AlGaInP μLEDs, as presented in Fig. 3.11. The results shown in Fig. 3.11(a) achieved size-independent EQE performance at 100 A/cm^2 while the EQE at low current density range was still less than that of the larger devices. There are two possible reasons for this observation. First, the normalized EQE was calculated based on light collected by placing a photodetector vertically on top of the device, where sidewall emission was unable to collect. Secondly, the sidewall treatment was not optimized, which was very likely, considering the sidewall treatment for AlGaInP μLEDs was realized very recently in a very limited amount of time. Therefore, true size-independent EQE characteristic in AlGaInP μLEDs can be achieved with additional optimizations in the sidewall treatment method.

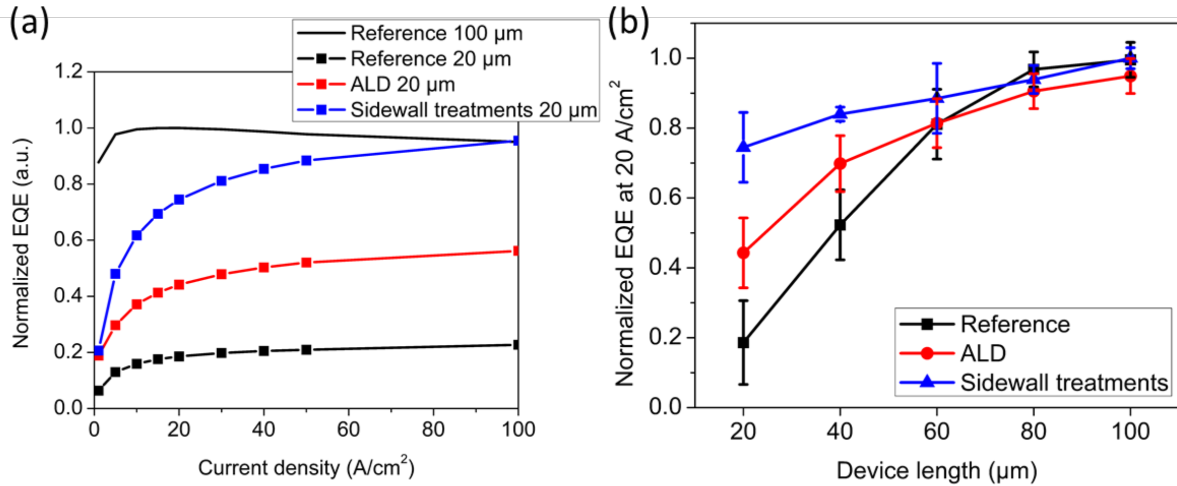

Figure 3.11. (a) The dependence of EQE on current density and (b) the size-dependent normalized EQE at 20 A/cm² with nearly optimized sidewall treatment techniques

3.4 Summary

In conclusion, due to the mature developments in AlGaInP material and device aspects, AlGaInP red µLEDs have outstanding optical properties than the state-of-the-art InGaN red devices and other commercially available red emitters, such as OLEDs and quantum dots. However, due to the high surface recombination velocity and minority diffusion length in AlGaInP material system, AlGaInP devices suffered from detrimental decrease in EQE as device dimensions shrink, where the EQE drop was more even severe compared to the case of InGaN devices. Because ALD sidewall passivation has been demonstrated to enhance the optoelectrical performances of InGaN µLEDs, the improvements of ALD sidewall passivation on AlGaInP devices were determined. Both the electrical and optical performances, in terms of current-voltage and light output power characteristics, were improved remarkably, suggesting ALD sidewall passivation is beneficial to the AlGaInP device performances. Furthermore, the drop in EQE was lessened by employing ALD sidewall passivation. The results indicated that size-independent

EQE performance can be realized in AlGaInP μLEDs by using proper sidewall treatments, and preliminary data is shown as evidence to support this hypothesis.

Reference

1. Huang, Y., Hsiang, E., Deng, M. & Wu, S. Mini-LED , Micro-LED and OLED displays : present status and future perspectives. *Light Sci. Appl.* (2020). doi:10.1038/s41377-020-0341-9
2. Hunt, R. W. G. & Pointer, M. R. Measuring Colour. *John Wiley Sons* (2011).
3. Tamaki, M. *et al.* A 3 . 9-inch LTPS TFT Full Color MicroLED Display with Novel Driving and Reflector Cavity Process. *SID 2020 Dig.* 111–114 (2020).
4. Zhao, Y. *et al.* Green Semipolar (20-2-1) InGaN Light-Emitting Diodes with Small Wavelength Shift and Narrow Spectral Linewidth. *Appl. Phys. Express* **6**, 062102 (2013).
5. Gou, F. *et al.* High-efficiency micro-LED displays with indistinguishable color shift. *Proc. SPIE* (2020). doi:10.1117/12.2543223
6. Pasayat, S. S. *et al.* Color-tunable < 10 μ m square InGaN micro- LEDs on compliant GaN-on-porous-GaN. *Appl. Phys. Lett.* **117**, 061105 (2020).
7. Zhuang, Z., Iida, D. & Ohkawa, K. Effects of size on the electrical and optical properties of InGaN-based red light-emitting diodes. *Appl. Phys. Lett* **116**, 173501 (2020).
8. Liu, Y., Wu, B., Wang, Y.-C., Tanyi, E. K. & Cheng, L.-J. Red emission carbon dots for microLED application. *Proc. SPIE* 14 (2019). doi:10.1117/12.2529778
9. Won, Y.-H. *et al.* Highly efficient and stable InP/ZnSe/ZnS quantum dot light-emitting diodes. *Nature* **575**, 634–638 (2019).
10. Leitão, M. F. *et al.* Pump-power-dependence of a CsPbBr 3 -in-Cs 4 PbBr 6 quantum dot color converter. *Opt. Mater. Express* **9**, 3504 (2019).
11. Wang, L. *et al.* Blue Quantum Dot Light-Emitting Diodes with High Electroluminescent Efficiency. *ACS Appl. Mater. Interfaces* **9**, 38755–38760 (2017).
12. Pickett, M. L., Gresty, N. C. & Hines, M. A. Heavy Metal-Free Quantum Dots Making Inroads for Consumer Applications. *SID Symp. Dig. Tech. Pap.* **47**, 425–427 (2016).

13. Pickett, N. L., Harris, J. A. & Gresty, N. C. Heavy Metal-Free Quantum Dots for Display Applications. *SID Symp. Dig. Tech. Pap.* **46**, 168–169 (2015).

14. Dai, X. *et al.* Solution-processed, high-performance light-emitting diodes based on quantum dots. *Nature* **515**, 96–99 (2014).

15. Zhu, R., Luo, Z. & Wu, S.-T. Light extraction analysis and enhancement in a quantum dot light emitting diode. *Opt. Express* **22**, A1783 (2014).

16. Robin, Y. *et al.* Insight into the performance of multi-color InGaN/GaN nanorod light emitting diodes. *Sci. Rep.* **8**, 1–8 (2018).

17. Wong, M. S., Nakamura, S. & DenBaars, S. P. Review—Progress in High Performance III-Nitride Micro-Light-Emitting Diodes. *ECS J. Solid State Sci. Technol.* **9**, 015012 (2020).

18. Kish, F. A. & Fletcher, R. M. Chapter 5 AlGalnP Light-Emitting Diodes. *Semicond. Semimetals* **48**, (1997).

19. Mukai, T., Yamada, M. & Nakamura, S. Characteristics of InGaN-Based UV/Blue/Green/Amber/Red Light-Emitting Diodes. *Jpn. J. Appl. Phys.* **38**, 3976–3981 (1999).

20. Seo, Y. G. *et al.* Orange a-plane InGaN/GaN light-emitting diodes grown on r-plane sapphire substrates. *Opt. Express* **19**, 12919 (2011).

21. Hwang, J.-I., Hashimoto, R., Saito, S. & Nunoue, S. Development of InGaN-based red LED grown on (0001) polar surface. *Appl. Phys. Express* **7**, 071003 (2014).

22. Robin, Y. *et al.* What is red? on the chromaticity of orange-red InGaN/GaN based LEDs. *J. Appl. Phys.* **124**, 183102 (2018).

23. Iida, D. *et al.* 633-nm InGaN-based red LEDs grown on thick underlying GaN layers with reduced in-plane residual stress. *Appl. Phys. Lett.* **116**, 1–5 (2020).

24. Alhassan, A. I. *et al.* Development of high performance green c- plane III-nitride light-emitting diodes. *Opt. Express* **26**, 5591–5601 (2018).

25. Li, P. P. *et al.* Very high external quantum efficiency and wall-plug efficiency 527 nm InGaN green LEDs by MOCVD. *Opt. Express* **26**, 33108 (2018).

26. Iida, D., Zhuang, Z., Kirilenko, P., Velazquez-Rizo, M. & Ohkawa, K. Demonstration of low forward voltage InGaN-based red LEDs. *Appl. Phys. Express* **13**, 031001 (2020).

27. Oh, C.-H., Shim, J.-I. & Shin, D.-S. Current- and temperature-dependent efficiency droops in InGaN-based blue and AlGaInP-based red light-

emitting diodes. *Jpn. J. Appl. Phys.* **58**, SCCC08 (2019).

28. Oh, S. H. *et al.* Semipolar III-nitride light-emitting diodes with negligible efficiency droop up to ~1 W. *Appl. Phys. Express* **9**, 7–10 (2016).

29. Schubert, E. F. Light-Emitting Diodes. *Cambridge Univ. Press* (2010). doi:10.1017/cbo9780511790546.013

30. Krames, M. R. *et al.* High-power truncated-inverted-pyramid (AlxGa1-x)0.5In0.5P/GaP light-emitting diodes exhibiting >50% external quantum efficiency. *Appl. Phys. Lett.* **75**, 2365–2367 (1999).

31. Chen, H.-W., Lee, J.-H., Lin, B.-Y., Chen, S. & Wu, S.-T. Liquid crystal display and organic light-emitting diode display: present status and future perspectives. *Light Sci. Appl.* **7**, 17168 (2018).

32. Boroditsky, M. *et al.* Surface recombination measurements on III-V candidate materials for nanostructure light-emitting diodes. *J. Appl. Phys.* **87**, 3497–3504 (2000).

33. Royo, P., Stanley, R. P., Ilegems, M., Streubel, K. & Gulden, K. H. Experimental determination of the internal quantum efficiency of AlGaInP microcavity light-emitting diodes. *J. Appl. Phys.* **91**, 2563–2568 (2002).

34. Bulashevich, K. A. & Karpov, S. Y. Impact of surface recombination on efficiency of III-nitride light-emitting diodes. *Phys. Status Solidi - Rapid Res. Lett.* **10**, 480–484 (2016).

35. Wong, M. S. *et al.* Improved performance of AlGaInP red micro-light-emitting diodes with sidewall treatments. *Opt. Express* **28**, 5787 (2020).

36. Losurdo, M., Capezzuto, P., Bruno, G., Perna, G. & Capozzi, V. N2-H2 remote plasma nitridation for GaAs surface passivation. *Appl. Phys. Lett.* **81**, 16–18 (2002).

37. Chobpattana, V., Mates, T. E., Mitchell, W. J., Zhang, J. Y. & Stemmer, S. Influence of plasma-based in-situ surface cleaning procedures on HfO 2/In0.53Ga0.47As gate stack properties. *J. Appl. Phys.* **114**, 0–4 (2013).

38. Chobpattana, V. *et al.* Nitrogen-passivated dielectric/InGaAs interfaces with sub-nm equivalent oxide thickness and low interface trap densities. *Appl. Phys. Lett.* **102**, 100–103 (2013).

39. Oh, J.-T. *et al.* Light output performance of red AlGaInP-based light emitting diodes with different chip geometries and structures. *Opt. Express* **26**, 11194 (2018).

40. Lee, S. W. *et al.* Origin of forward leakage current in GaN-based light-emitting devices. *Appl. Phys. Lett.* **89**, 132117 (2006).

41. Zhu, D. *et al.* The origin of the high diode-ideality factors in GaInN/GaN

multiple quantum well light-emitting diodes. *Appl. Phys. Lett.* **94**, 1–4 (2009).

42. Yang, H. S., Han, S. Y., Baik, K. H., Pearton, S. J. & Ren, F. Effect of inductively coupled plasma damage on performance of GaN-InGaN multiquantum-well light-emitting diodes. *Appl. Phys. Lett.* **86**, 1–3 (2005).

43. Ping, A. T. *et al.* Characterization of reactive ion etching-induced damage to n-GaN surfaces using schottky diodes. *J. Electron. Mater.* **26**, 266–271 (1997).

44. Jeng, M. J., Chang, Y. H., Chang, L. B., Huang, M. J. & Lin, J. C. Effective suppression of surface recombination of AlGaInP light-emitting diodes by sulfur passivation. *Japanese J. Appl. Physics, Part 2 Lett.* **46**, (2007).

4

µLEDs with chemical and sidewall treatments

4.1 µLEDs with Improved Performances

In previous chapters, the optoelectrical benefits of ALD sidewall passivation on AlGaInP and InGaN µLEDs have been addressed thoroughly, and it should be clear that µLEDs require more sophisticated sidewall passivation techniques than conventional LEDs to suppress the size effect[1,2]. Yet, the findings suggest that ALD sidewall passivation enhances µLED characteristics by suppressing sidewall damage and surface recombination, and hence sidewall damage remains in the devices and the size effect is lessened, not eliminated. There are multiple alternative methods to attenuate the influences of sidewall damage, including low-power etch and selective-area growth, and these approaches have demonstrated decent results[3–5]. However, these approaches take advantage of specific parameters, either in etching power or in growth, to achieve the desired performances. Therefore, the repeatability and accessibility for mass production are constrained to certain etching tools or growth conditions. In this

chapter, a method that consists of chemical and ALD sidewall treatments is introduced. More importantly, the size-independent characteristics are observed on μLEDs with chemical and sidewall treatments from 100×100 to 10×10 μm^2, which is the first demonstration of μLEDs with size-independent peak EQE feature. The idea of this technique is to provide a simple and universal method to mitigate the size effect, while maintaining high degree of tunability and flexibility for fabrication process design and other perspectives, and thus gives reliable device results regardless of the individual etching variables. The technique of chemical and sidewall treatments should be material-versatile, meaning the principle of this technique works not only in visible InGaN μLEDs but also in red AlGaInP and deep-UV AlGaN μLEDs. This chapter will emphasize the effects and disclose the details of chemical and sidewall treatments on InGaN μLEDs.

4.2 LEDs with Chemical Treatments

In the search of damage removal methods in LEDs, the uses of wet chemical treatments, including KOH, phosphoric acid (H_3PO_4), and ammonium sulfide ($(NH_4)_2S$), have been reported in the literature. Furthermore, the mechanisms of various wet chemical treatment techniques have been studied extensively, and the investigations of the effects using chemical treatments on LED performances have also been reported[6–10]. There are two types of chemical treatments for passivation. One terminates surface recombination by forming stronger bonds with Ga atoms (leading to larger bandgap) at the surfaces, and $(NH_4)_2S$ and other sulfur-based containing chemicals are passivating the III-V and III-nitride semiconductor

surface in this route. On the other hand, the other class of chemical treatment relies on the oxidation of GaN into its oxide form (Ga_2O_3) and the resulting oxide is dissolved in the solution. Most acidic and basic chemicals follow the oxidation mechanism, and photoelectrochemical (PEC) etching is one of the examples that utilizes the oxidation mechanism of GaN. Unlike the sulfur-based chemical treatment where it is a self-limiting reaction at the surface, the oxidation path may sound like to continue forever without stopping. Although this is the general concept of PEC etching for GaN liftoff, there are multiple factors that can be used to control the selectivity of oxidation, such as crystallographic planes[9]. In this chapter, KOH is the main chemical used to show the enhancements of chemical treatment. The effects of H_3PO_4 and $(NH_4)_2S$ are determined preliminarily, but their overall impacts on device are not explored, because the current μLED fabrication process is unable to adopt these two chemicals. More information about monitoring the KOH chemical treatment and the choice of chemicals will be addressed later.

After understanding the general mechanisms of chemical treatments, it is critical to identify the improvements using chemical treatments in conventional LEDs. For devices with chemical treatments, the forward- and reverse leakage current decrease significantly compared to devices without chemical treatments[7,11]. The reduction in leakage current is attributed to the removal of sidewall damage because of plasma bombardment[12–14]. Additionally, due to the etching nature of KOH, *m*-plane facet formation at the sidewalls is observed after

chemical treatment, where the overall sidewall profile can be vertically smooth or with facet depending on the treatment conditions[9]. The *m*-plane facet at the sidewalls could potentially be used to increase the light extraction efficiency of the device, although experimental data on the improvement with sidewall faceting has not been studied extensively.

4.3 Devices with Chemical and Sidewall Treatments

This section will first examine the capability of wet chemicals to integrate into the current μLED design and the issues with different chemicals, namely KOH and H_3PO_4, in the current process design. This part of the discussion is intended to help developing future μLED designs by revealing all the potential and known problems. After that, the effects of the combination of chemical and sidewall treatments will be presented. Because strong acidic and basic solutions are used for chemical treatment, it is ideal to perform the treatment after dry etching and before any dielectric or metal depositions to avoid degradation under extreme pH environment. As a result, the chemical treatment presented here was carried out after ITO and GaN etch and before IBD in the μLED process flow.

4.3.1 Influences of Different Chemicals

Even though GaN is chemically robust to almost all chemicals, ITO has already deposited on the *p*-GaN surface before the chemical treatment step, thus it is crucial to account for the chemical stability of ITO with different chemicals. The main reason that H_3PO_4 and $(NH_4)_2S$ did not incorporate into device analysis

is that both chemicals react with ITO, and the current fabrication process is not suitable for the use of H_3PO_4 and $(NH_4)_2S$. H_3PO_4 etched ITO rapidly and the lateral etch rate was significant, even if a SiO_2 protecting layer was used to cover the ITO layer. For example, 300 nm of sputter SiO_2 was deposited on top of 110 nm of ITO prior treating with H_3PO_4, and the ITO layer was removed after 10 minutes of treatment time. While $(NH_4)_2S$ did not etch ITO, it altered the optical appearance of ITO from blueish to yellowish color after the treatment depending on the treatment conditions. Hence, KOH or other basic derivatives was the only option with the current process. In fact, KOH roughened the ITO layer and could eventually remove the ITO layer. The reaction between ITO and KOH was slow and almost negligible at room temperature and the rate increased with temperature. Increase in series resistance and ITO surface roughness were the main drawbacks for over-exposing ITO to KOH, as shown in Fig. 4.1. The squared features were the device structures after mesa etch, where the ITO was located. As seen in Fig. 4.1, the ITO was darker, indicating a rougher surface after KOH treatment.

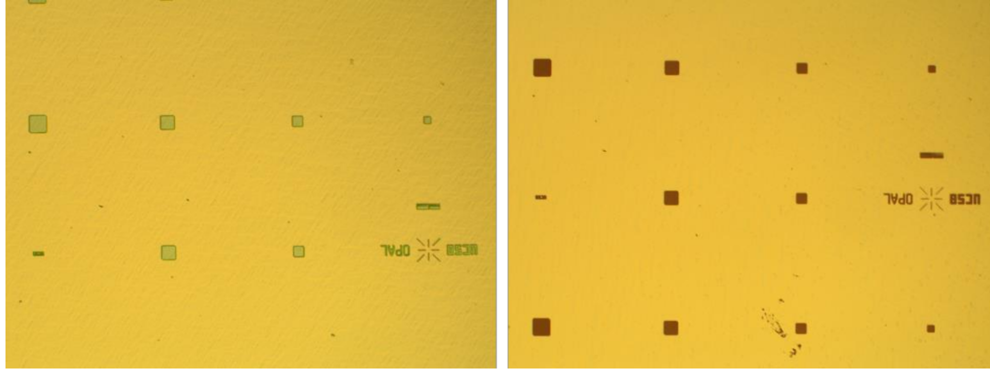

Figure 4.1. Optical micrographs before (left) and after (right) KOH treatment performed at 80°C for 40 minutes. This KOH condition was first used as a testing condition. The ITO should look identical before and after KOH treatment at room temperature for 40 minutes.

Despite of the disadvantages in process integration with ITO, there are several benefits by employing chemical treatment. First, facet sidewall profile can be realized by using KOH chemical treatment. The sidewall profile can be modified remarkably by using different chemical treatment parameters, including the choice of chemical, concentration, time, and temperature. Figure 4.2 shows the sidewall profiles of InGaN μLEDs with four chemical treatment conditions.

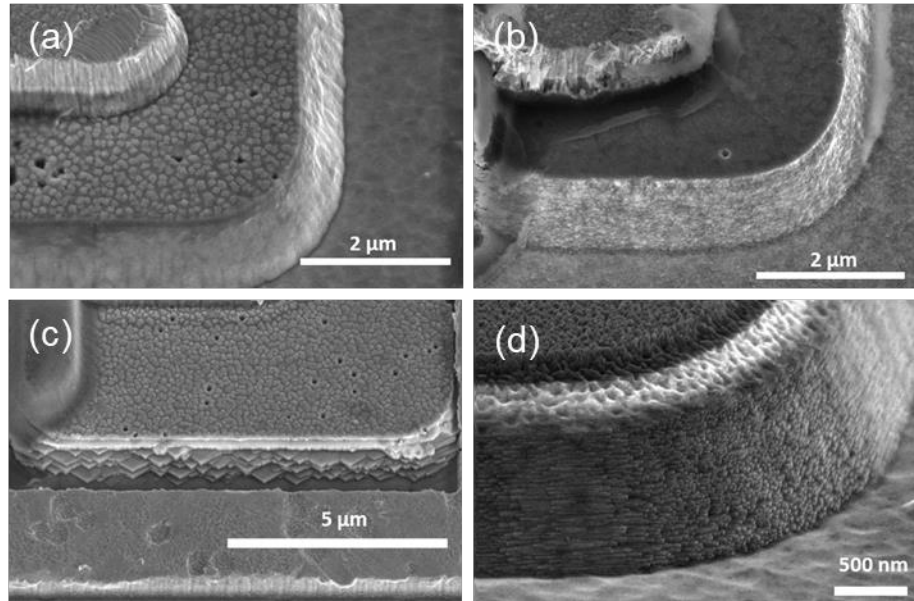

Figure 4.2. SEM images of sidewall profiles with different chemical treatment conditions: no chemical treatment (a), with H_3PO_4 for 10 minutes at room temperature (b), and KOH for 60 (c) and 40 (d) minutes at room temperature.

From Fig. 4.2, the impacts of each chemical treatment to sidewall profile should be obvious. Figure 4.2(a) presents the sidewall profile after $SiCl_4$ reactive ion etch (RIE) and without chemical treatment[15]. The resulting sidewall surface was rough with a sloped angle about 60-70° due to the physical bombardment of the etch, and all sidewall surfaces were the same before chemical treatments. Figure 4.2(b) illustrates the sidewall profile with H_3PO_4 treatment. The sidewall profile with H_3PO_4 treatment resulted in smoother surface while maintaining the identical tilted sidewall profile as in the case without chemical treatment. This means H_3PO_4 treatment preserved the geometric shape of the device and could be advantageous for devices with curved sidewall or other sidewall designs for light directionality purpose[16]. On the other hand, KOH treatment yielded sidewalls in various facet dimensions, ranging from micron- to nanoscale, by modulating the

treatment time. The facet formation has been observed and identified as *m*-plane facet, and more rigorous *m*-plane facet formation with larger facet feature can be achieved by increasing the treatment time or using other conditions[9,17]. The *m*-plane facet sidewall can be utilized to enhance the overall light extraction efficiency if desired, since light emitted from the active region is easier to escape from the device with the randomly textured sidewalls. Figure 4.3 shows the light output power-current density characteristics of devices with and without KOH chemical treatment.

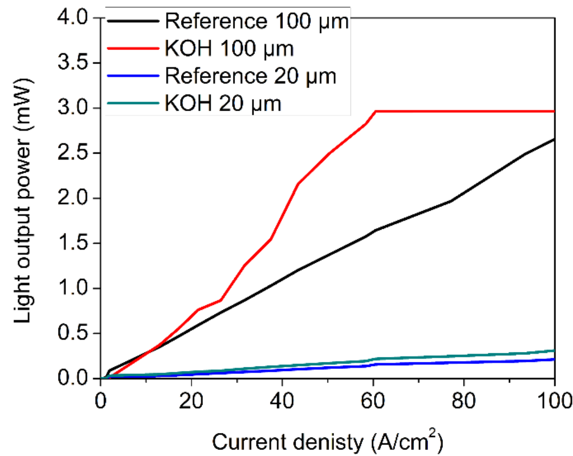

Figure 4.3. On-wafer light output power-current density performance of μLEDs with and without KOH treatment. The 100×100 μm² device reached the photodetector limit at about 60 A/cm². Reference indicates devices without chemical treatment.

As shown in Fig. 4.3, the enhancement in light output power was substantial in the 100×100 and 20×20 μm² devices. The better performance could be attributed to the improvement in light extraction efficiency caused by the *m*-plane facet sidewall or better IQE due to the removal of sidewall damage. The creation of the *m*-plane facet sidewall can be explained by the oxidation mechanism of GaN in KOH solution. For KOH chemical treatment, the etch rate

in nonpolar planes is an order of magnitude slower than that in polar *c*-plane, hence *m*-plane facet is thermodynamically favorable under KOH chemical treatment. Additionally, the oxidation mechanism is assisted by hole carrier generation and associated with thermodynamic redox potential, which the nonradiative recombination sites caused by sidewall damage are expected to have higher energy than equilibrium and with excess carriers[6,9]. Therefore, KOH chemical treatment is believed to remove nonradiative recombination sites created by dry etching while providing the unique *m*-plane facet sidewall characteristic. Another note, some reports indicated that the use of chemical treatment would enlarge pits formation on the GaN surface because of etching in the semi-polar planes[17]. This phenomenon is possible depending on the crystal quality and the treatment temperature, where the etch rate is more extreme with high dislocation material at elevated temperatures. Although the enlargement in pits was not observed at room temperature, surface smoothening after Cl_2 etching was noticed. Grassing is a common problem after RIE using Cl_2 as the etchant gas, instead of using $SiCl_4$, and it will result in highly roughened *n*-GaN surface. The use of KOH at 80°C would eliminate the grassing issue. This subsection addresses the treatment mechanism and the reason for choosing KOH, and the device performances with chemical treatment will be presented in the next subsection.

4.3.2 μLEDs with chemical treatment

The comprehensive investigations on the major effects of chemical treatment on GaN have been discussed, and this subsection will demonstrate the

device performances when incorporating chemical treatment. Figure 4.4 shows the EL images at 1 A/cm^2 of μLEDs with different chemical treatments.

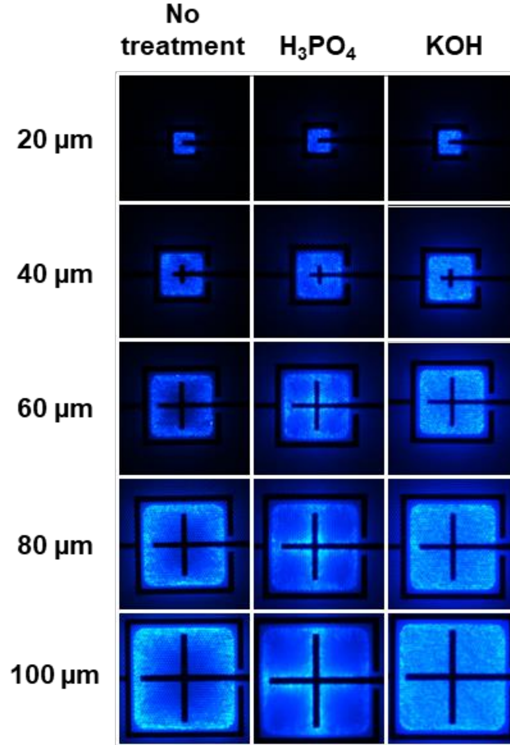

Figure 4.4. EL images of μLEDs with different chemical treatments at 1 A/cm^2

The devices without chemical treatment yielded similar EL behavior as the reference devices reported in chapter 2, where light emission was brighter at the edges for larger devices and homogenously dimmer emission for smaller devices. For the devices with H_3PO_4 treatment, current crowding issue was observed for devices greater than 40×40 μm^2. Since the area surrounding the metal contacts was brighter in larger devices, it suggested that current was not uniformly spread across the whole device and the current crowding was due to the resistive contact layer. This was attributed to the ITO etch with H_3PO_4, where the current spreading ability was dramatically reduced after the etch. This light emission

observation also verified current crowding is a problem for larger devices and current spreading is more uniform in smaller devices[18]. In contrast, the EL profiles with KOH treatment resulted in homogeneous light emission. This revealed KOH chemical treatment recovers sidewall damage from dry etching.

For the electrical characteristics, devices with chemical treatments showed lower forward leakage current than devices without chemical treatments, as illustrated in Fig. 4.5.

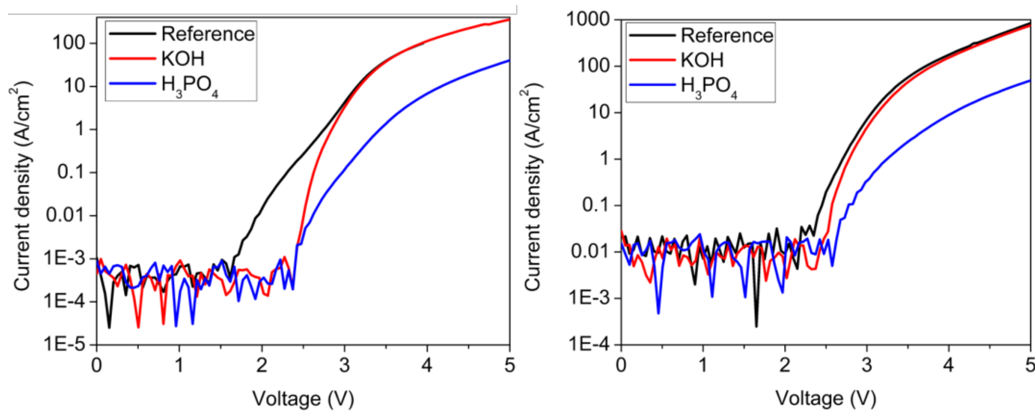

Figure 4.5. Forward current density-voltage characteristics of 100×100 μm² (left) and 20×20 μm² (right) devices with different chemical treatments.

For the 100×100 and 20×20 μm² devices, the devices without chemical treatment gained high forward leakage current compared to the devices with KOH or H_3PO_4 chemical treatments. This demonstrated chemical treatments are effective to mitigate leakage current generated by sidewall damage[7]. Nevertheless, the negative influence of chemical treatment can also be exemplified from Fig. 4.5. As mentioned previously, the primary concern of employing chemical treatment was the reaction to ITO that would lead to resistive device characteristic, and the device performance with H_3PO_4 chemical treatment was considered as a strong

evidence. Both KOH and H_3PO_4 chemical treatments were sufficient to greatly suppress leakage current, yet the achievable current densities at identical applied voltage from the two sets of devices provided distinctive feature that devices with H_3PO_4 treatment are outstandingly more resistive than the devices with KOH treatment. The excessive resistance penalty came from the faster ITO etch rate in H_3PO_4 than that in KOH. However, if ITO or other current spreading layers are not used, H_3PO_4 could serve as an alternative for replacing KOH, especially in the case of high Al content III-nitride materials for deep UV LEDs[6].

4.3.3 μLEDs with chemical treatment and ALD sidewall passivation

As discussed in chapter 2, ALD dielectric sidewall passivation effectively diminished the size effect by suppressing surface recombination and sidewall damage, and μLEDs with ALD sidewall passivation yielded exceptional device performances[1,2,19–21]. The combination of chemical treatment and ALD sidewall passivation should minimize the size effect and reduce the size-dependent efficiency characteristic due to sidewall damage, since chemical treatment removes sidewall defects and ALD sidewall passivation mitigates the influences of surface recombination[19,22]. This subsection will address the device performances with chemical and ALD sidewall treatments.

Depending on the facet dimensions, the formation of *m*-plane facet sidewall during KOH chemical treatment could offer greater light output power due to better light extraction efficiency as shown in Fig. 4.3, thus it is important to determine the sidewall profile to ensure the light extraction efficiency is similar

for fair comparison. Figures 4.6(a) and (b) present the sidewall profiles of the devices without and with chemical treatment discussed in this subsection, respectively.

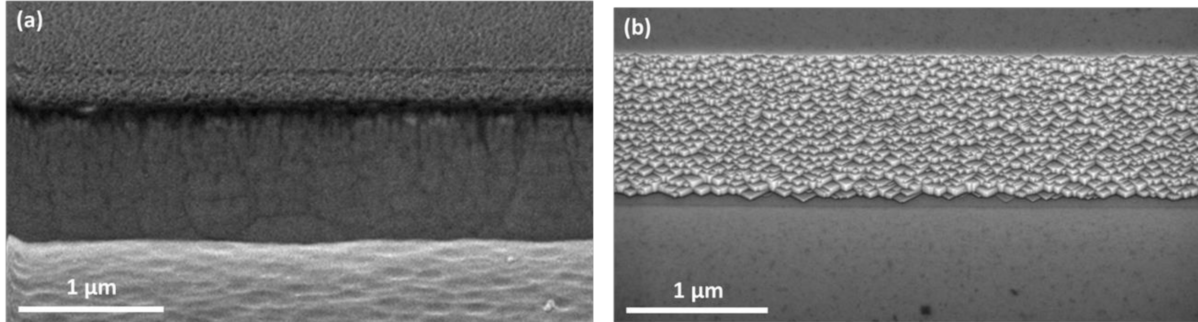

Figure 4.6. SEM images of sidewall profiles without (a) and with (b) sidewall treatments. These images are to show the light extraction efficiency is similar in both cases.

The facet sizes ranged from 50 to 200 nm, so the light extraction efficiency would not be affected significantly by the textured sidewall and the EQE comparison would be valid between the two cases. Note that the facet feature in Fig 4.6(b) was distinctive from that in Fig. 4.2(d) and this could be attributed from different epitaxy wafer were used, because the inherent epitaxial details, such as doping, would slightly affect the appearance of the *m*-plane facet formation.

The devices with chemical and sidewall treatments resulted in improved forward current density-voltage characteristics than devices without treatments, as shown in Fig. 4.7(a).

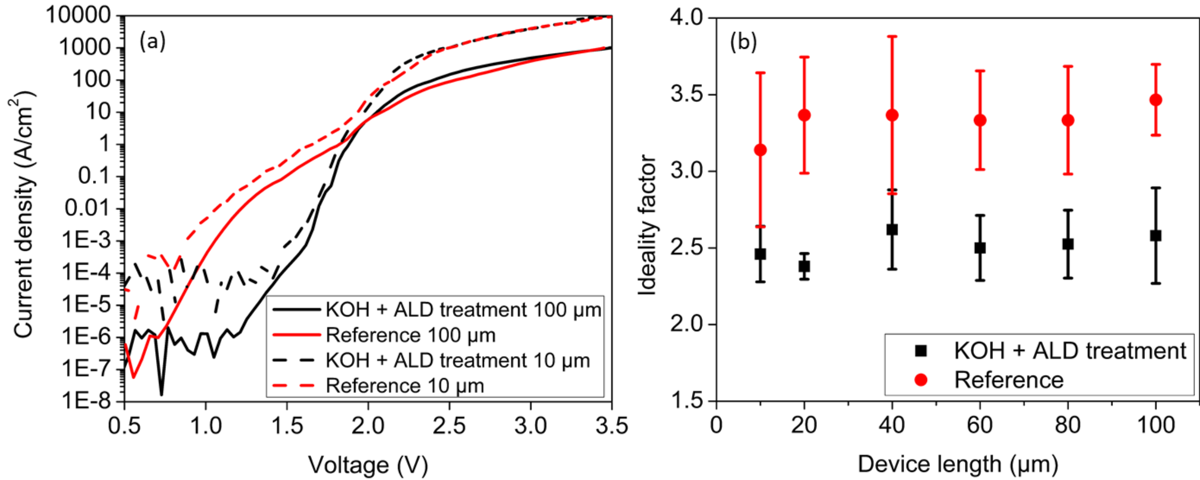

Figure 4.7. Current density-voltage characteristics (a) and ideality factor distribution (b) of devices with and without sidewall treatments.

The forward current density-voltage characteristics of devices with chemical and sidewall treatments yielded lower leakage current and sharper turn-on feature than devices without treatments. Moreover, from Fig. 4.7(b), the ideality factor for devices with sidewall treatments were closer to the ideal value than that of devices without sidewall treatments. Besides forward leakage current, the reverse leakage current was also lessened by utilizing sidewall treatments. Figure 4.8 shows the reverse leakage current density at -4 V with respect to different device sizes.

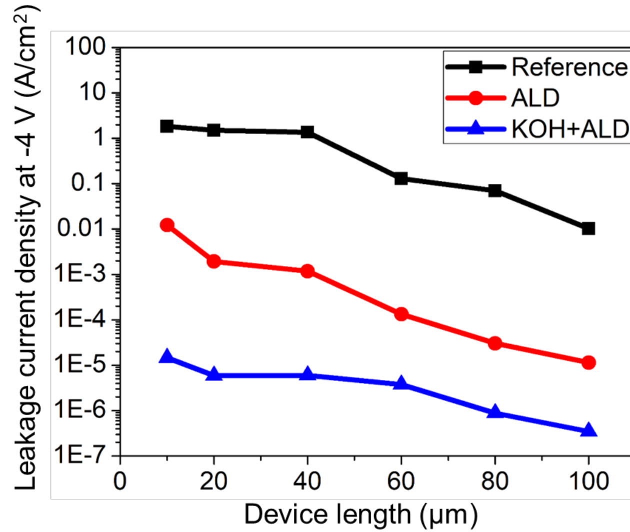

Figure 4.8. The dependence of leakage current density at -4 V on device dimensions using different sidewall treatments.

Similar to Fig. 2.8, the devices without sidewall treatments yielded the highest leakage current density at -4 V and devices with ALD sidewall passivation suppressed leakage current remarkably. However, the leakage current characteristics of the μLEDs with ALD sidewall passivation increased notably from 100×100 to 10×10 μm^2, showing the influences of sidewall damage. With the use of the combination of chemical and sidewall treatments, the leakage current density further reduced and was almost independent with size. The leakage current density was nearly decoupled with the device dimensions, suggesting the leakage current due to sidewall damage was greatly suppressed or removed, since the effects of sidewall damage should be strongly correlated to the perimeter-to-area ratio. Based upon the optoelectrical results, the device performances were enhanced with the combination of chemical and sidewall treatments, which was a consequence of the removal of sidewall damage and surface recombination. Therefore, the effects of sidewall damage and surface recombination should be

significantly suppressed or eliminated after utilizing chemical and sidewall treatments.

Lastly, the effects on the maximum EQE due to the sidewall treatments will be presented. Figure 4.9 (a) and (b) show the EQE performances of devices without and with sidewall treatments, respectively.

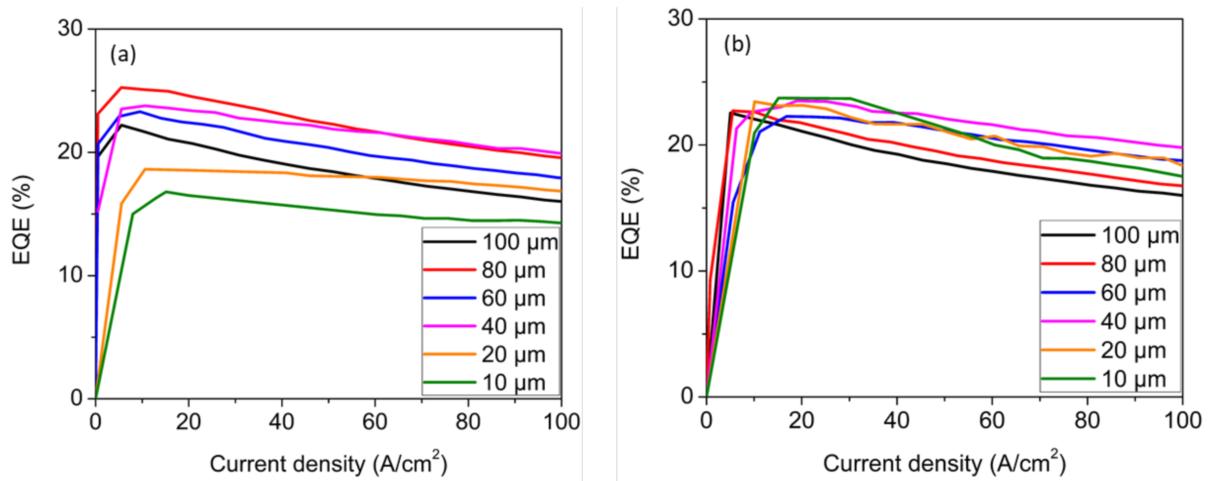

Figure 4.9. The dependence of EQE with current density for devices without (a) and with (b) sidewall treatments.

From Fig. 4.9 (a), the devices without sidewall treatments resulted in 30% decrease in peak efficiency by shrinking the device dimensions from 100×100 to 10×10 μm^2, and majority of the efficiency lost was observed from devices smaller than 40×40 μm^2. Because smaller devices have greater perimeter-to-area ratio, the influences of sidewall damage are more significant in small devices than in larger devices. Conversely, the decrease in peak EQE was within minimal variation for μLEDs with sidewall treatments as shown in Fig. 4.9 (b). The sustained peak EQE could be accounted for the reduction or elimination of sidewall damage, hence the peak efficiency was not affected by the size effect.

Figure 4.10 shows the peak EQE distribution of devices with and without sidewall treatments. The devices without sidewall treatments yielded a gradually decreasing trend as the size shrinks, while the devices with sidewall treatments maintained peak EQE with trivial deviations that could be attributed from fabrication or wafer uniformity.

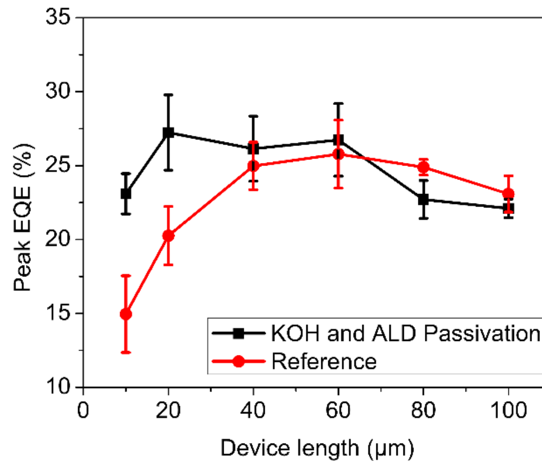

Figure 4.10. The EQE distribution of devices with and without sidewall treatments.

4.4 Summary

In short, this was the first demonstration on achieving size-independent peak EQE of InGaN μLEDs from 100×100 to 10×10 μm^2 by employing post-etch treatments. The idea of this work was to provide a universal and simple approach to remove the size effect in μLEDs. The method of the sidewall treatments consisted of the use of chemical treatment to eliminate sidewall defects and ALD passivation to mitigate surface recombination, which was scalable and offered high degree of flexibility for various device design. By tuning the chemical treatment conditions, different sidewall profiles could be obtained, and thus the

light extraction efficiency could also be enhanced. Based upon the device performances, devices with sidewall treatments resulted in better electrical characteristics, including lower forward- and reverse leakage current and reduced ideality factor. In terms of optical performance, greater light output power was demonstrated from devices with chemical treatment due to improved light extraction efficiency or IQE. As devices with chemical treatments yielded better light extraction efficiency and/or IQE, the EQE could theoretically be improved by modulating the chemical treatment parameters to give even higher EQE values.

References

1. Wong, M. S. *et al.* High Efficiency of III-Nitride Micro-Light-Emitting Diodes by Sidewall Passivation Using Atomic Layer Deposition. *Opt. Express* **26**, 21324–21331 (2018).
2. Wong, M. S. *et al.* Improved performance of AlGaInP red micro-light-emitting diodes with sidewall treatments. *Opt. Express* **28**, 5787 (2020).
3. Zhu, J. *et al.* Near-Complete Elimination of Size-Dependent Efficiency Decrease in GaN Micro-Light-Emitting Diodes. *Phys. Status Solidi Appl. Mater. Sci.* **1900380**, 1–6 (2019).
4. Lee, S. *et al.* A discrete core-shell-like micro- light-emitting diode array grown on sapphire nano-membranes. *Sci. Rep.* **10**, 7506 (2020).
5. Nedy, J. *et al.* Low damage dry etch for III-nitride light emitters. *Semicond. Sci. Technol.* **30**, 85019 (2015).
6. Zhuang, D. & Edgar, J. H. Wet etching of GaN, AlN, and SiC: A review. *Mater. Sci. Eng. R Reports* **48**, 1–46 (2005).
7. Yang, Y. & Cao, X. A. Removing plasma-induced sidewall damage in GaN-based light-emitting diodes by annealing and wet chemical treatments. *J. Vac. Sci. Technol. B Microelectron. Nanom. Struct.* **27**, 2337 (2009).
8. Martinez, G. L., Curiel, M. R., Skromme, B. J. & Molnar, R. J. Surface recombination and sulfide passivation of GaN. *J. Electron. Mater.* **29**, 325–331 (2000).
9. Yue, Y. *et al.* Faceted sidewall etching of n-GaN on sapphire by photoelectrochemical wet processing. *J. Vac. Sci. Technol. B, Nanotechnol.*

Microelectron. Mater. Process. Meas. Phenom. **32**, 061201 (2014).

10. Zhou, L. *et al.* Brief review of surface passivation on III-V semiconductor. *Crystals* **8**, 1–14 (2018).
11. Lin, C. F., Lin, C. M. & Jiang, R. H. Micro-square-array InGaN-based light-emitting diode with an insulated Ga2O3 layer through a photoelectrochemical process. *Jpn. J. Appl. Phys.* **51**, 01AG03 (2012).
12. Lee, J.-M., Huh, C., Kim, D.-J. & Park, S.-J. Dry-etch damage and its recovery in InGaN/GaN multi-quantum-well light-emitting diodes. *Semicond. Sci. Technol.* **18**, 530–534 (2003).
13. Lee, S. W. *et al.* Origin of forward leakage current in GaN-based light-emitting devices. *Appl. Phys. Lett.* **89**, 132117 (2006).
14. Cao, X. A. *et al.* Electrical effects of plasma damage in p-GaN. *Appl. Phys. Lett.* **75**, 2569–2571 (1999).
15. Yonkee, B. P., Young, E. C., DenBaars, S. P., Nakamura, S. & Speck, J. S. Silver free III-nitride flip chip light-emitting-diode with wall plug efficiency over 70% utilizing a GaN tunnel junction. *Appl. Phys. Lett.* **109**, 191104 (2016).
16. Zhang, Y. *et al.* Light extraction efficiency improvement by curved GaN sidewalls in InGaN-based light-emitting diodes. *IEEE Photonics Technol. Lett.* **24**, 243–245 (2012).
17. Stocker, D. A. & Schubert, E. F. Crystallographic wet chemical etching of GaN. **73**, 2654–2656 (1998).
18. Bulashevich, K., Konoplev, S. & Karpov, S. Effect of Die Shape and Size on Performance of III-Nitride Micro-LEDs: A Modeling Study. *Photonics* **5**, 41 (2018).
19. Le Maoult, C. *et al.* Analysis of InGaN surfaces after chemical treatments and atomic layer deposition of Al2O3 for μLED application. *Proc. SPIE* (2020). doi:10.1117/12.2544787
20. Huang Chen, S.-W. *et al.* Full-color monolithic hybrid quantum dot nanoring micro light-emitting diodes with improved efficiency using atomic layer deposition and nonradiative resonant energy transfer. *Photonics Res.* **7**, 416 (2019).
21. Lee, D., Lee, J., Park, J., Seong, T. & Amano, H. Improving the Leakage Characteristics and Efficiency of GaN-based Micro-Light-Emitting Diode with Optimized Passivation. *ECS J. Solid State Sci. Technol.* **9**, 055001 (2020).
22. Wong, M. S. *et al.* Size-independent peak efficiency of III-nitride micro-

light-emitting-diodes using chemical treatment and sidewall passivation. *Appl. Phys. Express* **12**, 097004 (2019).

5

Mass transfer of μLEDs

5.1 Liftoff Methods

For most of the display applications, mass transfer of red, green, and blue μLEDs with excellent yield and selectivity is highly desired for self-emissive μLED displays. Because conventional LED wafers are grown on sapphire or on silicon substrates with single color emission, three types of devices, red, green, and blue colors, are required to be removed from the substrates and transferred to display panels[1,2]. The liftoff principles and results of two developed liftoff methods, namely PEC liftoff and laser liftoff (LLO), on substrate removal of *c*-plane GaN devices from sapphire substrates will be discussed.

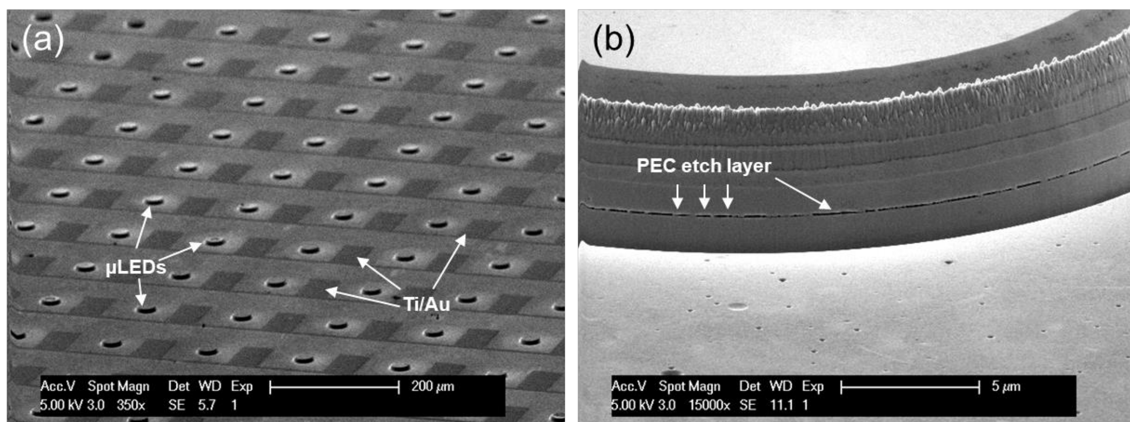

Figure 5.1. SEM images of (a) the PEC design and (b) the etch InGaN sacrificial layer

PEC liftoff relies on the oxidation of InGaN sacrificial layer, where it is intentionally grown below the LED epitaxy structure, with the assistance of photoexcitation and electrolyte (KOH or H_3PO_4)[3,4]. Moreover, since PEC is a redox reaction, metal electrodes are commonly used to reach reasonable liftoff rate. Figure 5.1(a) shows a SEM image of a liftoff mask design for PEC liftoff, where the device dimensions is about 20 μm in diameter, and Fig. 5.1(b) shows the etched InGaN layer after the PEC etch. Due to the needs of metal electrodes and InGaN sacrificial layer for the PEC reaction, more GaN material must be removed from the wafer and the LED epitaxy design needs to be different from the typical LED structure. Additionally, the PEC etch rate and the resulting interface, such as roughness, are highly dependent on the crystal orientation and electrolyte conditions[5,6]. Figure 5.2 shows the undercut interfaces of *c*-plane GaN on sapphire substrates using 0.01 M and 0.1 M KOH. From Fig. 5.2, the roughness increased with higher KOH concentration due to the higher etch rate in the nitrogen face of GaN[3]. However, the undercuts were imperfect where some regions of the device remain attached to the substrate, as indicated by the arrows. This connection issue would introduce undercut non-uniformity when scaling the substrate size and difficult to confirm whether the lateral etch is completed. Because the proposed mass transfer method takes advantage of the fluidic assembly feature, the use of PEC liftoff was not suitable in terms of scalability and *c*-plane GaN devices.

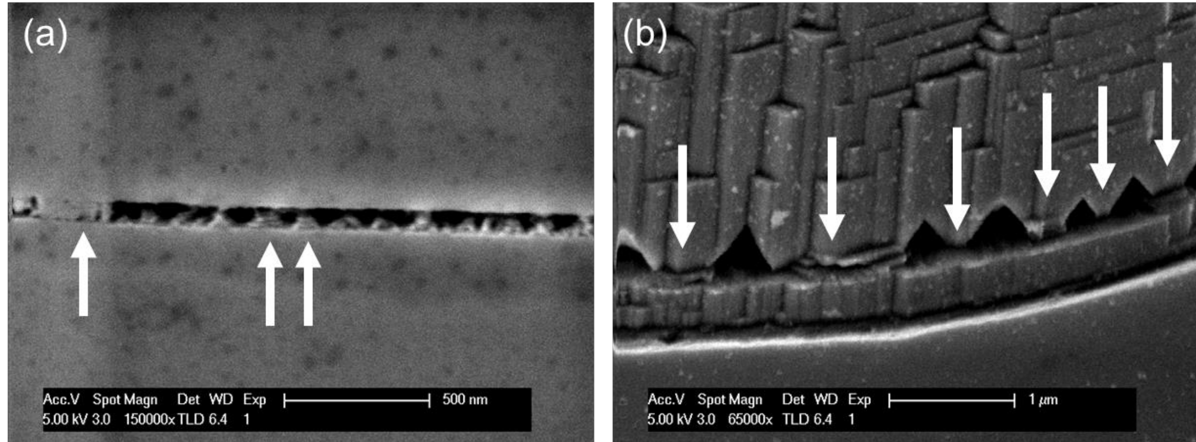

Figure 5.2. SEM images of InGaN sacrificial layer using (a) 0.01 M and (b) 0.1 M KOH after PEC liftoff. The arrows indicate the imperfect separations between the device and the substrate.

Besides PEC liftoff, LLO is another developed approach for substrate removal of GaN on sapphire substrate system, and this method has been employed extensively in a variety of industry processes[7,8]. The mechanism of LLO is based on the difference in absorption between the sapphire substrate and GaN, where sapphire is transparent and GaN absorbs at 266 nm. A high-power laser source can be used to excite the GaN layer at the GaN and sapphire interface, resulting in the delamination of GaN devices from the sapphire substrate[7,9,10]. Unlike PEC, LLO is a liftoff method that employs physical separation using high-power laser, so the device spacing on wafer can be significantly reduced compared to the PEC design, as shown in Fig. 5.3(a). The pitch between the 28×28 μm^2 devices was about 3.5 μm and the device surface after LLO and transferring to a silicon submount showed smooth interface. Moreover, the liftoff is independent of GaN crystal orientation and offers great versatility in scalability and uniformity under academic and commercial settings[7,9,11]. Nevertheless, due to the high-power nature of LLO, additional damage, even physical cracking, can be induced during

the liftoff process, as shown in Fig. 5.3(b)[7]. Since the LLO conditions including the laser power and the exposure time were not optimized, the liftoff process was imperfect and there were cracks in various locations across the whole 2-in sapphire wafer. Although LLO created damage and cracks in devices, it provided much rapid liftoff rate and outstanding scalability than PEC liftoff, LLO was used as the liftoff method described in this dissertation.

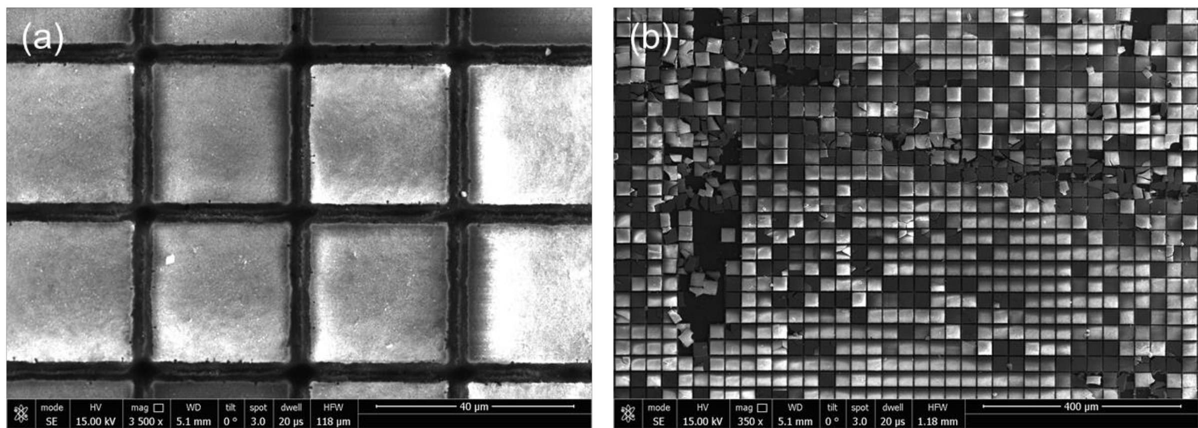

Figure 5.3. SEM images of (a) LLO design and (b) GaN devices on silicon submount after LLO

5.2 Fluidic Assembly with External Forces

Compared to OLEDs and self-emissive quantum dot LEDs, where solution-based inkjet printing is viable, µLEDs lack practical methods that provide rapid transfer rate[12–15]. Therefore, the transfer of µLEDs becomes a cost- and time-inefficient manufacturing process and results in expensive µLED displays[1]. Although transfer approaches using elastomeric stamps have been initially developed, the transfer performance relies significantly on precise alignments and is limited by the reliability of the plastic stamps[16,17]. On the other hand, fluidic assembly techniques using surface chemistry, gravity, or heat have been realized,

and many of them have shown quick transfer rates [18–21]. Most of the demonstrated fluidic assembly approaches depend on pre-patterned display panel for device alignment, where the movement control of devices is minimal and usually disorganized during the transfer process. This disordered characteristic is non-ideal for transfer in high volume, particularly in transferring three color devices for μLED displays, because this random nature can be material-costly and time-consuming and could introduce reliability issues.

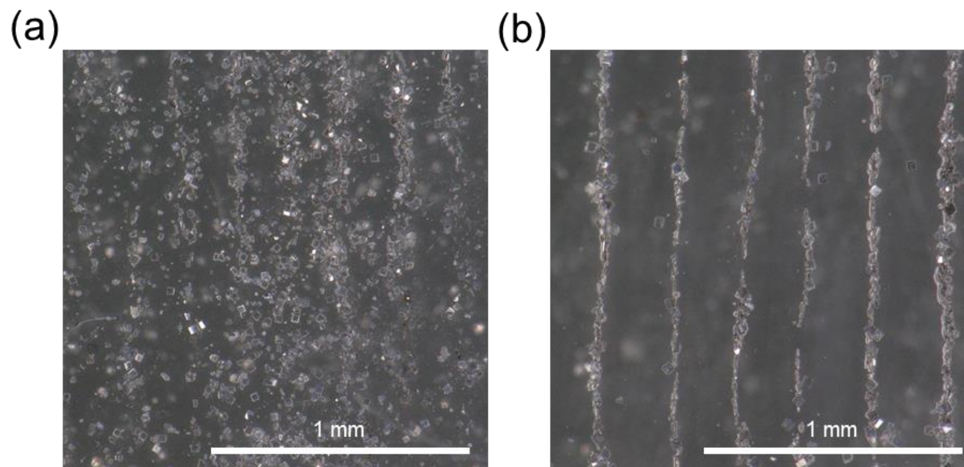

Figure 5.4. Micrographs of InGaN μLEDs (a) without and (b) with acoustic focusing aligning in isopropanol solution

To examine if acoustic focusing can align GaN μLEDs in isopropanol, 28×28 μm^2 devices were used. As shown in Fig. 5.4(a), the devices did not exhibit any ordering features without the use of acoustic focusing. However, by employing acoustic focusing, μLEDs assembled in lines with a distance of 200 μm between lines. The spacing between lines and other assembly parameters can be modulated by varying the wavelength and the amplitude of the acoustic wave, controlled by the resonant frequency and voltage supplied to the vibrating piezoelectric

actuator[22–24]. Figure 5.5 illustrates a schematic of the acoustic focusing channel design. When applying acoustic focusing, acoustic standing waves were created within the microfluidic printing channel, where the channel was 3 mm in width and 300 μm in height in this work. Depending on the acoustic wave, different numbers of node and anti-node were generated with their corresponding sinusoidal pressure forces, and lines of aligned devices were formed by the acoustic forces. Furthermore, since the acoustic forces rely merely on the contrasts in density and in the compressibility between the device and the fluid medium, this process is largely material versatile. Regardless of their chemical or electromagentic properties, semiconductor devices of nearly any solid materials, including InGaN, AlGaN, or AlGaInP, can be manipulated.

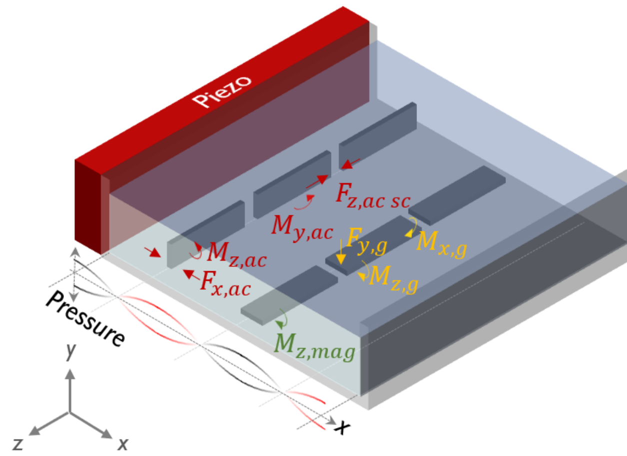

Figure 5.5. Schematic of the acoustic focusing channel design for device alignment in solution using acoustic focusing with labelled forces and moments from different fields

In Fig. 5.4(b), the alignment was not perfect because of the creation of defective materials during LLO. From Fig. 5.3(b), LLO provided uniform and rapid sapphire removal process in most areas, but it could also result in cracked and defective

devices due to the high-power LLO observed from the silicon wafer. The defective devices could reduce or disrupt the ability to manipulate the ordering of devices within the focused lines. Therefore, optimizations on the LLO conditions or alternative liftoff methods or substrates, including PEC liftoff and epitaxial lateral overgrowth, could be considered to obtain damage-free substrate removal techniques[3,25].

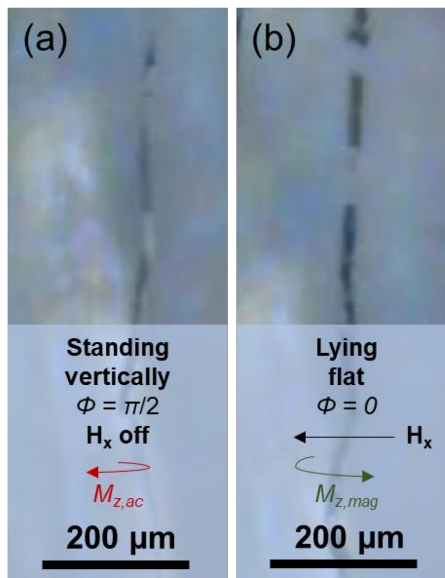

Figure 5.6. Micrographs of InGaN µLEDs (a) without and (b) with magnetic field when applying acoustic focusing in solution

Other than aligning the devices using acoustic focusing, it is important to control the proper device orientation during the transfer. Figures 5.6(a) and 5.6(b) present the microscope images of fluidic assembly of the µLEDs without and with an applied magnetic field while applying acoustic focusing, respectively. For devices without applying a magnetic field, the devices were ordered with an "edge-on" configuration, where the metal contacts were perpendicular to the printing surface. In contrast, the devices were assembled with a "face-on" configuration,

where the metal contacts were parallel to the printing surface, when applying magnetic field. This orientation was controlled by the applied acoustic and magnetic fields. Using the standing pressure wave alone, the devices were oriented "edge-on", because the pressure amplitude was high enough that the torque caused by the pressure differential across the width of the device overcomes the gravitational torque. Thus, magnetic field is required to rotate the devices into the "face-on" configuration for proper electrical contact.

5.3 Devices on Transparent Substrate

The current displays are typically built on glass or other transparent substrates for both LCDs or OLED displays[26–28]. To date, most μLEDs are analyzed either on-wafer or bonded on driving boards, and not many reports on the performances of μLEDs mounted on glass or transparent substrates, such as double-sided polished sapphire substrates[29–33]. Here, this section suggests a novel way to package μLEDs to have better understanding in the device characteristics when mounted on glass or sapphire. Traditional μLED packaging involves mounting the devices on silver headers, where some light will be absorbed by the headers[34–36]. By employing the filament design for μLED packaging, the device performances have demonstrated to be greater than conventional packaging, as shown in Fig. 5.7.

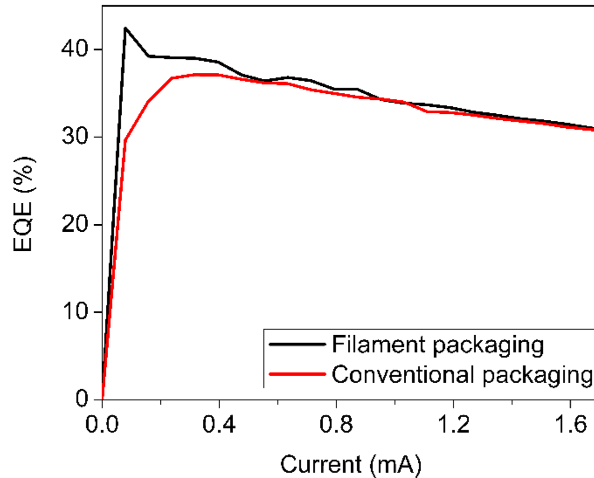

Figure 5.7. EQE comparison between filament and conventional packaging techniques

5.4 Summary

In short, a fluidic assembly approach of InGaN μLEDs using external forces was demonstrated. This fluidic assembly approach employed acoustic focusing and magnetic field to give precise control on device alignment and orientation, and the orientation of the assembled devices can be easily tuned by modulating the parameters of the external forces. This time-efficient fluidic assembly approach could serve as the high-throughput mass-transfer method to make products such as μLED displays at a reduced manufacturing cost and time. Besides the transfer method, the liftoff methods and packaging approaches for InGaN μLEDs have also been explored.

Reference

1. Ding, K., Avrutin, V., Izyumskaya, N., Özgür, Ü. & Morkoç, H. Micro-LEDs, a manufacturability perspective. *Appl. Sci.* **9**, 1206 (2019).

2. Wong, M. S., Nakamura, S. & DenBaars, S. P. Review—Progress in High Performance III-Nitride Micro-Light-Emitting Diodes. *ECS J. Solid State Sci. Technol.* **9**, 015012 (2020).

3. Hwang, D. *et al.* Photoelectrochemical liftoff of LEDs grown on freestanding c-plane GaN substrates. *Opt. Express* **24**, 22875 (2016).

4. Hwang, D. Epitaxial Growth, Nanofabrication, and Mass Transfer of InGaN Micro-LEDs for Displays. (2018).

5. Lee, S. *et al.* Demonstration of GaN-based vertical-cavity surface-emitting lasers with buried tunnel junction contacts. *Opt. Express* **27**, 31621 (2019).

6. Kearns, J. A., Back, J., Cohen, D. A., DenBaars, S. P. & Nakamura, S. Demonstration of blue semipolar (202¯1¯) GaN-based vertical-cavity surface-emitting lasers. *Opt. Express* **27**, 23707 (2019).

7. Wong, W. S. & Sands, T. Damage-free separation of GaN thin films from sapphire substrates. *Appl. Phys. Lett.* **72**, 599–601 (1998).

8. Delmdahl, R., Pätzel, R. & Brune, J. Large-area laser-lift-off processing in microelectronics. *Phys. Procedia* **41**, 241–248 (2013).

9. Ueda, T., Ishida, M. & Yuri, M. Separation of thin GaN from sapphire by laser lift-off technique. *Jpn. J. Appl. Phys.* **50**, 1–6 (2011).

10. Kelly, M. K. *et al.* Large Free-Standing GaN Substrates by Hydride Vapor Phase Epitaxy and Laser-Induced Liftoff. *Jpn. J. Appl. Phys.* **38**, L217–L219 (1999).

11. Iida, D. *et al.* Laser lift-off technique for freestanding GaN substrate using an in droplet formed by thermal decomposition of GaInN and its application to light-emitting diodes. *Appl. Phys. Lett.* **105**, 7–10 (2014).

12. Won, Y.-H. *et al.* Highly efficient and stable InP/ZnSe/ZnS quantum dot light-emitting diodes. *Nature* **575**, 634–638 (2019).

13. Wang, L. *et al.* Blue Quantum Dot Light-Emitting Diodes with High Electroluminescent Efficiency. *ACS Appl. Mater. Interfaces* **9**, 38755–38760 (2017).

14. Levermore, P. P. *et al.* Ink-Jet-Printed OLEDs for Display Applications. *SID Symp. Dig. Tech. Pap.* **47**, 484–486 (2016).

15. Dai, X. *et al.* Solution-processed, high-performance light-emitting diodes based on quantum dots. *Nature* **515**, 96–99 (2014).

16. Cok, R. S. *et al.* Inorganic light-emitting diode displays using micro-transfer printing. *J. Soc. Inf. Disp.* **25**, 589–609 (2017).

17. Bower, C. A. *et al.* Emissive displays with transfer-printed assemblies of 8 µm × 15 µm inorganic light-emitting diodes. *Photonics Res.* **5**, A23 (2017).

18. Cho, S., Lee, D. & Kwon, S. Fluidic self-assembly transfer technology for micro-LED display. *2019 20th Int. Conf. Solid-State Sensors, Actuators*

Microsystems Eurosensors XXXIII 402–404 (2019).

19. Fang, J. & Böhringer, K. F. Parallel micro component-to-substrate assembly with controlled poses and high surface coverage. *J. Micromechanics Microengineering* **16**, 721–730 (2006).

20. Snyder, E. J., Chideme, J. & Craig, G. S. W. Fluidic self-assembly of semiconductor devices: A promising new method of mass producing flexible circuitry. *Jpn. J. Appl. Phys.* **41**, 4366 (2002).

21. Saeedi, E., Kim, S. S., Etzkorn, J. R., Meldrum, D. R. & Parviz, B. A. Automation and yield of micron-scale self-assembly processes. *Proc. 3rd IEEE Int. Conf. Autom. Sci. Eng. IEEE CASE 2007* 375–380 (2007). doi:10.1109/COASE.2007.4341776

22. Collino, R. R. *et al.* Deposition of ordered two-phase materials using microfluidic print nozzles with acoustic focusing. *Extrem. Mech. Lett.* **8**, 96–106 (2016).

23. Collino, R. R. *et al.* Acoustic field controlled patterning and assembly of anisotropic particles. *Extrem. Mech. Lett.* **5**, 37–46 (2015).

24. Melchert, D. S. *et al.* Flexible Conductive Composites with Programmed Electrical Anisotropy Using Acoustophoresis. *Adv. Mater. Technol.* **4**, 1–8 (2019).

25. Gandrothula, S. *et al.* An approach to remove homoepitaxially grown GaN layers by cleavage from the substrate surface. *Appl. Phys. Express* **13**, 041003 (2020).

26. Chen, H.-W., Lee, J.-H., Lin, B.-Y., Chen, S. & Wu, S.-T. Liquid crystal display and organic light-emitting diode display: present status and future perspectives. *Light Sci. Appl.* **7**, 17168 (2018).

27. Harding, M. J., Horne, I. P. & Yaglioglu, B. Flexible LCDs Enabled by OTFT. *SID Symp. Dig. Tech. Pap.* **48**, 793–796 (2017).

28. Lin, Y. *et al.* Mini-LED and Micro-LED: Promising Candidates for the Next Generation Display Technology. *Appl. Sci.* **8**, 1557 (2018).

29. Tian, P. *et al.* Size-dependent efficiency droop of blue InGaN micro-light emitting diodes. *Appl. Phys. Lett.* **101**, 231110 (2012).

30. Olivier, F. *et al.* Influence of size-reduction on the performances of GaN-based micro-LEDs for display application. *J. Lumin.* **191**, 112–116 (2017).

31. Liu, Z. J., Wong, K. M., Keung, C. W., Tang, C. W. & Lau, K. M. Monolithic LED microdisplay on active matrix substrate using flip-chip technology. *IEEE J. Sel. Top. Quantum Electron.* **15**, 1298–1302 (2009).

32. Liu, Z., Chong, W. C., Wong, K. M. & Lau, K. M. GaN-based LED micro-

displays for wearable applications. *Microelectron. Eng.* **148**, 98–103 (2015).

33. Wong, M. S. *et al.* Improved performance of AlGaInP red micro-light-emitting diodes with sidewall treatments. *Opt. Express* **28**, 5787 (2020).

34. Wong, M. S. *et al.* High Efficiency of III-Nitride Micro-Light-Emitting Diodes by Sidewall Passivation Using Atomic Layer Deposition. *Opt. Express* **26**, 21324–21331 (2018).

35. Wong, M. S. *et al.* Size-independent peak efficiency of III-nitride micro-light-emitting-diodes using chemical treatment and sidewall passivation. *Appl. Phys. Express* **12**, 097004 (2019).

36. Hwang, D., Mughal, A., Pynn, C. D., Nakamura, S. & DenBaars, S. P. Sustained high external quantum efficiency in ultrasmall blue III-nitride micro-LEDs. *Appl. Phys. Express* **10**, 032101 (2017).

6

Conclusion

6.1 Challenges in μLED Displays

In this dissertation, the focus has been on the size effect, where the EQE drops significantly as device dimensions shrink. Based upon the results from the dissertation and related work, μLEDs below 10 μm have shown enhanced optoelectrical characteristics by employing methods described in previous chapters, including ALD sidewall passivation and chemical treatment[1–4]. Although the size effect is a major challenge for μLED displays, there are other crucial issues for realizing μLED displays for mass production. First, the mass transfer has the greatest impact to the manufacturing cost of μLED displays, because the ideal mass transfer approach should offer rapid transfer rate with excellent yield and selectivity[5–9]. Both high transfer rate and selectivity are extremely important for μLED displays, as the transfer rate governs the manufacturing time and cost and the selectivity controls the number of defective pixels in the display panel. Without fulfilling these two objectives, μLED displays would remain expensive for typical commercial products[10]. Consider other potential candidates for next-generation display applications, including self-

emissive quantum-dot LEDs, OLEDs, and laser displays, the transfer aspect is not a problem[11–14]. Hence, the mass transfer issue is unique to μLED displays, and should be addressed as soon as possible.

Other than mass transfer, utilizing red, green, and blue colors for mass production is another challenge. As mentioned in chapter 3, InGaN red LEDs suffer from poor optical and efficiency characteristics, and conventional AlGaInP red LEDs tolerate with high drop in efficiency due to surface recombination[15–18]. Additionally, conventional InGaN devices have *c*-plane crystal orientation when grown on silicon or sapphire substrates, where the wavelength shift in *c*-plane devices is the most severe due to the QCSE and would affect the display quality significantly. The QCSE is not the only source that introduces wavelength shift, since the shift in wavelength can also be caused by growth-related variations[10,19]. As a result, other alternatives have been applied to demonstrate full-color μLED displays. Among all alternative routes, color conversion using quantum dots is one of the popular approach, because the color quality is modulated by the choice of quantum dots and monolithic μLEDs, usually blue or UV-A emission, can be used for excitation[10,20,21]. Nevertheless, quantum dots also have their own issues for color conversion materials, such as in the material, transfer, and reliability perspectives[22–24]. Other than the use for color conversion, quantum dots can also be employed for self-emissive LEDs, and self-emissive quantum dot LEDs are getting more attention in recent years[11,25]. If self-emissive quantum dot LEDs are possible, the manufacturing cost for μLED displays with quantum dot color

conversion might be more expensive. Therefore, because of the uncertainty in all approaches, different methods that realize full-color μLED displays are still ongoing.

6.2 Outlook

From the literature, transfer in solution has demonstrated faster transfer rate than transfer methods using stamps or carrier substrates, possibly because the transfer rate is limited by the stamp dimensions[10]. Thus, mass transfer using fluidic assembly can deliver much faster transfer rate than the stamping methods. The main disadvantage of fluidic assembly is the random motion during the transfer, and the uncontrollable transfer mechanism can harm the yield and selectivity, since the irregular movement has no control in device alignment or orientation. Because fluidic assembly using external forces is gaining increasing research attention, the fluidic assembly transfer approach described in chapter 5 provides potential useful insight for future fluidic transfer[26].

For full-color displays, this dissertation reveals the possibility of AlGaInP and InGaN μLEDs with size-independent EQE characteristic, which adds supportive insights to full-color μLEDs, where AlGaInP devices are used for red and InGaN devices are used for blue and green emitters. Because InGaN red LEDs would require more time for better development in terms of the optical and efficiency performances, AlGaInP red μLEDs serve as an alternative until the InGaN red LED technology is mature and applicable for mass production.

Although this dissertation concentrates μLEDs for display applications, there are a variety of potential applications for μLEDs, including biomedical and short-range communication[27–29]. The issues discussed above remain valid for other μLED applications, so any improvements in the μLED color and transfer aspects would be beneficial for the overall μLED development.

6.3 μLED Process Followers

1. Aqua regia three times, 10 min each (only for InGaN samples with metal on surface, do not do this with AlGaInP samples)
2. Hydrochloric acid dip for 40 seconds (AlGaInP samples use 1:10 $HCl:H_2O$ for 60 seconds)
3. Electron beam evaporation for heated ITO deposition, 110 nm, 680°C
4. Stepper 2 mask 1 (AlGaInP requires sputter SiO_2 hard mask for mesa etch)
5. Hard mask SiO_2 etch with ICP 2 for AlGaInP samples only, recipe #101
6. ITO etch with RIE 2 using MHA chemistry
7. Mesa etch (RIE 5 for GaN and Unaxis for AlGaInP)
8. Chemical treatment
9. Stepper 2 mask 2
10. IBD for ODR deposition (12_BY_7_layer for InGaN and 12_MW_11_layer)
11. ALD sidewall passivation at 300°C

12. Stepper 2 mask 3

13. ALD dielectric material removal using BHF

14. Metal deposition (Al/Ni/Au for InGaN and Ge/Au/Ni/Au for AlGaInP)

15. Inspect samples before testing and measurements

6.4 Conclusion

The dissertation provides first demonstrations on recovery of μLED performances, including the optoelectrical and efficiency performances. Before this, the drop in EQE has been observed by several reports and the causes have been identified as surface recombination and sidewall damage. The post-etch sidewall treatment techniques described here offers a universal and straightforward method to suppress or mitigate the influences of sidewall damage and surface recombination resulting in the enhancements in device performances and size-independent EQE characteristic. Moreover, proper sidewall treatments, with the same concepts, are material-versatile and can be applied to not only InGaN visible μLEDs but also AlGaInP red and AlGaN UV LEDs. With the adaptable nature of the sidewall treatments, the size effect and the need of long-wavelength devices are resolved.

Reference

1. Wong, M. S. *et al.* High Efficiency of III-Nitride Micro-Light-Emitting Diodes by Sidewall Passivation Using Atomic Layer Deposition. *Opt. Express* **26**, 21324–21331 (2018).

2. Wong, M. S. *et al.* Size-independent peak efficiency of III-nitride micro-light-emitting-diodes using chemical treatment and sidewall passivation.

Appl. Phys. Express **12**, 097004 (2019).

3. Ley, R. T. *et al.* Revealing the importance of light extraction efficiency in InGaN / GaN microLEDs via chemical treatment and dielectric passivation. *Appl. Phys. Lett* **116**, 251104 (2020).

4. Wong, M. S. *et al.* Improved performance of AlGaInP red micro-light-emitting diodes with sidewall treatments. *Opt. Express* **28**, 5787 (2020).

5. Yeh, H. J. J. & Smith, J. S. Fluidic self-assembly for the integration of GaAs light-emitting diodes on si substrates. *IEEE Photonics Technol. Lett.* **6**, 706–708 (1994).

6. Snyder, E. J., Chideme, J. & Craig, G. S. W. Fluidic self-assembly of semiconductor devices: A promising new method of mass producing flexible circuitry. *Jpn. J. Appl. Phys.* **41**, 4366 (2002).

7. Jacobs, H. O., Tao, A. R., Schwartz, A., Gracias, D. H. & Whitesides, G. M. Fabrication of a cylindrical display by patterned assembly. *Science (80-.).* **296**, 323–325 (2002).

8. Park, S. *et al.* Printed Assemblies of Inorganic Light-Emitting Diodes for Deformable and Semitransparent Displays. *Science (80-.).* **325**, 977–982 (2009).

9. Lee, C. H. *et al.* Flexible inorganic nanostructure light-emitting diodes fabricated on graphene films. *Adv. Mater.* **23**, 4614–4619 (2011).

10. Ding, K., Avrutin, V., Izyumskaya, N., Özgür, Ü. & Morkoç, H. Micro-LEDs, a manufacturability perspective. *Appl. Sci.* **9**, 1206 (2019).

11. Won, Y.-H. *et al.* Highly efficient and stable InP/ZnSe/ZnS quantum dot light-emitting diodes. *Nature* **575**, 634–638 (2019).

12. Maimone, A. & Wang, J. Holographic Optics for Thin and Lightweight Virtual Reality. *ACM Trans. Graph. 39, 4, Artic.* **67**, 14 (2020).

13. Levermore, P. P. *et al.* Ink-Jet-Printed OLEDs for Display Applications. *SID Symp. Dig. Tech. Pap.* **47**, 484–486 (2016).

14. Singh, M., Haverinen, H. M., Dhagat, P. & Jabbour, G. E. Inkjet printing-process and its applications. *Adv. Mater.* **22**, 673–685 (2010).

15. Pasayat, S. S. *et al.* Color-tunable < 10 μ m square InGaN micro- LEDs on compliant GaN-on-porous-GaN. *Appl. Phys. Lett.* **117**, 061105 (2020).

16. Robin, Y. *et al.* What is red? on the chromaticity of orange-red InGaN/GaN based LEDs. *J. Appl. Phys.* **124**, 183102 (2018).

17. Hwang, J.-I., Hashimoto, R., Saito, S. & Nunoue, S. Development of InGaN-based red LED grown on (0001) polar surface. *Appl. Phys. Express*

7, 071003 (2014).

18. Oh, J.-T. *et al.* Light output performance of red AlGaInP-based light emitting diodes with different chip geometries and structures. *Opt. Express* **26**, 11194 (2018).

19. Li, H. *et al.* Study of efficient semipolar (11-22) InGaN green micro-light-emitting diodes on high-quality (11-22) GaN/sapphire template. *Opt. Express* **27**, 24154 (2019).

20. Liu, Y., Wu, B., Wang, Y.-C., Tanyi, E. K. & Cheng, L.-J. Red emission carbon dots for microLED application. *Proc. SPIE* 14 (2019). doi:10.1117/12.2529778

21. Jung, T., Choi, J. H., Jang, S. H. & Han, S. J. Review of Micro-light-emitting-diode Technology for Micro-display Applications. *SID Symp. Dig. Tech. Pap.* **50**, 442–446 (2019).

22. Pickett, N. L., Harris, J. A. & Gresty, N. C. Heavy Metal-Free Quantum Dots for Display Applications. *SID Symp. Dig. Tech. Pap.* **46**, 168–169 (2015).

23. Manders, J. R. *et al.* High efficiency and ultra-wide color gamut quantum dot LEDs for next generation displays. *J. Soc. Inf. Disp.* **23**, 523–528 (2015).

24. Huang Chen, S.-W. *et al.* Full-color monolithic hybrid quantum dot nanoring micro light-emitting diodes with improved efficiency using atomic layer deposition and nonradiative resonant energy transfer. *Photonics Res.* **7**, 416 (2019).

25. Dai, X. *et al.* Solution-processed, high-performance light-emitting diodes based on quantum dots. *Nature* **515**, 96–99 (2014).

26. Eo, Y. J. *et al.* Enhanced DC-Operated Electroluminescence of Forwardly Aligned p/MQW/n InGaN Nanorod LEDs via DC Offset-AC Dielectrophoresis. *ACS Appl. Mater. Interfaces* **9**, 37912–37920 (2017).

27. Wong, M. S., Nakamura, S. & DenBaars, S. P. Review—Progress in High Performance III-Nitride Micro-Light-Emitting Diodes. *ECS J. Solid State Sci. Technol.* **9**, 015012 (2020).

28. Kim, T. *et al.* Injectable, Cellular-Scale Optoelectronics with Applications for Wireless Optogenetics. *Science (80-.).* **340**, 211–216 (2013).

29. Rein, M. *et al.* Diode fibres for fabric-based optical communications. *Nature* **560**, 214–218 (2018).